Institute of Chemistry
University of Lübeck
Director: Prof. Dr. Thomas Peters

Small Ligand Effectors of Bio-macromolecules: Exploration of Novel α-Glucosidase Inhibitors and NMR Investigation of $tRNA^{Phe}$-bound Aminoglycosides

A thesis presented in part fulfilment of the requirements for the doctoral degree of the University of Lübeck
Faculty of Technical and Natural Sciences

Submitted by:
Syed Shahzad ul Hussan

Lübeck, 2005

1. Berichterstatter: PD Dr. Thomas Weimar

2. Berichterstatter: Prof. Dr. Peter K. Müller

Tag der Mündlichen Prüfung: 26.05.2005

Druck genehmigt: Lübeck, 26.05.2005

Contents

Abbreviations and Symbols used

η	Magnitude of NOE enhancement
τ_c	Correlation time
AGEs	Advanced Glycation End-products
CD	Circular Dichroism
COSY	Correlated Spectroscopy
DNA	Deoxyribonucleic Acid
G	6-Dideoxy-2,6-diaminoglucopyranose
HDV	Hepatitis Delta Virus
HIV	Human Immunodeficiency Virus
Hz	Hertz
I	6-Dideoxy-2,6-diaminoglucopyranose
IC_{50}	Inhibitor concentration that inhibits an enzymatic reaction by 50 %
IDDM	Insulin Dependent Diabetes Mellitus
kDa	Kilodalton
K_i	Dissociation constant for enzyme-inhibitor complex
K_m	Michaelis-Menten constant
k_p	Rate constant for the rate determining step of enzyme-catalyzed reaction.
K_s	Dissociation constant for enzyme-substrate complex
ρ	Longitudinal relaxation rate constant
MD Simulation	Molecular Dynamics Simulation
MLEV	Composite Spin-Lock Pulse by Malcom Levitt
NIDDM	Non-insulin Dependent Diabetes Mellitus
NMR	Nuclear Magnetic Resonance
NOE	Nuclear Overhauser Enhancement
NOESY	Nuclear Overhauser and Exchange Spectroscopy
R	Ribofuranose
RNA	Ribonucleic Acid
RNase P	Ribonuclease P
ROE	Rotating frame Overhauser Enhancement
rpm	Round per minute

RRE	Rev Response Element
S	2-Deoxystreptamine
SEM	Standard Error of the Mean
SPR	Surface Plasmone Resonance
STD	Saturation Transfer Difference
TAR	Trans-activation Response region
Tat	Trans-activating Regulatory Protein
TOCSY	Total Correlation Spectroscopy
Tris	Tris(hydroxymethyl)-aminomethan
tRNA	Transfer Ribonucleic Acid
$tRNA^{Phe}$	Phenylalanine-specific Transfer RNA
TrNOE	Transferred Nuclear Overhauser Enhancement
TrROE	Transferred Rotating frame Overhauser Enhancement
TSP	3-(Trimethylsilyl) propionic acid
V_{max}	Maximum velocity of enzyme-catalyzed reaction.
V_{maxi}	Maximum velocity of enzyme-catalyzed reaction in the presence of an inhibitor.
YPD	Yeast extract peptone glucose
γ	Gyromagnetic ratio
σ	Cross relaxation rate constant
ω	Precession frequency

1 Introduction

1.1 Drug Resistance and New Drug Discovery

Microorganisms and viruses have developed several resistance mechanisms, which enable them to evade the effects of antimicrobial and antiviral drugs (McKeegan *et al.*, 2002). Consequently, many of them have become resistant to various drugs. For instance, anti-tuberculosis drug resistance have been found in up to 68% patients in some countries (Kim, 2002). Two leading anti-malarial medicines have become ineffective in many Asian countries and a third is effective in only half of the patients (Barat & Bloland, 1997). Many anti-retroviral drugs have become ineffective against HIV and hepatitis virus due to the development of resistance in viral strains (Kuritzkes, 2002). Not only the health care systems but also the food industries are permanently threatened by the microorganisms and viruses. Keeping in view the on going ability of microorganisms and viruses to develop resistance against different generations of drugs, there is continues need to develop new drugs to combat the drug resistant strains. In this respect, RNA structures are considered as the important targets for the development of new antibacterial, antifungal and antiviral drugs.

1.2 Role of RNA in Biological Processes and RNA as a Potential Target for Therapeutic Intervention

RNA molecules have multifaceted roles in fundamental and highly conserved cellular processes. Starting with RNA as primer for the replication of DNA, RNA molecules have a comprehensive role in the replication and transfer of genetic information from the nucleotide to the amino acid sequence (Judson, 1980). The recent high-resolution structures of ribosome have revealed that RNA is a key component in the structure of ribosome, responsible for peptide bond formation during protein biosynthesis (Harms *et al.*, 2001; Moore & Steitz, 2002). Besides messenger RNA and ribosomal RNA, transfer RNA is a third kind of RNA molecule, which is directly involved in the process of protein synthesis. After aminoacylation with a specific amino acid, tRNA decodes the triplet at the messenger RNA and delivers individual amino acids to the peptide chain.

Ability of catalysis along with the storage and transfer of genetic information makes RNA a functionally versatile bio-molecule. Self-splicing pre-ribosomal RNA (rRNA) was the first discovered RNA molecule having catalytic activity (Kruger, 1982). Ribonuclease P (RNase P) is another example of catalytic RNA that catalyzes the endonucleolitic 5' maturation of tRNA in all kingdoms of life. It is this cleavage of pre-mature tRNA by RNase P which forms the active form of the tRNA molecule (Guerrier-Takada *et al.*, 1983). The hammerhead, hepatitis delta virus (HDV) and hairpin ribozymes are small RNA structures, which catalyze the site-specific self-cleavage and mediate the rolling-circle replications of virus-like RNAs, HDV and plant virus satellite RNAs, respectively. Catalytic RNA molecules play major roles in RNA processing and replication of viral genome. For example, HIV uses small structural RNA elements known as *trans*-activation response region (TAR) and Rev response element (RRE) to recruit the viral regulatory proteins, Tat and Rev to control the viral gene expression. As far as structural properties of RNA molecules are concerned, they can adopt diverse three-dimensional architectures like proteins with the formation of pockets and cavities where shape specific binding can be achieved.

Diverse roles of RNA molecules in biological processes and their high structural variability and complexity, make RNA molecules promising targets for therapeutic intervention. Many antibiotics that are known to interfere with the protein synthesis mechanism, these antibiotics predominantly target the ribosomal RNA molecules rather than ribosomal proteins (Vicens & Westhof, 2003). A class of small molecules that is known to bind various RNA molecules are aminoglycosides (Tor, 2003).

1.3 Aminoglycosides

Aminoglycosides belong to a therapeutically important class of antibiotics that is the oldest known class of broad-spectrum antibacterial agents having activity against Gram-negative and Gram-positive bacteria as well as mycobacteria (Jiang *et al.*, 1999). Therefore, these antibiotics have long been used against various pathogens.

The denomination, aminoglycoside, has been derived from structural architecture of these molecules. Aminoglycosides are constituted of amino-sugars glycosidically linked to an aminocyclitol aglycone. Based on aminocyclitol type (streptidine, 2-deoxystreptamine or fortamine) aminoglycosides can be classified into three major classes. 2-Deoxystreptamine containing aminoglycosides represent the largest group of aminoglycosides and this group is

further classified based on the linkage of amino sugars to the non-sugars. Neomycin B, paromomycin and lividomycin belong to one separate subgroup having a pyranose glycosidically linked to C4 and a furanose glycosidically linked to C5 of the deoxystreptamine ring. Kanamycin A and B, tobramycin and gentamycin belong to a further subgroup having a 2-deoxystreptamine ring glycosilated at C4 and C6.

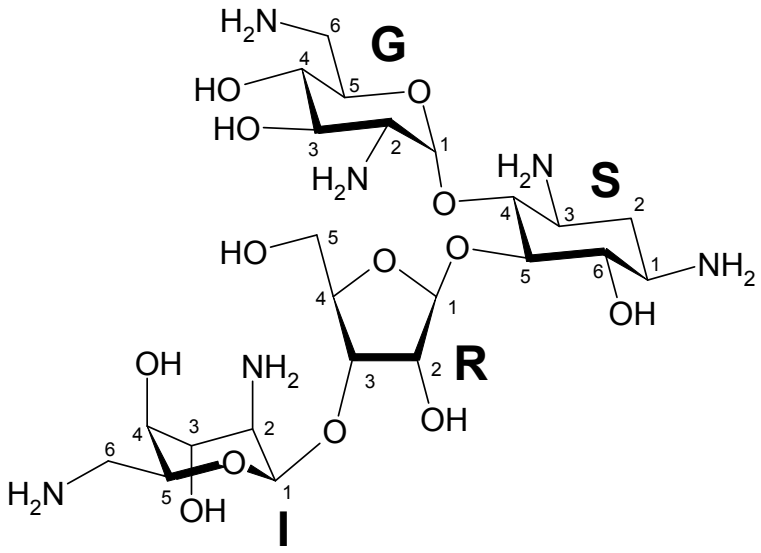

Figure-1.1: Structural scheme of Neomycin B and its subunits, ribostamycin and neamine. Neomycin B comprises of four rings, 6-dideoxy-2,6-diaminoglucopyranose (G), 2-deoxystreptamine (S), ribofuranose (R) and 2,6-diamino-2,6-dideoxyidopyranose (I). Ribostamycin comprises of G, S and R rings whereas neamine consists of only two rings G and S.

Some aminoglycosides can bind specifically to the RNA component of bacterial ribosomes which leads to miscoding during translation and ultimately to bacterial cell death (Blanchard *et al.*, 1998; Carter *et al.*, 2000). Aminoglycosides are also known to interfere with the function of viral RNA besides the prokaryotic RNA. Aminoglycosides can bind to the two regulatory RNA elements, RRE and TAR of HIV mRNA. Binding of aminoglycosides to these elements inhibits the binding of cognate viral proteins Rev and Tat to RRE and TAR respectively, consequently stops the viral replication (Zapp *et al.*, 1993; & Mei *et al.*, 1995). Aminoglycosides have also been reported to bind HDV ribozymes (Rogers *et al.*, 1996), hammerhead ribozymes (Stage *et al.*, 1995; Clouet-d'Orval *et al.*, 1995) and group I intron (von Ahsen *et al.*, 1991; Wank *et al.*, 1994). Binding of these molecules to ribozymes can inhibit the catalytic activities of the ribozymes. tRNA molecules are also a potential target for aminoglycosides since binding of these effector molecules can lead to the conformational

changes in the tRNA molecule which results in the inhibition of aminoacylation process of the tRNA (Kirk & Tor, 1999; Walter *et al.*, 2002). Consequently, protein biosynthesis is inhibited.

Aminoglycosides have been long sought remedy for tuberculosis and other bacterial infections. However, their side effects of renal and auditory toxicity at high doses, has led to decrease their use (Forge & Schacht, 2000). These side effects of aminoglycosides have also urged the need for the discovery of new and more specific drugs. For the rational drug development, the detailed structural information of effector molecules specifically bound to RNA molecules is required. Information about the interaction of aminoglycosides with RNA molecules is still very limited. Few crystal structures of complexes of RNA and effector molecules have been resolved in recent years. These structures of the complexes have provided important information of binding sites of the effector molecules in the RNA structures and the orientation of bound effector molecules. Only a few of these crystal structures have provided sufficient information of conformational properties of these bound effector molecules. Conformational information especially in the flexible molecules like aminoglycosides is crucial for rational drug design. Often x-ray crystallography does not resolve the small ligands bound to macromolecule and crystal packing forces can introduce structural changes in the crystal, especially at the interface between the macromolecule and the ligand. The recently published crystal structure of a complex between $tRNA^{Phe}$ from yeast and neomycin B is resolved at 2.6 Å and parts of the complex, including the binding site of the neomycin B, display high crystallographic B-factors (Figure 1.2) (Mikkelsen *et al.*, 2001). A closer inspection of the aminoglycoside in this crystal structure reveals several configuration errors.

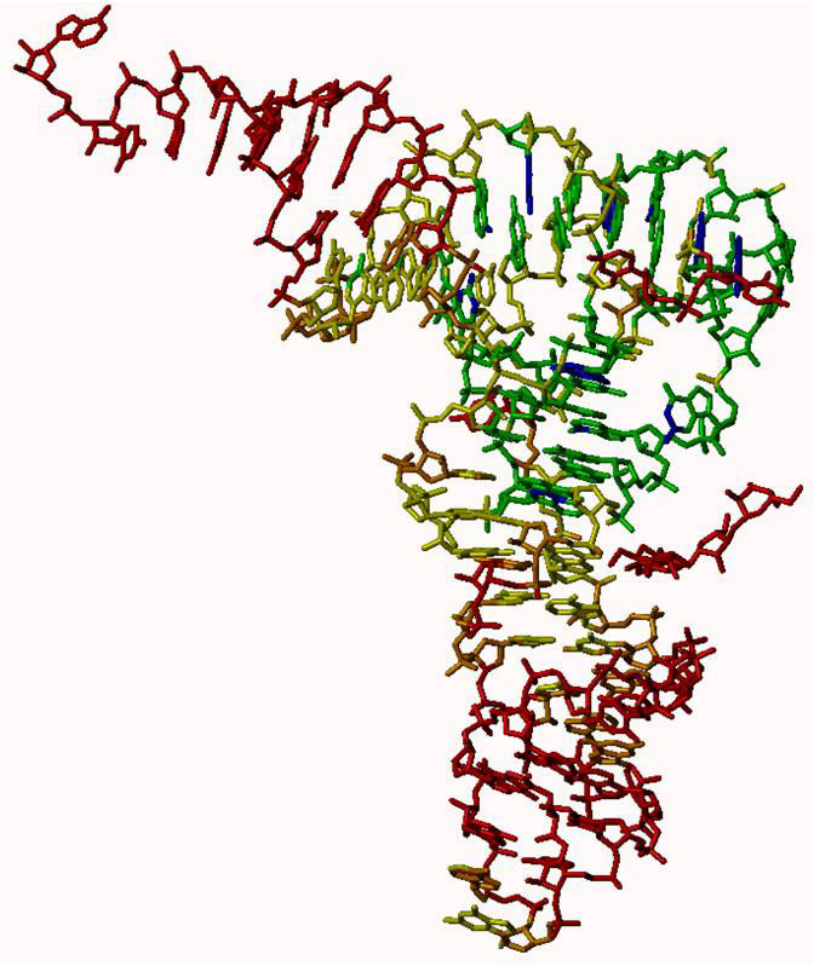

Figure-1.2: Crystal structure of the $tRNA^{Phe}$-neomycin B complex. Red coloured region showing high B factor values, which also include the region containing bound neomycin B.

1.4 Enzymes and their Characteristics

Enzymes are bio-catalytic molecular devices that determine the pattern of chemical transformations. Catalytic power and specificity is the most striking feature of these molecules. Enzymes play a crucial role in catalyzing the reactions because of their capacity to specifically bind to a wide variety of substrates. Specificity is the main characteristic that distinguishes the enzymes from general chemical catalysts. Enzymes are protein in nature. However, ribozymes (catalytic RNA) are the only non-protein macromolecules having catalytic potential like enzymes (Wu *et al.*, 1989).

Study of enzymes provides the key to the knowledge of biological system. Enzymes are responsible for the complete metabolism of food during which nutrient molecules are degraded, chemical energy is transformed and macromolecules are formed which in turn construct the cells and tissues. Enzymes accelerate the biochemical reactions by the factor of millions (hydration of CO_2 is 10^7 times faster in the presence of carbonic anhydrase enzyme

comparative to non-enzymatic reaction) (Stryer, 1995). Enzymes increase the rate of reaction by lowering the free energy of activation (amount of energy a reactant needs to be converted into the product) (Figure 1.3). This lowering of activation energy is nothing but bringing the substrates together in optimal orientation using the intermolecular forces and catalyzing the reaction by stabilizing the transition state. Enzyme substrate complex formation is an important step in the process of catalysis. This complex is formed through the non-covalent interactions between active site of an enzyme and substrate. Active site of enzyme is a small portion of enzyme structure consists of a few amino acids or nucleotides (in case of ribozymes), which directly involves in catalysis. Active site may be constituted of amino acids that are far apart in the primary structure but come in close proximity in three-dimensional structures to form the pocket of active site (Donald & Judith, 1990).

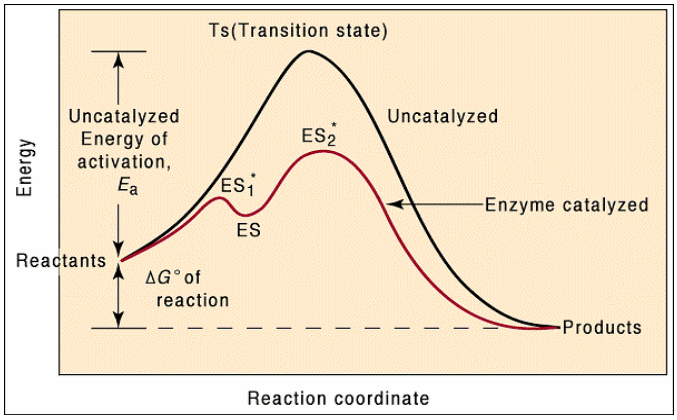

Figure-1.3: Diagram showing the effect of enzyme on activation energy of a reaction.

1.5 Classification of Enzymes

Enzymes can be classified into six main groups according to the types of reactions they catalyze (Table 1.1).

Table-1.1: Enzyme classification based on reaction catalyzed.

Groups of enzymes	Types of reactions catalyzed
1- Oxidoreductases	Oxidation-reduction reaction
2- Transferases	Transfer of functional groups
3- Hydrolases	Hydrolysis reaction
4- Lyases	Group elimination to form double bonds
5- Isomerases	Isomerization
6- Ligases	Bond formation coupled with ATP hydrolysis

1.6 Enzyme Inhibition and its Therapeutic Significance

Inhibition of enzymes is one of the most significant strategies for drug development. A large number of well-known and effective drugs act by inhibiting certain enzymes. Penicillin and aspirin, which are considered very important medicines in the history, act by inhibiting transpeptidase (penicillin binding protein) and cyclooxygenase enzymes, respectively (Vane, 1971; Izaki *et al.*, 1966). Moreover, some of the very successful drugs developed in last few decades, for instance (AZT) 3′-azido-3′-deoxythymidine against HIV (Parthasarathy & Kim, 1988), acarbose against diabetes (Bischoff, 1994) and clavulanic acid, which is used to fight bacterial resistance (Conner, 1985), are the inhibitors of reverse transcriptase, α-glucosidase and β-lactamase enzymes, respectively.

1.7 α-Glucosidase Enzymes

α-Glucosidase enzymes catalyze the hydrolysis of α-glycosidic bond of the oligosaccharides to release the monosaccharide unit.

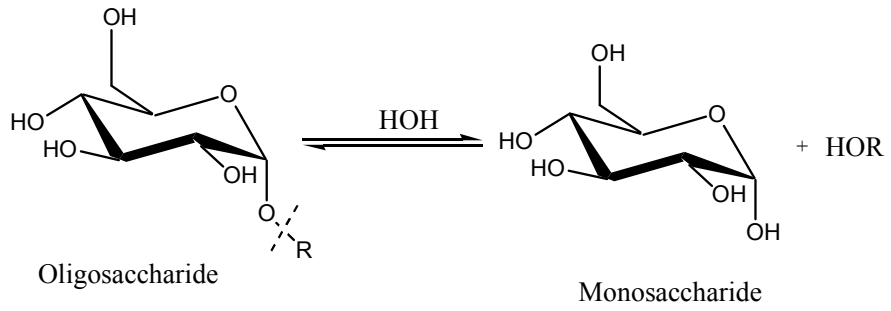

Figure-1.4: α-Glucosidase catalyzed hydrolysis of oligosaccharide

1.7.1 Classification of α-Glucosidase Enzymes on the Basis of Substrate Specificity

Various types of α-glucosidases are widely distributed in microorganisms, plants and animal tissues. α-Glucosidases are classified into three main types on the basis of substrate specificity. (a) Maltase and isomaltase, capable of hydrolysing synthetic arylglucosides such as phenyl α-glucopyranoside and *p*-nitrophenyl α-glucosides more rapidly than malto-oligosaccharides such as maltose and isomaltose (α-glucosidase from Saccharomyces). (b) α-Glucosidases that can catalyze the hydrolysis of malto-oligosaccharides more rapidly (α-glucosidase from *Aspergillus niger*). (c) α-Glucosidases that are capable of hydrolysing

α-glucan as well as malto-oligosaccharides (α-glucosidase from pig serum and sugar beat) (Yoshikawa *et al.*, 1994).

1.7.2 Intestinal α-Glucosidases

The small intestine harbours four membrane-bound glycohydrolases, sucrase-isomaltase maltase-glucoamylase, lactase and trehalase. The combined actions of the maltase-glucoamylase and sucrase-isomaltase complexes, each having two different active sites, further degrade the starch-derived products of α-amylase digestion. Each of the subunits in these complexes has maltase and maltotriose activity, hydrolysing the α(1→4) glycosidic bonds of non-reducing glucose units. In human, the sucrase-isomaltase is responsible for three different catalytic activities: (1) it is responsible for about 80% of the maltase and maltotriase activity in the small intestine by hydrolysing maltose and maltotriose (Semenza, 1986). (2) The isomaltase subunit of this complex is also responsible for the hydrolysis of dextrins at their α(1→6) glycosidic linkages, therefore releasing non-reducing α(1→6) glycosidically bound glucose residues. (3) The sucrase subunit of this complex catalyzes the hydrolysis of sucrose to release monomers. The maltase-glucoamylase complex is responsible for complete glucoamylase activity and about 20% maltase activity. These two complexes are true exoglucosidases, as they release free monomeric glucose from their di- and oligomeric substrates.

Lactase is responsible for the hydrolysis of lactose. Lactose is present in milk and is very important for the growth and survival of young mammals. In small intestine, lactase is the only enzyme that performs the essential β(1→4) galactosidase activity. It is therefore, a fundamental enzyme during post-natal mammalian development. Trehalase is responsible for the hydrolysis of trehalose (Van Beers *et al.*, 1996). Trehalose is found in honey, seafood and beer.

1.8 Inhibition of α-Glucosidase and Management of Diabetes

α-Glucosidase inhibition plays a crucial role in managing diabetes, especially to avoid associated complications. Diabetes has been divided into two types, insulin dependent diabetes mellitus (IDDM) and non-insulin dependent diabetes mellitus (NIDDM). IDDM is developed when insulin secreting β-cells of pancreas are progressively damaged by autoimmune system of the body. Consequently, their ability to secrete insulin gets impaired

progressively. In NIDDM, impaired insulin secretion is not as progressive as in IDDM. Insulin resistance (insulin stimulation of tissue glucose uptake is relatively reduced despite the presence of normal insulin levels) is a cause of NIDDM in 80% patients (Unger & Grundy, 1985) which deteriorates the conditions by diminishing the insulin secretion from pancreas by the toxic effect of glucose on β-cells. More than 90% diabetic patients are diagnosed with NIDDM (Martin & Patricia, 1996).

The most damaging aspect of diabetes mellitus is late complications associated with it. The rate of such disorders affecting eyes, kidneys, arteries and nerves is up to 25 times higher in diabetic patients comparative to non-diabetic individuals (Puls & Bischoff, 1983). Longer manifestation of these chronic disorders may cause severe consequences. Diabetes is considered as an independent risk factor for cardiovascular disease. Two to four times increase of morbidity and mortality in diabetic patients is due to coronary heart diseases (CHD). Coronary heart diseases is found in 40 to 50% diabetic patients, hypertension is found in about 50%, cerebrovascular diseases in 15%, peripheral artery diseases in 30% and retinopathy is found in up to 50% diabetic patients (Jarrett, 1989). The rate of these associated complications increases steadily with the increase of duration of diabetes. Hyperglycaemia, increased blood glucose levels, plays a central role in the development of these chronic complications (DeFronzo *et al.*, 1992).

1.8.1 Mechanisms for the Development of Diabetes-Associated Complications

1.8.1.1 Advanced Glycation End-Products (AGEs)

Formation of so called, AGEs, is one of the mechanisms responsible for the development of diabetes associated complications. High blood glucose levels chemically modify various intracellular and extra-cellular macromolecules. Free amino groups are irreversibly condensed with sugar and form highly reactive Schiff bases. Lysine is one of the amino acids especially involved in this condensation reaction. The Schiff bases subsequently, undergo a chemical rearrangement to more stable Amadori products. These products in turn degrade into a number of highly reactive compounds, which react again with free amino groups and form various intermediates and AGEs. Formation of AGEs plays a significant role in several complications of aging and diabetes, including etherosclerosis and renal diseases. AGEs may accumulate on long-lived tissue proteins, for instance collagen. Formation of these AGEs on proteins may alter their tertiary structures. In addition to structural modifications of normal

matrix proteins, many plasma proteins may be trapped in the matrix by the reactive AGEs situated on the matrix proteins, which further enhance the thickness of basement membrane (Bruce & Timon, 1995; Brownlee, 1992).

1.8.1.2 The Polyol Pathway

Normal route of glucose metabolism is changed significantly at high blood glucose levels. In such conditions, glucose is reduced to sorbitol by the action of aldose reductase and then oxidised to fructose by the enzyme polyol dehydrogenase. Aldose reductase has a low affinity for glucose therefore, glucose is metabolised also through this pathway when hyperglycaemia prevails. This alternate pathway of glucose metabolism is known as polyol pathway. Aldose reductase has been found in many tissues including nerves, retina, retinal micro vessels and glumeruli. At higher glucose levels, polyol pathway contributes to glucose metabolism as much as 30%. Metabolism of glucose through polyol pathway leads to the accumulation of polyol because these sugar alcohols cannot pass through the cell membrane. The accumulation of sorbitol may have a role in diabetes associated complications especially retinopathy and renal disorders. The third mechanism for the development of diabetes-associated complications is the toxic effect of glucose on pancreatic β-cells. However, the reason of this toxic effect is still unclear. This effect may be due to decrease in glucose transporter-2 (Johnson *et al.*, 1990).

1.8.2 Role of Insulin in Glucose Metabolism

Insulin, secreted from the β-cells of pancreas is responsible to maintain blood glucose levels. Increase in plasma glucose levels rapidly stimulates insulin secretion. Insulin in turn, stimulates glucose uptake in peripheral tissues especially in skeletal muscles and inhibit the formation of glucose by the processes of glycogenolysis and gluconeogenesis (hepatic glucose production) (Reaven & Chen, 1988).

1.8.3 Management of NIDDM

The main objective of anti-diabetic therapy in both IDDM and NIDDM is to achieve consistency in normal blood glucose levels to prevent diabetes-associated late complications. Different strategies have been applied to manage diabetes that include insulin injections, hypoglycaemic agents and diet therapy. Insulin injections are useful only in IDDM, where pancreatic β-cells cannot secrete insulin in a sufficient quantity. In case of NIDDM, insulin

injections are not useful as this can cause hyperinsulinaemia. Oral hypoglycaemic agents like sulphonylureas function by stimulation of insulin secretion. These agents are not useful in NIDDM when the insulin resistance is a primary factor for developing the disease. More over, these agents have adverse effect of hypoglycaemia that, in severe case, can lead to permanent neurological disorders or death (Joe & Arshag, 2000).

1.8.3.1 Diet Therapy

As mono-, di- and polysaccharides, carbohydrates represent not only major part of the diet quantitatively but also the main source of energy. Diet therapy plays an important role especially at early stages of NIDDM to keep the blood glucose levels to normal and can avoid other complications. However, the patients, with diet therapy have to divide their carbohydrate uptake into 5 to 7 small portions spread over the day that disturbs their normal life.

1.8.3.2 α-Glucosidase Inhibition

The most important dietary carbohydrate components are starch and sucrose, which have to be broken down enzymatically by α-glucosidase to absorbable monosaccharides. Process of conversion of oligosaccharides into monosaccharides takes place in the distal portion of small intestine. However, the lower part of the intestine, ileum is not involved in this digestion process of carbohydrates yet this part contains all the enzymatic activity for carbohydrate digestion (Newcommer & McGill, 1966). Starch the biggest component of human diet, constitute a mixture of amylose and amylopectin. Glucose units are linked by α(1→4) glycosidic bonds in amylose units as well as in amylopectins, however, amylopectins also contain branch points formed by α(1→6) glycosidic bonds between the glucose units. Other important carbohydrate component of human diet is sucrose, found in many fruits and some vegetables. Sucrose consists of glucose and fructose units linked by β(1→2) glycosidic linkage. Starch digestion starts in the mouth by salivary α-amylase that converts starch into a mixture of maltose and maltotriose, and limit dextrin in small portion. This process also continues in the small intestine by the action of pancreatic α-amylase. Amylase does not release glucose by acting directly on glycosidic bond at the end of polymer chain because it is not a true exoglucosidase. Finally, in the intestine large quantity of maltose produced from starch, and sucrose as a dietary component, need to be digested as absorbable monosaccharides. The digestion of disaccharide is catalyzed by a complex mixture of α-glucosidases present in the epithelium of small intestine. Inhibition of these enzymes in small

intestine slows down the process of digestion that spreads up to distal part of small intestine. This slowing down of digestion leads to prolonged absorption of monosaccharides from intestine to blood. Ultimately, it helps in avoiding postprandial hyperglycaemia that in turn is very effective in managing non-insulin-dependent diabetes especially to avoid the onset of later complications (Bischoff, 1994; Arshag & Jerome, 1999). In case of α-glucosidase inhibition, there is no caloric loss in the form of discharge of undigested carbohydrate components from the body. This is just delaying and prolonging the process of digestion and absorption (Holt *et al.*, 1996).

1.9 α-Glucosidase Inhibition and Anti-viral Drugs

α-Glucosidase inhibitors have also been found to possess broad-spectrum antiviral activity. This activity is because of their potential to inhibit trimming glucosidases involved in the biosynthesis of the *N*-linked oligosaccharides on the envelope glycoproteins (Van den Broek *et al.*, 1996). Many α-glucosidase inhibitors have been found to possess anti-HIV (Human Immuno Deficiency Virus) activity. 1-Deoxenojirimycin, castanospermine and their several derivatives inhibit the HIV replication (Taylor *et al.*, 1991; Papandreou *et al.*, 2002). Inhibition studies on α-glucosidase enzyme, therefore, can lead to the development of new drugs not only for the management of diabetes but also for the viral diseases.

1.10 Natural Products and their Therapeutic Significance

Natural products are the primary source of pharmacophores against many diseases that subsequently leads to structural based drug design. Natural products have been an important source for drug discovery since ages. It is estimated that some 20,000 species of higher plants are used medicinally throughout the world and plants are the primary source of medicine in the developing world. Approximately 250,000 flowering plants are known to exist and only 15% of these have yet been analysed for their medicinal properties (Balandrin *et al.*, 1993). This makes the flowering plants an important source for the drug discovery especially against the challenging diseases. Many well-known drugs listed in the modern pharmacopoeia have their origins in nature that includes drugs for infectious and non-infectious diseases (Tagboto & Townson, 2001). Acarbose, antidiabetic drug that was isolated from fermentation broth of the Actinoplanes (Schmidt *et al.*, 1977), is one of the several examples of drugs derived from natural products. Vinblastine and vincristine that were isolated from *Catharanthiis roseus* are the clinically used drugs against various forms of cancers (Mahidol *et al.*, 1998)

2 Objectives

The aim of these studies was to investigate the complexes of three aminoglycosides from the neomycin B family, neamine, ribostamycin and neomycin B (Figure 1.1) with $tRNA^{Phe}$, and identify the new inhibitors of α-glucosidase enzymes.

The particular focus of the investigation of bindings of aminoglycosides to tRNA was:

(1) Optimising the conditions for NMR experiments of the complexes
(2) Determining the bioactive conformations of the aminoglycosides through transferred nuclear Overhauser enhancement (trNOE) experiments in combination with force field calculations.

2.1 Optimising the Conditions for NMR Experiments

Due to the high pKa values of amino groups of aminoglycosides, these molecules are protonated at physiological pH and therefore charged (Robert & Coxon, 1983). Therefore, most of the aminoglycosides behave as polycationic molecules at physiological pH. In neomycin B, out of six amino groups, five have pKa values between 7.6 and 8.8. Only the 3-amino group on ring S has a pKa of 5.7 (Overval *et al.*, 1995). RNA molecules are polyanionic due to their negatively charged backbone consisting of riboses and phosphoric esters. Electrostatic interactions between positively charged ammonium groups of aminoglycosides and negatively charged RNA molecules can be among the major deriving forces for the binding strength of these molecules (Wang & Tor, 1997). However, these electrostatic interactions can also be the source of unspecific binding of aminoglycosides to RNA molecules, which may lead one to wrong interpretation of the bioactive conformation and binding affinities of these molecules. Therefore, in order to determine the bioactive conformation of the aminoglycosides these unspecific interactions were to be minimized.

2.2 Determining the Bioactive Conformations of Aminoglycosides

The glycosidic linkages in aminoglycosides are very flexible and allow a large degree of conformational freedom. In aqueous solution, these molecules can adopt a large number of conformations but they bind to a macromolecule in a specific bioactive conformation. The trNOE technique was to be used to calculate the inter hydrogen atom distances and these

distances were to be used as constraints in the force field calculations to determine the bioactive conformations of the aminoglycosides.

2.3 α-Glucosidase Inhibition

Keeping in view the therapeutic importance of α-glucosidase inhibition, the focus of these studies was:

- To identify the new inhibitors of α-glucosidase enzyme by screening the focused libraries of compounds isolated from natural sources, using high throughput *in vitro* screening methods.
- To explore the binding modes and binding affinity of the active compounds identified in the initial screening, through the kinetic evaluations.
- To determine the toxic effects of the inhibitors using DNA damaging and brine shrimp assays for toxic studies so that only the non-toxic compounds could be used for further experiments.
- To identify the lead compounds by the comparison of inhibitory potential of the different classes of compounds.
- To investigate the α-glucosidase inhibitory potential of the most active compounds, *in vivo* for their therapeutic relevance, by determining their hypoglycaemic effects in animal models.

3 Theory

3.1 NMR Spectroscopy

3.1.1 Nuclear Overhauser Enhancement (NOE)

When two spins, usually called *I* and *S*, experience each other's magnetic dipole moment a dipole-dipole interaction phenomenon called cross-relaxation can transfer magnetization through space from one spin to the other. Thus the signal intensity of spin *I* changes when the equilibrium state of a neighboring spin *S* is disturbed by saturation (*S* refers originally to the saturated spin) or inversion with radio-frequency pulses. The change in intensity arising from this dipolar interaction is called Nuclear Overhauser Enhancement (NOE) (Noggel & Schirmer, 1971). The intensity change of spin *I* is governed by the three transition probabilities for zero-, one- and double quantum transitions, namely W_{0IS}, W_{1I} and W_{2IS}, respectively, which describe the cross-relaxation pathways in an idealized two-spin system. With these transition probabilities, the intensity change of spin *I* with time is defined by the Solomon equation as:

$$\frac{dI_Z}{dt} = -(I_Z - I_Z^0)(W_{0IS} + 2W_{1I} + W_{2IS}) - (S_Z - S_Z^0)(W_{2IS} - W_{0IS}) \qquad (3.1)$$

In equation 3.1, S_Z and I_Z are the longitudinal components of the magnetization of spins *S* and *I* (S_Z^0 and I_Z^0 at time zero). The Solomon equation is strictly applicable only for an idealized spin system, that is, for two isolated spins that are not scalar coupled and that exist in a rigid and isotropically tumbling molecule. Depending on tumbling rate, the zero- and double quantum transition probabilities cause negative and positive NOE enhancements, respectively. The difference between these probabilities (W_{2IS} - W_{0IS}), called the cross-relaxation rate constant (σ_{IS}), describes the rate of dipole-dipole transitions giving rise to the NOE enhancement, and therefore defines how fast an NOE enhancement is transferred between spins *I* and *S*. The term $W_{0IS} + 2W_{1I} + W_{2IS}$ is called the dipolar longitudinal relaxation rate constant (ρ_{IS}) and is part of the relaxation mechanism responsible for restoring the

equilibrium state of spin *I*. Incorporating these definitions, and taking into account that, while saturating spin *S* at steady state $dI_Z/dt = S_Z = 0$, we obtain:

$$\frac{I_Z - I_Z^{\,0}}{S_Z^{\,0}} = \frac{\sigma_{IS}}{\rho_{IS}} \tag{3.2}$$

Since the longitudinal components of spins *S* and *I* at the beginning of the experiment are identical ($S_Z^{\,0} = I_Z^{\,0}$), $S_Z^{\,0}$ can be further substituted by $I_Z^{\,0}$ to give the maximum steady state NOE enhancement η for spin *I* after saturation of spin *S*:

$$\eta = \frac{I_Z - I_Z^0}{I_Z^0} = \frac{\gamma_S}{\gamma_I} \frac{\sigma_{IS}}{\rho_{IS}} \tag{3.3}$$

The relationship between the two gyromagnetic ratios (γ_S and γ_I) means that equation 3.3 is also applicable to systems in which *I* and *S* are spins with different precession frequencies (ω), such as ^1H and ^{13}C, which give rise to a heteronuclear NOE. For a homonuclear ^1H-^1H NOE $\gamma_S = \gamma_I$.

3.1.1.1 Dependence of NOE on Molecular Motion

The transition probabilities, and therefore also σ_{IS} and ρ_{IS}, depend strongly on the precession frequencies (ω) of the spins and the overall correlation time (τ_c) of the molecule, which is a measure of the rate of reorientation in solution. The variation of the homonuclear NOE with the rate of reorientation of the molecule is presented in Figure 3.1 for a given precession frequency (ω). For molecules that tumble rapidly in solution, for example small organic compounds in organic solvents, a maximum theoretical NOE enhancement of +50 % is obtained. This region of the NOE curve is often called the extreme narrowing limit. Large molecules, such as proteins or polysaccharides or nucleic acids, tumble much slower and result in a maximum theoretical NOE enhancement of -100 %. Using the transition probabilities, we see that for short correlation times (small molecules) W_{2IS} dominates and leads to a positive NOE, whereas for large molecules (with long correlation times) the W_{0IS} transition is dominant, leading to negative NOE effects. Between these two extremes there is a region corresponding to intermediate tumbling where NOE changes sign and even becomes zero when $W_{2IS} = W_{0IS}$. In this region magnitude and sign of NOE is very sensitive to the molecular motion (Claridge, 1999).

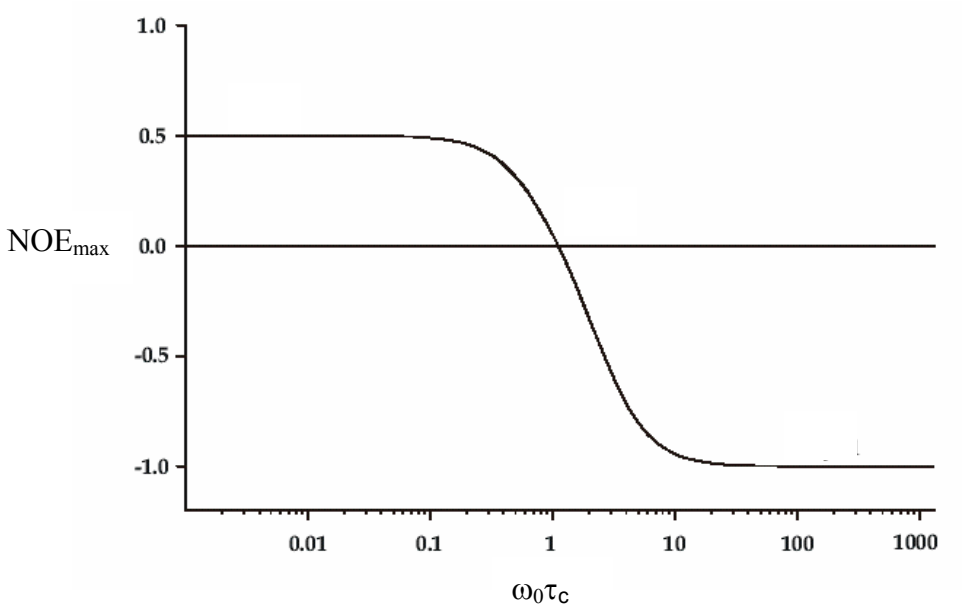

Figure-3.1: Dependence of the maximum homonuclear NOE enhancement on the product of the spectrometer frequency (ω_0) with the overall correlation time of the molecule (τ_c) $\omega\tau_c$ for a two-spin system. Saturation of the source spin was assumed (steady-state NOE conditions). In the case of inverted spins (transient NOE experiments) the dependence is almost identical, but starts at an enhancement of +0.38 for rapidly tumbling molecules (extreme narrowing limit).

3.1.2 NOE and Inter Nuclear Distance

In reality we are not working with idealized spin-systems and the longitudinal dipolar relaxation between spins *I* and *S* is not the only relaxation mechanism present. In such real molecules the NOE enhancement is inversely proportional to the distance (r) between the nuclei.

$$\eta \sim \frac{\tau_c}{r^6} \tag{3.4}$$

Given a NOE between a pair of nuclei (C and D), which are separated by a known distance, it is possible to determine the distance between two other nuclei (A and B) using the simple relationship shown in equation 3.5. This method is referred to as the two-spin approximation.

$$\frac{NOE_{AB}}{NOE_{CD}} = \frac{r^{-6}_{AB}}{r^{-6}_{CD}} \quad . \tag{3.5}$$

These information of inter hydrogen atom distances are very helpful to determine the three dimensional structure of the molecule.

3.1.3 Transferred Nuclear Overhauser Enhancement (trNOE)

TrNOE is the NOE measured on averaged ligand resonances when ligand is in an exchange between its free solution sate and a macromolecule-bound state at a rate on the relaxation time scale and measured enhancement reflects the geometry of the ligand in the bound state (Jackman & Cotton, 1975). TrNOE effects are negative in sign because of long correlation time of the complex. Therefore, the existence of binding may be easily deduced from visual inspection, since NOE effects for small molecule (ligand) are usually positive.

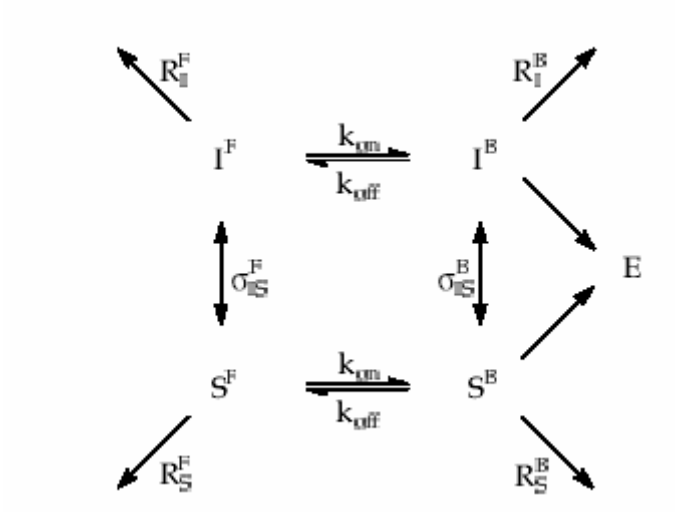

Figure-3.2: Two-spin system in a ligand molecule exchanging between its free and bound state. R stands for longitudinal relaxation rates at different states, σ represents cross relaxation rate constant and E indicates spin diffusion.

Figure 3.2 shows a simple two-spin system with two-site exchange with free and bound states. Both Spins I and S are present on a ligand. Exchange equilibrium for this system can be written as:

$$E + L \underset{k_{-1}}{\overset{k_1 [E]}{\rightleftharpoons}} EL \qquad (3.6)$$

E stands for free receptor, L stands for free ligand and EL represents ligand-receptor complex.

Binding constant for this reaction is written as:

$$K = \frac{k_1}{k_{-1}} = \frac{[EL]}{[E][L]} \tag{3.7}$$

The basis of trNOE experiment is that σ^B, the cross relaxation rate constant in slowly tumbling bound state should be larger than the σ^F, the cross relaxation rate in rapidly tumbling free state of the ligand (see the Figure 3.2). The averaged cross relaxation rate for fast exchange on relaxation time scale can be written as:

$$\langle \sigma \rangle = N^F \sigma^F_{IS} + N^B \sigma^B_{IS} \tag{3.8}$$

N is denoted for the mole fraction.

The limitation for trNOE that $\langle \sigma \rangle$ should be dominated by σ^B can be fulfilled when:

$$N^B \sigma^B_{IS} >> N^F \sigma^F_{IS} \tag{3.9}$$

Condition for the expression 3.9 depends upon affinity constant K for the formation of complex, distance r_{IS} in both states and the relative tumbling rates in free and bound state. If ligand is just weakly bound, N^B will be insufficient and trNOE does not appear due to insufficient availability of ligand in the bound state to contribute to overall relaxation process. On the other hand, if the ligand is extremely tightly bound, rate of exchange between free and bound states is not sufficient for the suitable magnetization flux to occur between them and this affects against the development of trNOE. The correlation time (τ_c) of the complex should be much larger than that of the free ligand. The more slowly the reorientation of the complex taken place, larger will be σ^B_{IS} and the condition favours the development of trNOE (Neuhaus & Williamson, 2000). All these factors have to taken into account during the trNOE experiments.

3.1.4 Spin Diffusion

In case of spin diffusion, apart from direct enhancements between hydrogen atoms close in space other spins may mediate the exchange of magnetization thus producing the negative cross peaks between hydrogen atoms far apart from each other (Kalk & Berendsen, 1976;

Akasaka *et al.*, 1978). These peaks have the same sign as those coming from direct enhancements through trNOE effects. Thus, spin diffusion may lead to a wrong trNOE-derived conformation of the bound ligand.

3.1.5 Identification of Spin Diffusion by trROE Experiments

When the magnetization of spins is locked in the x-y plane of the coordinate system which rotates with the speed and direction of nuclear precession (called the rotating coordinate system or rotating frame) with a long and weak pulse (spin-lock pulse) dipolar relaxation leads to so called ROE effects (Rotating frame Overhauser Enhancement). In ROE as well as trROE experiments, direct cross peaks always show positive sign relative to the diagonal signals (Arepalli *et al.*, 1995). Spin diffusion via one relay proton leads to negative cross peaks that can easily be distinguished from direct interactions. In trROE experiments, usually more than one relay protons are involved leading to cancellation of respective cross peaks. Therefore, if a cross peak is observed in trNOE spectrum and absent in trROE spectrum, it can be concluded that cross peak in the trNOE spectrum originated from spin diffusion.

3.1.6 Saturation Transfer Difference (STD) NMR

Macromolecules like proteins and RNAs consist of a large system of hydrogen atoms tightly coupled by dipole-dipole interactions. Selective saturation of macromolecule resonances results in a rapid spread of the magnetization over the entire macromolecule through spin diffusion. Further intermolecular transfer of this magnetization from the macromolecule to the ligand leads to progressive saturation of the ligand resonances in contact with the macromolecule (Figure 3.3). STD spectra therefore, help to define the contact area between ligand and macromolecule (Mayer & Meyer, 2001).

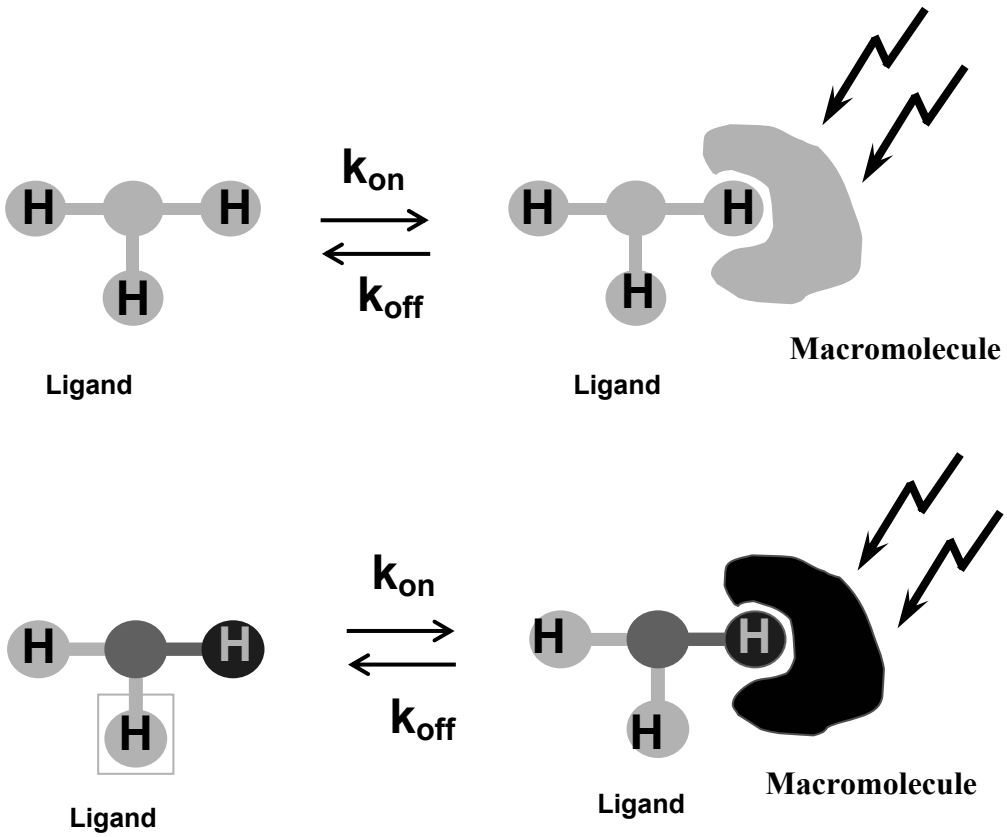

Figure-3.3: Schematic representation of STD NMR, when resonances of macromolecule are selectively saturated magnetization is also transferred to ligand in fast exchange between its free and bound states. Part of ligand that is in close proximity to macromolecule receives maximum magnetization. Dark coloured surface indicates the higher level of magnetization is transferred to that region.

3.2 Molecular Modelling

Computational technique that can provide insight into the behaviour of molecular systems is known as molecular modelling.

3.2.1 Force Field and Molecular Mechanics

In molecular mechanics, electronic motions are ignored and energy of a molecule is calculated as the function of nuclear position. According to Born-Oppenheimer approximation, the much smaller mass of the electrons comparative to nuclei means that they can rapidly adjust to any change in the nuclear position. Thus, the energy of molecule in its ground electronic state can be considered as function of nuclear coordinates. Change in nuclear position can be the result of just a single bond rotation or the movement of a large

number of atoms in a molecule. If some or all nuclei change their positions relative to each other, energy is changed.

$$\nu\left(r^{N}\right) = \sum_{bonds}\frac{k_i}{2}\left(l_i - l_{i,0}\right)^2 + \sum_{angles}\frac{k_i}{2}\left(\theta_i - \theta_{i,0}\right)^2 + \sum_{torsion}\frac{V_n}{2}\left(1+\cos\left(n\omega-\gamma\right)\right)+$$
$$\sum_{i=1}^{N}\sum_{j=i+1}^{N}\left(4\varepsilon_{ij}\left[\left(\frac{\sigma_{ij}}{r_{ij}}\right)^{12}-\left(\frac{\sigma_{ij}}{r_{ij}}\right)^{6}\right]+\frac{q_i q_j}{4\pi\varepsilon_0 r_{ij}}\right) \quad (3.10)$$

In expression 3.10, $\nu(r^N)$ represents the potential energy which is the function of the position (r) of N particles. First term in the equation 3.10 models the interactions between bonded atoms and gives the value of energy when the bond length l_i deviates from the reference value $l_{i,0}$. The second term represents the factor of valence angle and, third term in the expression denotes for torsion angles and calculates the energy change as the bond rotates. Fourth term is non-bonded term, which is calculated for all pairs of atoms that are in different molecule or in the same molecule but separated by at least three bonds. Non-bonded term is modelled using a Coulomb potential term for electrostatic interaction or Lennard-Jones potential for van der Walls interactions. Force field is an important tool in the modelling techniques as it can give the information about various sorts of energy, which in tern helps to decide which trajectory belongs to the most stable structure (Leach, 1996).

3.2.2 Molecular Dynamics (MD) Simulation

All molecules are in motion except at absolute zero. The motion can be associated with overall translation, rotation or vibration, which are related to the temperature and pressure of the system. More importantly from a conformational perspective, some of the motions are internal. These internal motions can drastically alter the conformation of the molecule, particularly through torsion angle rotation. In MD simulations the motion is divided into very short time steps (Δt = 1-2 fs). Given the position (x) of a particle at time t, its new position after time Δt may be obtained from the familiar Taylor expansion:

$$x(t+\Delta t) = x(t) + v(t)\Delta t + \frac{1}{2}a(t)\Delta t^2 + \ldots \quad (3.11)$$

Where v = atomic velocity and a = acceleration.

This is an infinite series and for practical implementation it must be truncated. Several methods have been proposed for the treatment of this truncation. The method of Verlet is one of the most common. The Verlet algorithm uses the positions and accelerations at time t and the positions from the previous step (t - Δt) to compute the new positions at $t + \Delta t$. The equations for the positions at ($t + \Delta t$) and ($t - \Delta t$) are:

$$x(t+\Delta t) = x(t) + v(t)\Delta t + \frac{1}{2}a(t)\Delta t^2 \tag{3.12}$$

$$x(t-\Delta t) = x(t) - v(t)\Delta t + \frac{1}{2}a(t)\Delta t^2 \tag{3.13}$$

These may be added together and rewritten to give the position at $t + \Delta t$ as:

$$x(t+\Delta t) = 2x(t) - x(t-\Delta t) + a(t)\Delta t^2 \tag{3.14}$$

The accelerations are computed from the force field by solving Newton's first law:

$$F_i = -\frac{\partial V}{\partial x_i} = m_i a_i \tag{3.15}$$

where, V is the potential energy function (i.e. the force field).

MD simulation is therefore, a computational method of studying the motions and the conformational space of molecular system by integration of the classical Newtonian equations of motion providing the potential energy function and its associated force field. Different information obtained through experiments can be used as constraints in MD simulation to get an experimentally derived ensemble (Bush & Martin-Paster, 1999; van Gunsteren & Berendsen, 1982).

3.3 Enzyme Kinetics

Enzyme kinetics deals with the factors affecting the rates of enzyme-catalyzed reactions. The important factors in this regard are enzyme concentration, ligand concentrations (substrates, products, inhibitors and activators), pH, ionic strength, and temperature. Studies of these factors provide the in depth knowledge of the nature of the enzyme-catalyzed reaction. For example, by varying the concentrations of substrate and product, it is possible to deduce the kinetic mechanism of the reaction. During kinetic studies, rate of disappearance of substrate or rate of appearance of product is measured under controlled conditions of temperature, pH and ionic strength of suitable buffer, and concentrations of substrate and enzyme (Segel, 1975).

3.3.1 Michaelis-Menten Equation

The simplest expression to explain enzyme-catalyzed reaction is one-substrate, one-product reaction that is based on the assumption that product, P is irreversibly formed with the regeneration of enzyme, E through the formation of intermediate enzyme-substrate, ES complex.

$$E + S \underset{k_{-1}}{\overset{k_1}{\rightleftharpoons}} ES \xrightarrow{k_p} E + P \tag{3.16}$$

The reaction rate is simply the rate of formation of product that can be written as:

$$v = \frac{d[P]}{dt} = k_p[ES] \tag{3.17}$$

Kinetic expression in most of the enzymes can be derived from steady state assumption according to that:

Rate of formation of [ES] is equal to rate of dissociation of [ES] in both directions (to form product and regenerate free substrate)

At steady state $$\frac{d[ES]}{dt} = 0 \tag{3.18}$$

Taking into account the steady state conditions kinetic expression can be solved to equation 3.19

$$v = \frac{k_p[E]_t[S]}{[S] + K_m} \tag{3.19}$$

$$k_p[E]_t = V_{max} \tag{3.20}$$

Expression 3.20 explains the saturation conditions when all the enzyme molecules in the reaction mixture are busy in carrying out catalysis in the presence of very high substrate concentration [S]. So the expression 3.19 becomes:

$$v = \frac{V_{max}[S]}{[S] + K_m} \tag{3.21}$$

In expression 3.21, V_{max} represents the maximum reaction velocity attained when enzyme is saturated with substrate. Numerical value of K_m (Michaelis-Menten constant) relates the velocity of enzyme-catalyzed reaction to the substrate concentration. K_m is numerically equivalent to the substrate concentration that yields half-maximal reaction velocity.

When $[S] = K_m$

Then expression 3.21 becomes

$$v = \frac{V_{max}[K_m]}{[K_m] + K_m} = \frac{1}{2}V_{max} \tag{3.22}$$

K_m Value is the characteristic of an enzyme so it helps to compare the activity of same type of enzymes from different sources using same substrate.

3.3.2 Lineweaver-Burk Plot

It is very difficult to determine the V_{max} value through hyperbolic curve obtained by plotting v versus [S] directly according to the expression 3.21 (Michaelis-Mentin equation). However, the rearrangement of Michaelis-Menten equation into the linear form produces Lineweaver-Burk plot or double reciprocal plot.

By rearranging expression 3.21

$$\frac{1}{\mathrm{v}} = \frac{K_m}{V_{\max}[\mathrm{S}]} + \frac{1}{V_{\max}} \tag{3.23}$$

So straight line is obtained by plotting 1/v versus 1/[S] according to the expression 3.23, which is helpful to determine all important kinetic constants.

3.4 Enzyme Inhibition and Types of Inhibitors

Enzyme inhibition is slowing down the process of catalysis on binding of certain molecules to the enzyme. Enzyme inhibition is one of the most important regulatory devices of biochemical reactions in living system. Inhibitors can be irreversible and reversible. Irreversible inhibitors bind very tightly to enzyme, some times even covalently. They dissociate back very slowly. Nerve gas, diisopropylphosphofluoridate irreversibly inhibits the acetylcholinesterase enzyme (Domschke & Erdmann, 1969). Reversible inhibitors bind to the enzyme through week interactions like hydrophobic interactions, hydrogen bonding and week electrostatic interactions. They are characterized by rapid dissociation of enzyme inhibitor complex. Reversible inhibitors have been classified into four types based on their mechanisms:

a) Competitive inhibitors
b) Noncompetitive inhibitors
c) Uncompetitive inhibitors
d) Mixed-type inhibitors

3.4.1 Competitive inhibitors

Competitive inhibitors bind to the free enzyme in a way that prevents substrate binding to the active site of the enzyme. They mostly resemble or mimic, in their structural features with

substrate and compete with the substrate for the binding site of the enzyme. As a result, the substrate is prevented from binding to the same active site when inhibitor is present at high concentration. A competitive inhibitor diminishes the rate of catalysis by reducing the proportion of the enzyme active site bound by substrate.

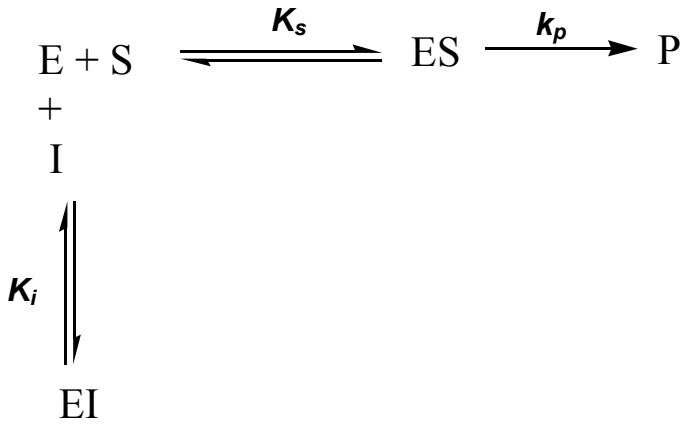

Figure-3.4: Reaction scheme for competitive inhibition. K_s is the dissociation constant for enzyme substrate complex, K_i is the dissociation constant for enzyme-inhibitor complex and k_p is the rate constant for rate determining step.

The initial velocity of enzyme-catalyzed reaction is proportional to ES (enzyme substrate) complex. Since substrate and inhibitor compete with each other for the same site of enzyme, so priority for binding largely depends upon concentration. Characteristic feature of competitive inhibition is that at any fixed concentration of inhibitor, velocity of the reaction can be made equal to the velocity that is in the absence of inhibitor, by just increasing the concentration of the substrate. Thereby, the entire enzyme can be converted to ES form. Consequently, V_{maxi}, the maximum velocity in the presence of competitive inhibitor can be equal to $V_{max,}$ the maximum reaction velocity in the absence of inhibitor. However, the substrate concentration required to derive the whole enzyme to ES form in the presence of competitive inhibitor is higher than that would be in the absence of inhibitor. Therefore, apparent $K_{m,}$ the concentration of substrate related to half- maximal velocity in the presence of inhibitor, increases.

The steady state kinetic expression in the presence of competitive inhibitor can be derived by considering that, the total enzyme [E]t is present in three forms: free enzyme [E] enzyme-substrate complex [ES] and enzyme-inhibitor complex [EI] (Figure 3.4).

$$v = \frac{V_{max}[S]}{K_m\left(1 + \frac{[I]}{K_i}\right) + [S]} \tag{3.24}$$

Expression 3.24 is different from expression 3.21, the usual Michaelis-Menten equation, in that the factor (1+[I]/K_i) is present as multiplied to the term K_m. Therefore, K_m is increased in the presence of competitive inhibitor and V_{max} remains the same. E is the only form of enzyme having affinity for the substrate to form ES intermediate complex (Figure 3.4). (1+[I]/K_i), is the [I] dependent factor that describes the distribution of enzyme between the E and EI forms. Velocity equation for competitive inhibition in double reciprocal form can be written as:

$$\frac{1}{v} = \frac{K_m}{V_{max}}\left(1 + \frac{[I]}{K_i}\right)\frac{1}{[S]} + \frac{1}{V_{max}} \tag{3.25}$$

Thus, the slope of the plot increases by the factor (1+ [I]/K_i) and the intercept at 1/v-axis will not be affected. Second reciprocal plot with higher inhibitor concentration will intercept the 1/v-axis at the same point but with higher value of slope to define higher K_m value.

3.4.2 Noncompetitive Inhibitors

Noncompetitive inhibitors bind either to free enzyme or ES (enzyme substrate) complex at a site different from the substrate-binding site of enzyme. Binding of both inhibitor and substrate to enzyme is quite independent of each other and random. The resulting ESI complex is catalytically inactive. Inactivation of ESI complex may be due to the conformational changes in enzyme structure induced by the inhibitor that consequently prevent the proper positioning of the catalytic site to catalyze the reaction.

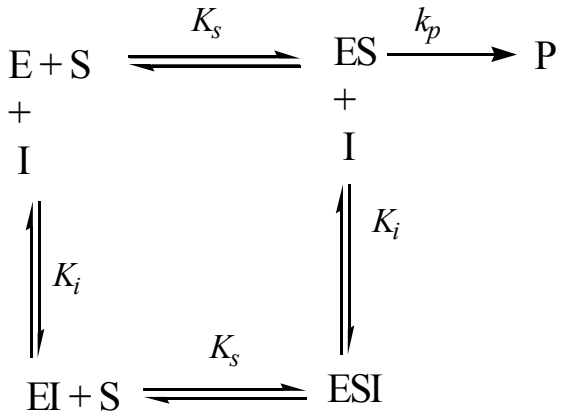

Figure-3.5: Reaction scheme for noncompetitive inhibition.

At any infinite concentration of substrate, whole enzyme cannot be driven to productive ES form. In the presence of inhibitor even at very minute concentration, a proportion of enzyme remains in non-productive ESI form regardless the concentration of substrate. Consequently, V_{maxi} (maximum velocity in the presence of noncompetitive inhibitor) will always be less than V_{max} (maximum velocity in the absence of inhibitor) and K_m value will remain the same. Kinetic expression in the presence of noncompetitive inhibitor can be derived by considering total enzyme $[E]_t$ is present in four forms: free enzyme, [E]; enzyme-substrate complex, [ES]; enzyme-inhibitor complex, [EI] and enzyme-substrate-inhibitor complex, [ESI] (Figure 3.5).

$$\frac{v}{\frac{V_{max}}{\left(1+\frac{[I]}{K_i}\right)}} = \frac{[S]}{K_m + [S]} \tag{3.26}$$

Expression 3.26 contains the term $(1 + [I]/K_i)$ as divided by the V_{max} indicating that the V_{max} value decreases in the presence of noncompetitive inhibitor. In such conditions enzyme substrate complex is present in productive ES and nonproductive ESI form at any substrate and inhibitor concentrations thus decrease the steady state level of ES that results in the decrease in V_{max} value. The factor $(1 + [I]/K_i)$ can be considered as the [I] dependent factor that describes the distribution of enzyme-substrate complex between ES and ESI form. Velocity equation for noncompetitive inhibition in the reciprocal form can be written as:

$$\frac{1}{v} = \frac{K_m}{V_{max}}\left(1 + \frac{[I]}{K_i}\right)\frac{1}{[S]} + \frac{1}{V_{max}}\left(1 + \frac{[I]}{K_i}\right) \tag{3.27}$$

Expression 3.27 shows that both, slope and intercept at 1/v-axis, increase by the factor of $(1 + [I]/K_i)$ in the presence of noncompetitive inhibitor. If the slope and 1/v-axis intercept increase by the same factor then 1/S-intercept point will remain the same and thus K_m is not affected.

3.4.3 Uncompetitive Inhibitors

Uncompetitive inhibitors reversibly bind to ES complex only and form inactive ESI complex (Figure 3.6).

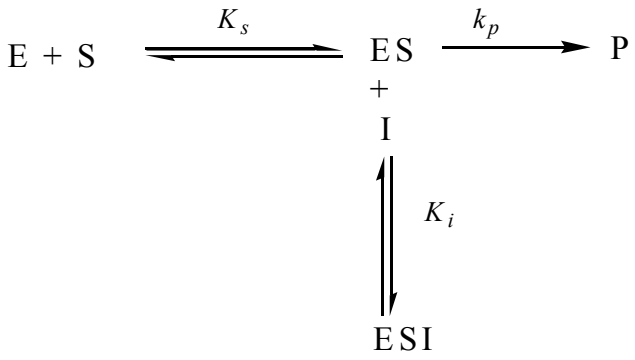

Figure-3.6: Reaction scheme for uncompetitive inhibition.

In case of uncompetitive inhibition, at any infinite concentration of substrate, some proportion of enzyme remain exists in non-productive ESI form and V_{maxi}, is less than V_{max}. The steady state velocity equation for uncompetitive inhibition can be written as:

$$\frac{v}{\frac{V_{max}}{\left(1 + \frac{[I]}{K_i}\right)}} = \frac{[S]}{\frac{K_m}{\left(1 + \frac{[I]}{K_i}\right)} + [S]} \tag{3.28}$$

According to expression 3.28 both V_{max} and K_m decrease with the increase of uncompetitive inhibitor concentration. Equation 3.28 can be written in the reciprocal form as:

$$\frac{1}{v} = \frac{K_m}{V_{max}} \frac{1}{[S]} + \frac{1}{V_{max}} \left(1 + \frac{[I]}{K_i} \right) \tag{3.29}$$

According to expression 3.29 slope of the curve remains the same in the presence of uncompetitive inhibitor but intercept at 1/v-axis increases by the factor of $(1 + [I]/K_i)$. Therefore, when inhibitor concentration increases the point of 1/v-intercept gets higher and different parallel curves are obtained each of these intercept x-axis at different points (Segel, 1993).

3.4.4 Mixed-type Inhibitors

Mixed-type inhibitors bind either to free enzyme or enzyme-substrate ES complex. In the presence of mixed-type inhibitor, a proportion of enzyme remains in non-productive ESI form regardless the concentration of substrate, so the V_{maxi} is less than $V_{max.}$ Characteristic feature of mixed-type inhibition is that enzyme has higher affinity for substrate in its E form than EI form. Consequently, apparent K_s value is larger than the K_s value (Figure 3.7). In other words, K_m value increases in the presence of mixed-type inhibitor because more quantity of substrate is required by enzyme to get half-maximal reaction velocity.

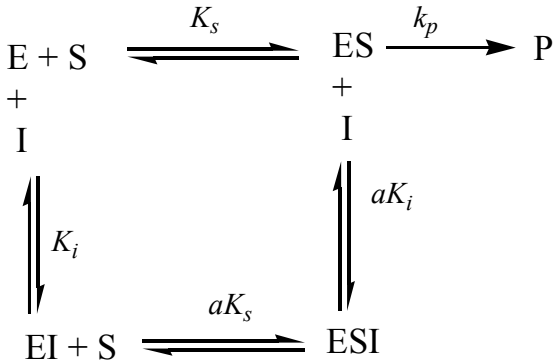

Figure-3.7: Reaction scheme for linear mixed-type inhibition

Steady state velocity equation for linear mixed type inhibition can be written as:

$$\frac{\mathrm{v}}{\frac{V_{\max}}{\left(1+\frac{[\mathrm{I}]}{aK_i}\right)}} = \frac{[\mathrm{S}]}{K_m\frac{\left(1+\frac{[\mathrm{I}]}{K_i}\right)}{\left(1+\frac{[\mathrm{I}]}{aK_i}\right)}+[\mathrm{S}]} \tag{3.30}$$

Expression 3.30 shows that $V_{\max}$ as well as K_m values are affected in the presence of mixed-type inhibitor.

3.5 Dixon Plot

Dixon plot is used to determine the K_i value and to identify the type of inhibition involved during the inhibition study of a particular enzyme. Dixon plot is produced between reciprocal of reaction velocity, 1/v and inhibitor concentrations, [I]. In order to produce the Dixon plot the velocity equation is rearranged to such a linear form in which [I] is the varied ligand. Example of competitive inhibition is taken to rearrange the Lineweaver equation into velocity equation for Dixon plot, as follow:

$$\frac{1}{\mathrm{v}} = \frac{K_m}{V_{\max}[\mathrm{S}]}\left(1+\frac{[\mathrm{I}]}{K_i}\right)+\frac{1}{V_{\max}}$$

After rearranging

$$\frac{1}{\mathrm{v}} = \frac{K_m}{V_{\max}[\mathrm{S}]}+\frac{K_m[\mathrm{I}]}{V_{\max}[\mathrm{S}]K_i}+\frac{1}{V_{\max}}$$

$$\frac{1}{\mathrm{v}} = \frac{K_m}{V_{\max}[\mathrm{S}]K_i}[\mathrm{I}]+\frac{1}{V_{\max}}\left(1+\frac{K_m}{[\mathrm{S}]}\right) \tag{3.31}$$

In the1/v versus [I] plot, factor $\frac{K_m}{V_{\max}[\mathrm{S}]K_i}$ provides the value of slope and the factor $\frac{1}{V_{\max}}\left(1+\frac{K_m}{[\mathrm{S}]}\right)$ provides the intercept of the curve at 1/v-axis. –[I] value at the intersection of two curves drawn for two particular substrate concentrations, gives the K_i value.

3.6 Reaction Mechanism and Active-sites of α-Glucosidase Enzymes

Mechanism of hydrolysis of α-glycosidic linkage of an oligosaccharide by α-glucosidase enzyme involves acid/base or oxocarbenium ion mechanism. Two acidic residues participate in this catalytic process. Carboxylate group promotes oxocarbenium ion formation, while the carboxylic group attacks the oxygen of glycosidic linkage. Subsequently, hydroxyl ion of water displaces the oxocarbenium ion through an S_N1 mechanism to complete the reaction (Figure 3.8). Two acidic residues, Asp-14 (aspartic acid-14) and Glu-276 (Glutamic acid-276) have been identified as being involved in the process of catalysis in yeast α-glucosidase (E.C 3.2.1.20) (McCarter & Withers, 1996; Howard & Wither, 1998). In case of mammalian sucrase-isomalatase, complex Asp-505 and Asp-1394 are active site residues in each of the two homologous active sites of the enzyme complex (Seiya, 1997).

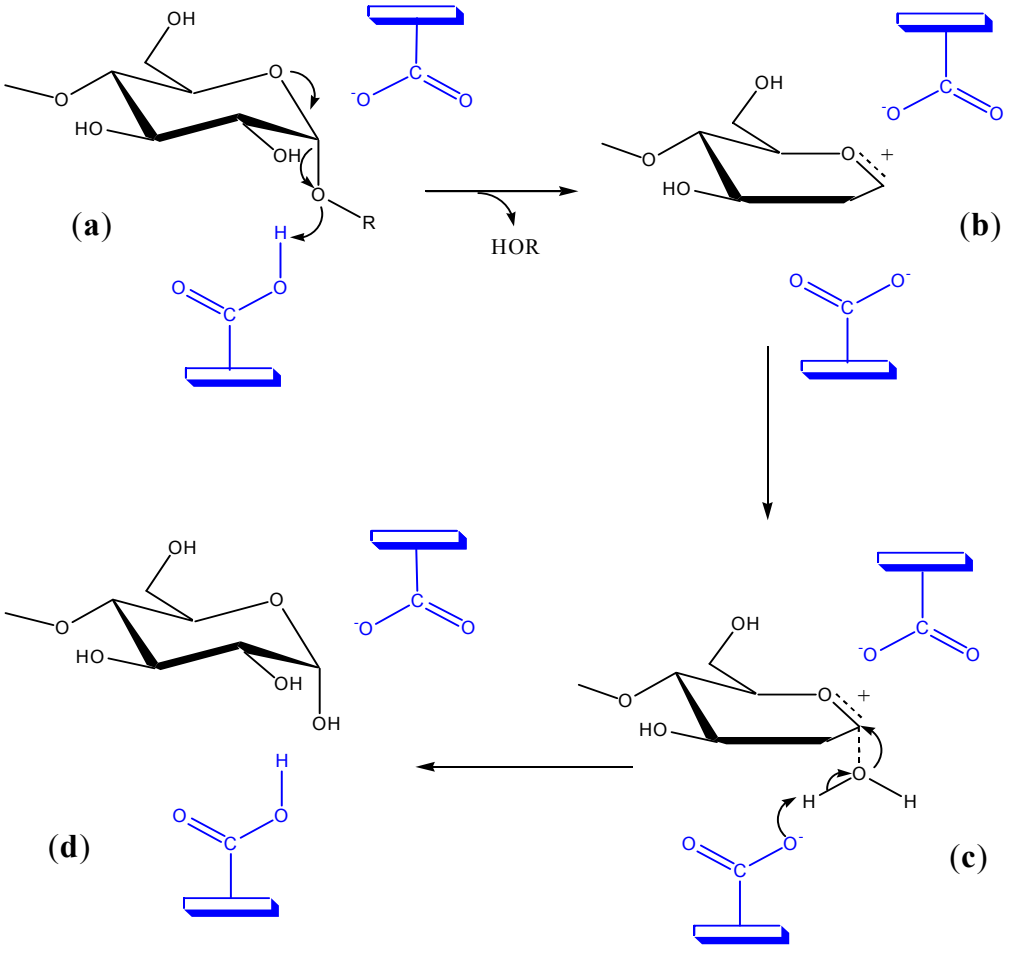

Figure-3.8: Mechanism of hydrolysis of α-glycosidic linkage by α-glucosidase enzyme. (a) Carboxylic group attacks the glycosidic oxygen, splits the glycosidic linkage and form the oxocarbenium ion intermediate, (b) oxocarbenium ion intermediate is stabilized by carboxylate group of other acid residue of the enzyme, (c) hydroxyl ion of water displaces the oxocarbenium ion through an S_N1 mechanism and (d) monosaccharide with α-anomer is formed.

4 Results and Discussion

4.1 Optimising the Conditions for NMR Experiments

In the very first NMR experiment with ribostamycin and $tRNA^{Phe}$, the NOE pattern of free ribostamycin and the mixture of ribostamycin with $tRNA^{Phe}$ did not change. The sign of the NOE effects changed from positive to negative, indicating that the small ligand bound to the macromolecule. Further on one-dimensional NMR experiments with the mixture of ribostamycin and $tRNA^{Phe}$ showed very broad signals (Figure 4.1) which indicated long residence times of the ribostamycin in the RNA-bound state. These experiments suggested that several ribostamycin molecules bound to $tRNA^{Phe}$, most likely due to unspecific electrostatic interactions (see section 2.1). In order to minimize these unspecific electrostatic interactions, we used Mg^{2+} as a competitor of aminoglycosides. In the course of titration with Mg^{2+}, we observed that with the increasing Mg^{2+} concentrations the line-width of ribostamycin signals decreased indicating a decreasing residence time of ribostamycin in the bound state (Figure 4.2). Above a concentration of 30 mM Mg^{2+}, the line-width did not narrow considerably. The same type of titration was also performed with neamine and neomycin B and with similar results. These results were also verified by performing surface plasmon resonance experiments with immobilized $tRNA^{Phe}$ (Szilaghi *et al.*, 2005) and finally a concentration of 30 mM Mg^{2+} was chosen for all further NMR experiments. Now a clear difference of the NOE pattern was observed between free aminoglycosides and the mixture of the aminoglycosides with $tRNA^{Phe}$ which indicated a conformer selection of the aminoglycosides.

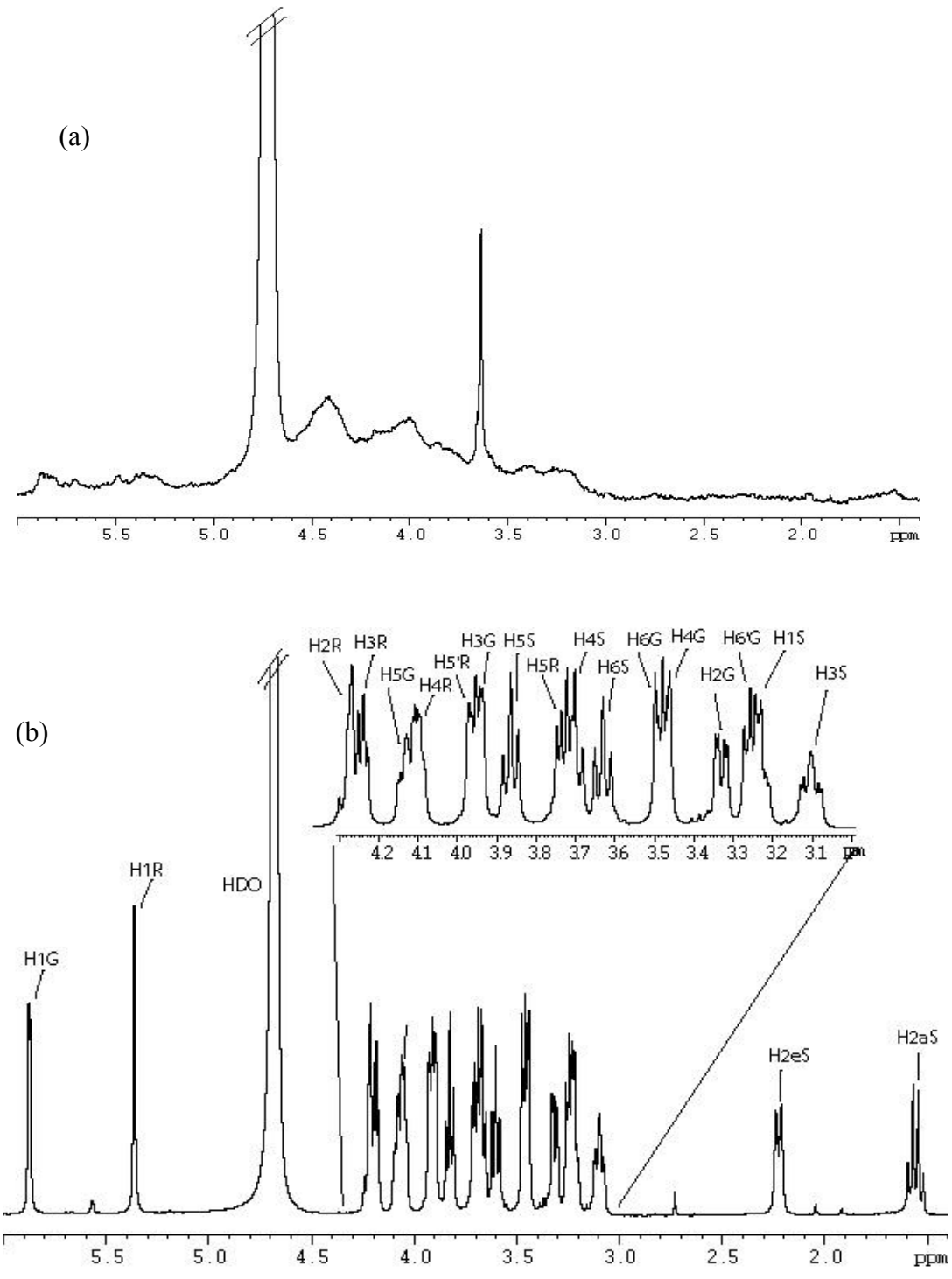

Figure-4.1: (a) ^{1}H NMR spectrum of ribostamyin and the $tRNA^{Phe}$ mixture without Mg^{+2} in comparison to the ^{1}H NMR spectrum of free ribostamycin (b).

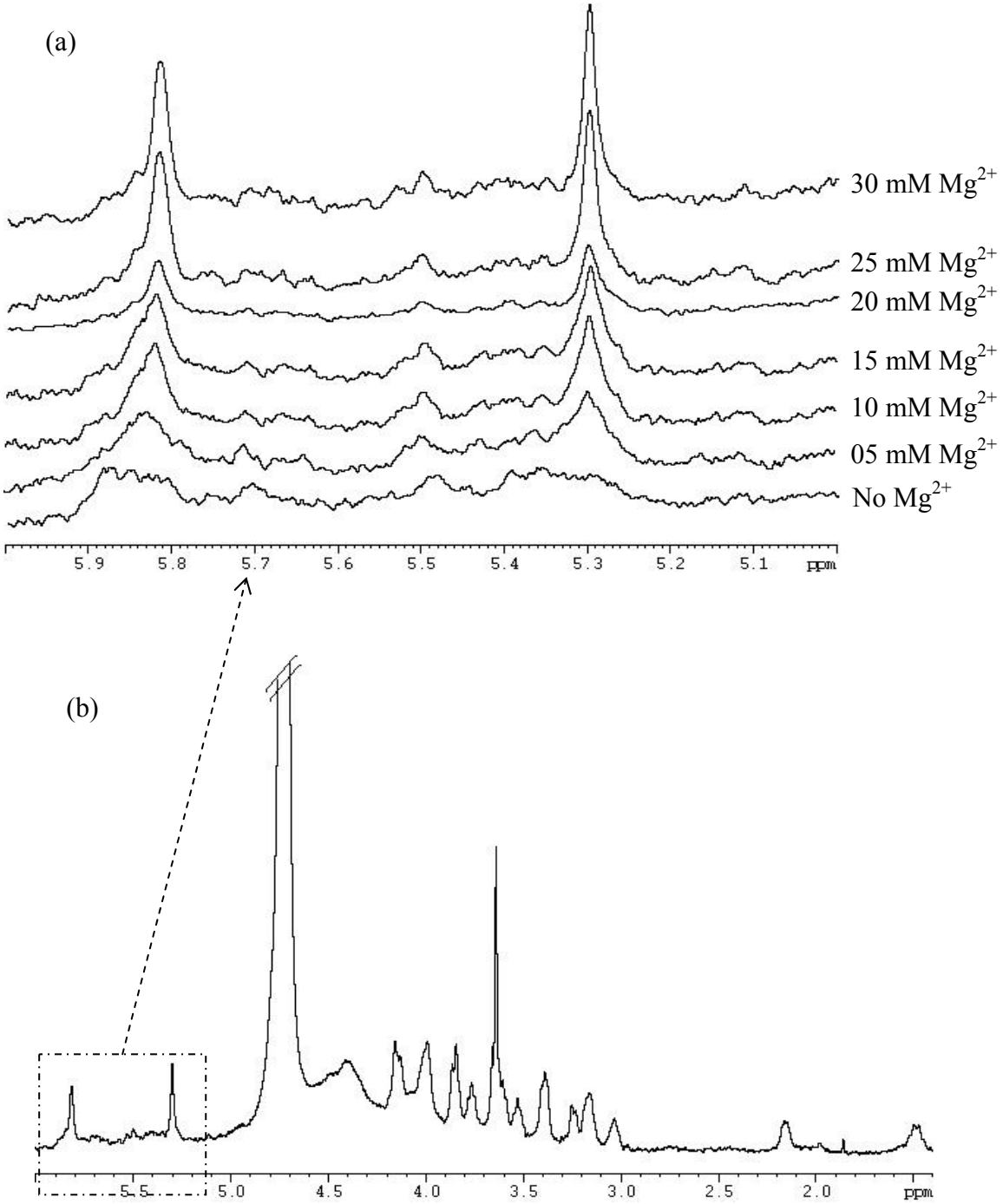

Figure-4.2: (a) Section of the anomeric resonances of the ^{1}H NMR spectra of the mixture of ribostamycin and $tRNA^{Phe}$ at different Mg^{2+} concentrations, (b) complete ^{1}H NMR spectrum of the mixture of ribostamycin and $tRNA^{Phe}$ in the presence of 30 mM Mg^{2+}.

In order to determine the effect of aminoglycosides and Mg^{2+} on the native structure of $tRNA^{Phe}$, circular dichroism (CD) experiments with $tRNA^{Phe}$ and neamine, ribostamycin and neomycin B were carried out. In these CD experiments, it was found that with increasing neomycin B concentrations, the intensity of CD signals decreased (Figure-4.3) indicating that neomycin B reduced the native helical contents of $tRNA^{Phe}$. Similar experiments were carried

out in the presence of Na^+ and Mg^{2+}. In the presence of 30 mM Mg^{2+}, no decrease of the intensity of the CD signals with increasing neomycin B concentrations could be observed (Figure 4.4). This indicated that the presence of Mg^{2+} stabilized the $tRNA^{Phe}$ structure. This stabilizing effect was not found with monovalent ions like Na^+. From these NMR, SPR and CD experiments it could be concluded that Mg^{2+} ions stabilize the native helical structure of tRNA and that divalent ions help to avoid unspecific interactions between the negatively charged RNA backbone and the positively charged aminoglycosides. Therefore, for all further NMR experiments a buffer containing 30 mM Mg^{2+} was used.

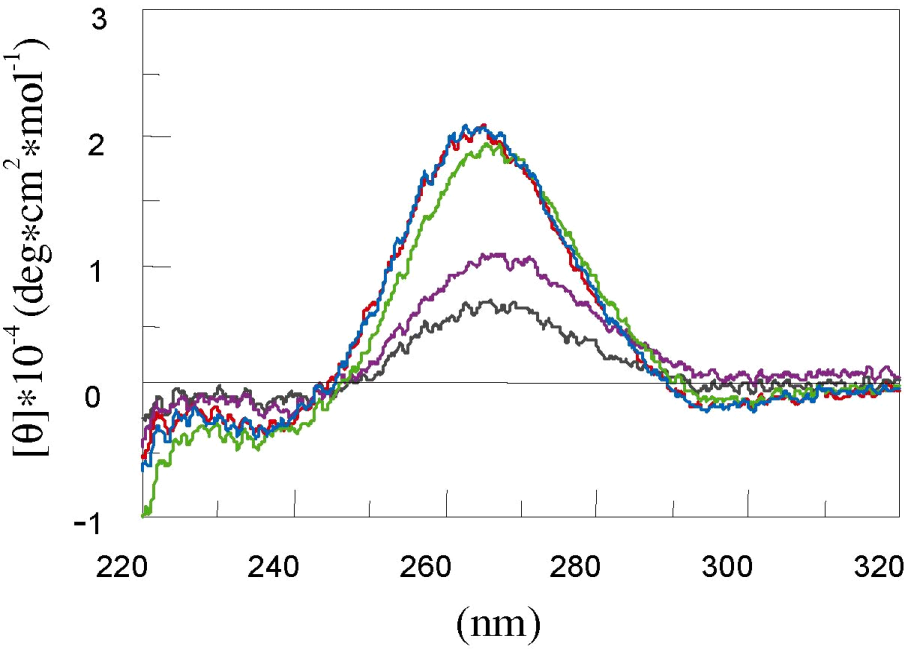

Figure-4.3: CD spectra of $tRNA^{Phe}$ with different concentrations of neomycin B. Blue, only tRNA at 20 µM concentration; red, tRNA and neomycin B (1:1); green, 10 fold excess of neomycin B; purple, 25 fold and black 50 fold excess of neomycin B relative to $tRNA^{Phe}$.

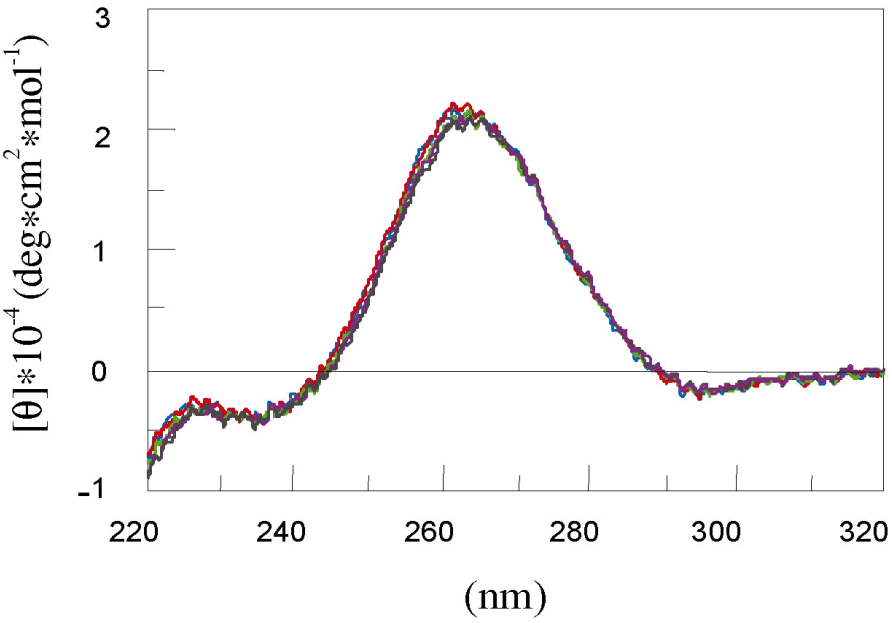

Figure-4.4: CD spectra of $tRNA^{Phe}$ with different concentrations of neomycin B and 30 mM $MgCl_2$ showing no decrease in intensity.

Kirk & Tor have investigated the inhibition of Pb^{2+} mediated cleavage of $tRNA^{Phe}$ by different aminoglycosides and found that there was a correlation between the number of amino groups on aminoglycosides and Pb^{2+} mediated cleavage of $tRNA^{Phe}$ (Kirk & Tor, 1999). According to their observations, Neo-Neo (Figure 4.5a) was 20 times more effective than neomycin B for the inhibition of Pb^{2+} mediated cleavage of $tRNA^{Phe}$. Neo-Neo has twice the number of amino groups as neomycin B. Its 20 times higher binding affinity as compared to neomycin B indicates the role of number of amino groups in this inhibition. Tor *et al.* found that tobramycin inhibited the hammerhead ribozyme more effectively than kanamycin B although both compounds contain the same number of amino groups. The only difference between the two molecules is the presence of an additional hydroxyl group in kanamycin B at C3, in proximity to amino group, which makes it less basic as compared to tobramycin (Figure 4.5) (Tor *et al.*, 1998). Wang & Tor determined the effect of pH on the binding affinity of tobramycin and kanamycin B to hammerhead ribozyme. At lower pH, difference of binding affinity of tobramycin and kanamycin B reduced significantly (Wang & Tor, 1997). Tobramycin had higher binding affinity to the hammerhead ribozyme than kanamycin B due to its more basic character but at lower pH, this effect was less pronounced. Thus the difference of binding affinity of these two aminoglycosides got narrowed at lower pH. These examples indicate that the presence of a higher number of positive charges (protonated amino groups) on aminoglycosides and the higher basicity of the amino groups enhance the binding

affinity of aminoglycosides to the RNA. This shows that electrostatic interactions between positively charged aminoglycosides and negatively charged RNA molecules play an important role in their interactions. On the other hand, spermine has the same number of amino groups as in kanamycin A (Figure 4.5) but it is 10 times less effective than kanamycin A for the inhibition of Pb^{2+}mediated cleavage of $tRNA^{Phe}$ even though it is more basic and likely to be higher charged at physiological pH as compared to kanamycin A[3]. These observations indicate that not only the specific number of protonated amino functions but also their three-dimensional representation plays an important role for the binding of aminoglycosides to RNA.

In the course of optimising the conditions, the unspecific interactions between aminoglycosides and $tRNA^{Phe}$ were successfully minimized using Mg^{2+} as a competitor for electrostatic interactions. Orval *et al*. have reported the similar results that the inhibition of the cleavage of the hammerhead ribozyme by neomycin B was reduced by increasing the concentration of Mg^{2+} ions (Overval *et al.*, 1995). Thus, the results described in previous section (section 4.1) are in agreement with the reported results.

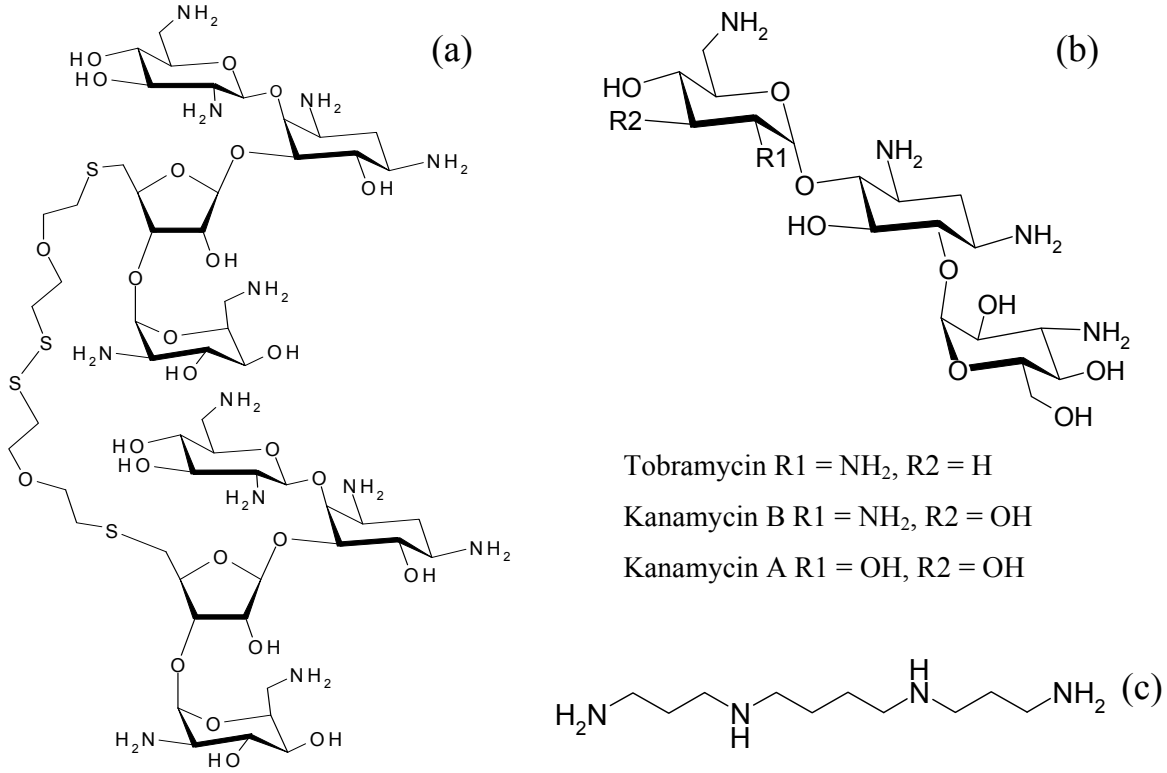

Figure-4.5: (a) Structure of the synthetic aminoglycoside dimmer neo-neo, (b) structural scheme for tobramycin, kanamycin A and kanamycin B, (c) structure of spermine.

4.2 Conformational Analysis of Aminoglycosides

For the determination of the bioactive conformations of aminoglycosides, their structural and conformational properties in the free state were also required. The structural and conformational properties of Neomycin B have already been investigated (Asensio *et al.*, 2002; Botto & Coxon, 1984). However, in order to make a comparison of the data of aminoglycosides in their tRNA-bound state and in the free state, experiments under the similar conditions had to be performed. Therefore, a conformational analysis of neamine, ribostamycin and neomycin B was done before doing the experiments with the mixtures of aminoglycosides and tRNA.

4.2.1 Conformational Analysis of Neamine

4.2.1.1 NMR Experiments

For the conformational analysis of neamine, ^{1}H, COSY, TOCSY and NOESY spectra of neamine in tris buffer were acquired. No large signal shifts were observed when ^{1}H spectra were acquired in deuterium oxide or tris buffer. Chemical shifts and NOE details of neamine obtained through these NMR experiments were then compared to those reported in literature (Botto & Coxon, 1984; Asensio *et al.*, 2002). Two rings 2,6-diamino-2,6-dideoxy-α-D-glucopyranosyl (G) and 2-deoxystrepamine (S) (Figure 1.1) were found to have two isolated proton spin systems as determined by 2D-COSY and 2D-TOCSY experiments. The information about inter ring NOE contacts was used to determine the conformational properties of neamine at the glycosidic linkage. The information about intra ring NOEs along with scalar coupling values was used to determine the ring conformations. Strong NOE contacts for H2G-H4G and H3G-H5G and very weak NOE signals for H2G-H3G and H4G-H5G in the 2,6-diamino-2,6-dideoxy-α-D-glucopyranose ring (G) were consistent with the trans-diaxial orientation of neighboring hydrogen atoms (H2G-H3G, H3G-H4G and H4G-H5G) of this ring which in turn suggested the presence of $^{4}C_{1}$ chair conformation. The configuration at C1 was determined from the scalar coupling constant between H1G and H2G which was found to be 4 Hz. This value was consistent with the gauche orientation for these two hydrogen atoms that in turn indicated the presence of the α-anomer. For the 2-deoxystrepamine ring (S) strong NOEs for H2Sa-H4S, H2Sa-H6S, H4S-H6S, H1S-H3S, H1S-H5S and H3S-H5S were observed which indicated a trans-diaxial relation of vicinal

hydrogen atoms in the ring. These observations supported the presence of a $^4C_1$ ring chair conformation in which all the hydroxyl and amino groups were in the equatorial orientation.

Four inter ring NOEs, H1G-H4S, H1G-H5S, H1G-H3S and H5G-H4S were observed for free neamine. Since the presence of all four NOEs was not consistent with any single conformation around the glycosidic linkage, observation of all these four NOEs indicated a large flexibility of this glycosidic linkage. H1G and H4S are positioned directly at the glycosidic linkage and therefore showed very strong NOE contact with each other. H1G also showed NOE contacts with H3S as well as with H5S, on both sides of H4S. These two NOE contacts supported the existence of two different conformational families at the glycosidic linkage because these two NOE contacts were not possible in a single conformation (Figure 4.6).

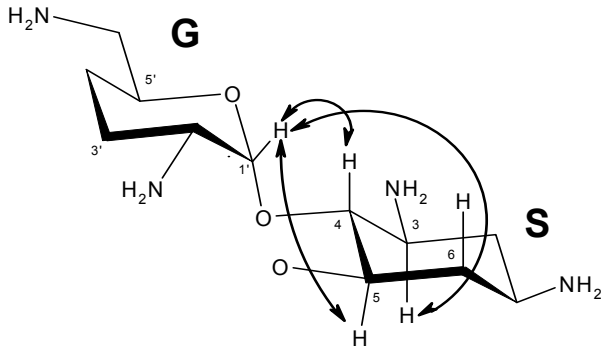

Figure-4.6: Inter ring NOE contacts of neamine. Hydroxyl groups have been removed for simplicity. NOE contacts of H1G with H3S and H5S indicates large conformational flexibility about the glycosidic linkage as these two NOE are not satisfied by a single conformation about the glycosidic linkage.

4.2.1.2 Grid Search Analysis

In order to gain information about the low energy conformations at the glycosidic linkage of neamine, a grid search analysis was performed. From this grid search, a potential energy plot of neamine was created (see the methodology chapter). Four conformational regions with a low energy were identified from this potential energy map (Figure 4.7). The global minimum energy conformation for neamine was found to be at ϕ/ψ = -60° /-60°. Further three local minimum energy conformations at ϕ/ψ = -40°/60°, 40°/40° and ϕ/ψ = -40/180 were found to be connected to the global minimum energy region through a shallow valley. Similar energy

regions in the potential energy plot of these two rings have also been described by (Asensio *et al.*, 2002).

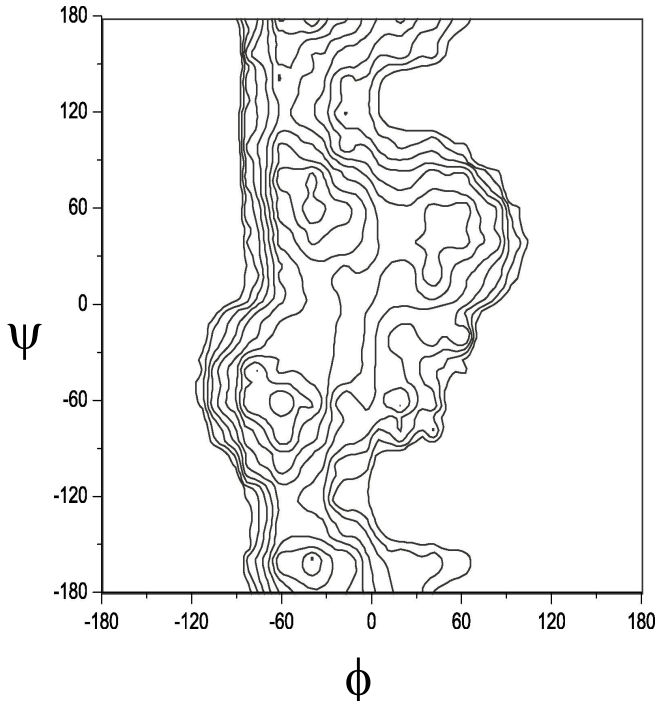

Figure-4.7: Potential energy plot of neamine obtained as the function of the glycosidic torsion angles ϕ and ψ.

4.2.2 Conformational Analysis of Ribostamycin

Ribostamycin has a ribose ring (R) connected to the neamine moiety (Figure 1.1).

4.2.2.1 NMR Experiments

Ribostamycin was found to comprise of three isolated spin systems of scalar coupling as determined by 2D-COSY and TOCSY experiments. These three spin systems correspond to the three rings of ribostamycin glycosidically linked to each other (Figure 1.1). The NMR data for the two rings G and S (neamine moiety) of ribostamycin was found to be consistent with the data for neamine (see section 4.2.1). Information about the conformational properties of the glycosidic linkage between ring R and S was obtained from six inter ring NOEs (H1R-H5S, H1R-H4S, H1R-H6S, H2R-H6S, H1G-H2R and H1G-H3R). The appearance of these inter ring NOEs (Figure 4.8) were not consistent with a single conformation at this glycosidic linkage. H1R and H5S are directly connected through glycosidic linkage and therefore showed a strong NOE effect. H1R also showed NOE contacts to H4S and H6S.

These two NOEs point to different conformational families. These observations indicated the presence of at least two different conformational families being populated at the R/S glycosidic linkage on account of the flexibility of this molecule.

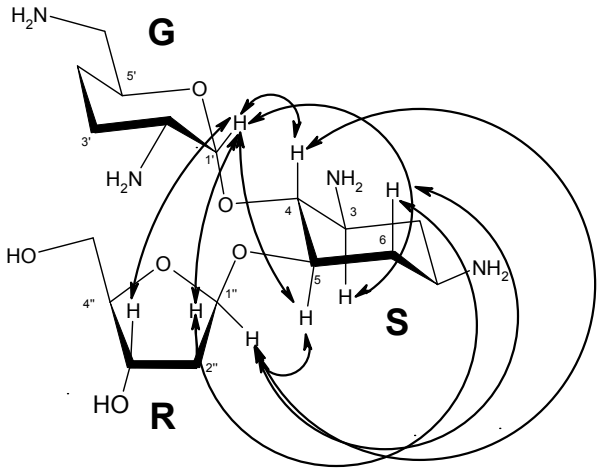

Figure-4.8: Inter ring NOE contacts of ribostamycin.

4.2.2.2 Grid Search Analysis

In order to determine the low energy regions of ribostamycin, potential energy plots for both glycosidic linkages were produced by performing a grid search analysis. For the G/S glycosidic linkage of ribostamycin, minimum energy regions were found in the same regions of conformational space as it has been described in the case of neamine (see section 4.2.2). In the case of the R/S glycosidic linkage also four minimum energy regions were observed at ϕ/ψ = -30°/40°, 180°/50°, 60°/30° and 60°/180°. The global minimum energy was located at ϕ/ψ = -30°/40° (Figure 4.9 b). These observations about the conformational properties of ribostamycin were also in agreement with the results described by (Asensio *et al.*, 2002)

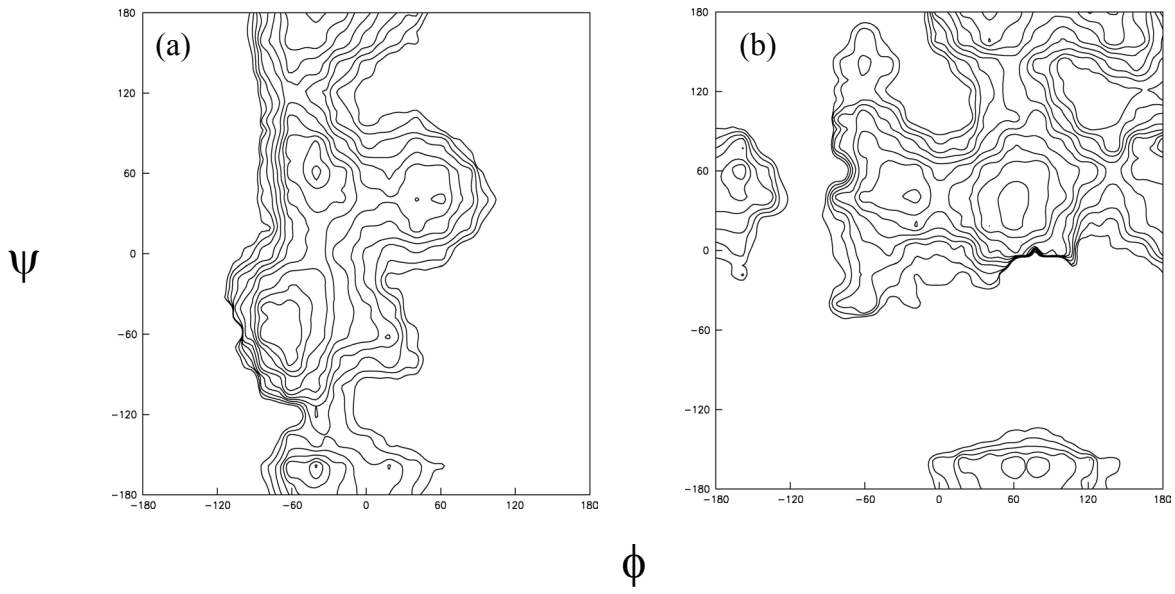

Figure-4.9: Potential energy plots of ribostamycin, (a) for the G/S glycosidic linkage and (b) for the R/S glycosidic linkage.

4.2.3 Conformational Analysis of Neomycin B

Neomycin B (Figure 1.1) comprises of four rings with a 2,6-diamino-2,6-dideoxyidopyranose (I) linked to ribostamycin.

4.2.3.1 NMR Experiments

The NMR data for the three rings G, S and R (ribostamycin moiety) of neomycin B was found to be consistent with the data for neamine and ribostamycin (see sections 4.2.1 and 4.2.2). The determination of the ring conformation of the 2,6-diamino-2,6-dideoxyidopyranose (I) ring was more complicated. At first sight, the data for this ring (I) looked very similar to that of ring G but a closer inspection of intra ring NOE contacts and hydrogen-hydrogen coupling constant values indicated a striking difference of the ring conformations. The coupling constant for H1I-H2I was around 2 Hz, which was consistent with the gauche orientation for these two hydrogen atoms. Very strong NOE signals were observed for H1I-H5I, which indicated that H1I and H5I had a *syn*-diaxial orientation. This suggested that the bulky aglycone at C1 and the aminomethyl group at C5 are in an equatorial orientation (β–anomer). The small coupling constant between axially oriented H1I and H2I (2 Hz) was consistent with the equatorial orientation of H2I. Almost equally strong NOEs

were observed for H1I-H2I, H2I-H3I, H3I-H4I and H4I-H5I which indicated the presence of gauche orientations for all these vicinal hydrogen atom pairs. Furthermore, comparison of proton chemical shifts for ring G and I supported an equatorial orientation of the ring hydrogen atoms of I ring. H1I appeared upfield to H1G which was consistent with an axial orientation of H1I (β-anomer) and an equatorial orientation of H1G (α-anomer). On the other hand, chemical shifts of H2I, H3I and H4I were at lower field relative to those of respective hydrogen atoms of ring G (Figure 4.10) which suggested an equatorial orientation for H2I, H3I and H4I and an axial orientation for respective hydrogen atoms in ring G. Also, the hydrogen atoms of ring I were found to have smaller coupling constants as compared to those of the ring G which suggested the gauche type arrangement for vicinal hydrogen atoms that in turn supports the equatorial orientation for H2I, H3I and H4I.

Several inter ring NOEs were observed in the case of neomycin B. Inter ring NOE data for the first three rings, G, S and R (ribostamycin unit) of neomycin B was found to be identical to the ones observed for ribostamycin. Information about the conformational preferences between rings R and I of neomycin B was obtained from five inter ring NOE effects (H1I-H3R, H1I-H2R, H1I-H4R, H2I-H2R and H2I-H3R). These five NOE effects cannot be satisfied by any single conformation about the glycosidic linkage. H1I and H3R are directly connected through glycosidic linkage and therefore showed a strong NOE contact. H2R and H4R are present on the two sides of H3R therefore the strong NOE effects H1I-H2R and H1I-H4R pointing to different conformational families at this glycosidic linkage (Figure 4.11).

Thus, the observed NOE data showed a weighted average of the different conformations at glycosidic linkages indicating the conformational flexibility in neomycin B. Four inter ring NOE effects (HIG-H3S, H1G-H3R, H1R-H4S and H1I-H4R) were observed in addition to those reported by (Asensio *et al.*, 2002) based on their selective 1D NOE experiments with neomycin B. The observation of even more NOE contacts than the reported ones supports the reported results about the existence of conformational flexibility in neomycin B.

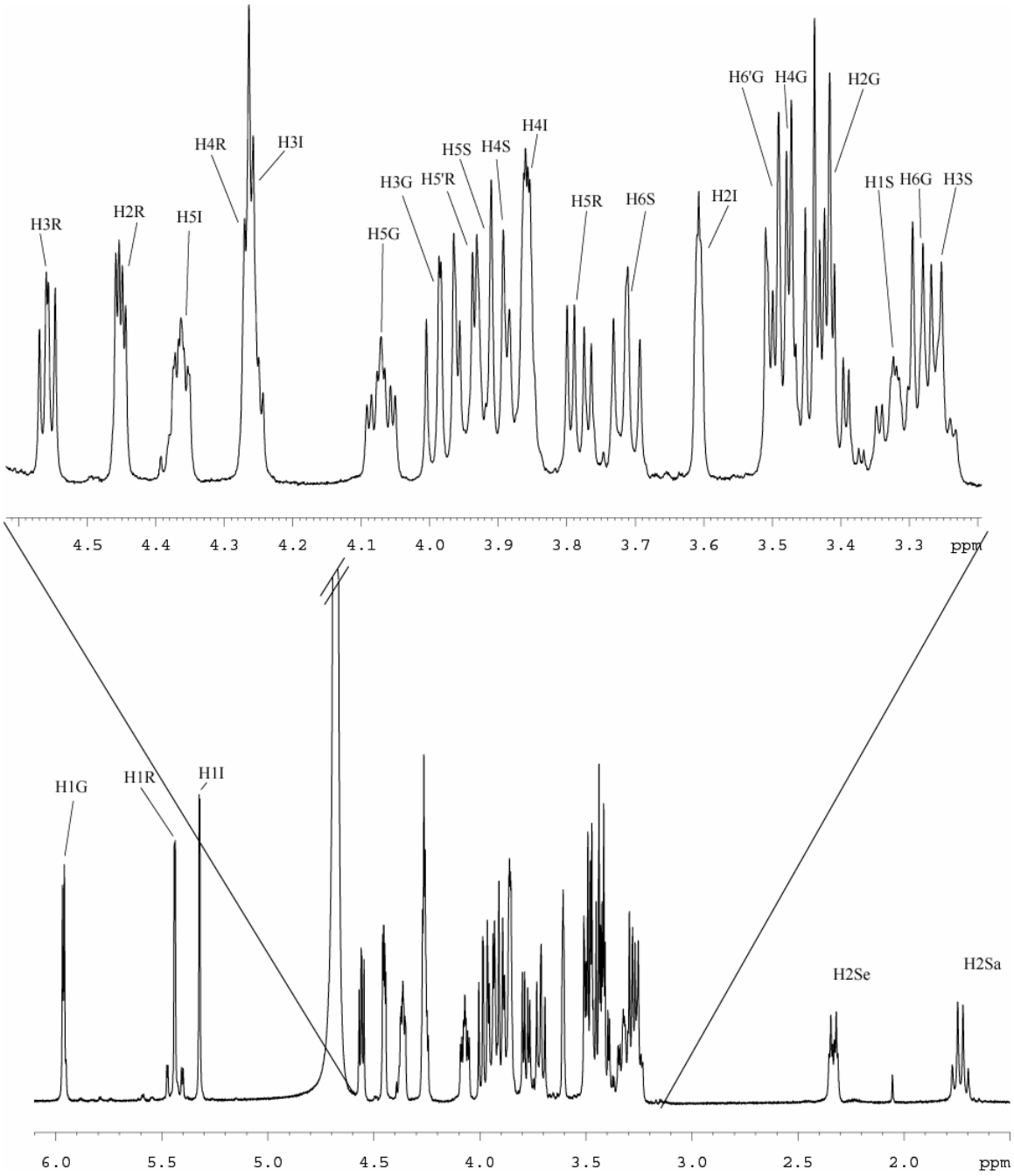

Figure-4.10: ^{1}H NMR spectrum of neomycin B.

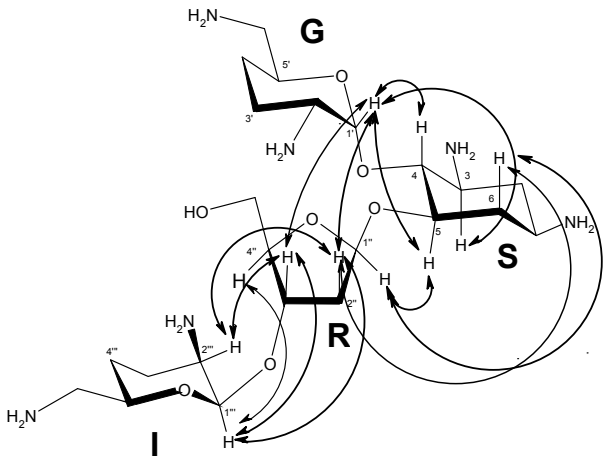

Figure-4.11: Inter ring NOE contacts in neomycin B.

4.2.3.2 Grid Search Analysis

The potential energy map for the G/S glycosidic linkage of neomycin B was found to be very similar to those of neamine and ribostamycin (sections 4.2.1.2 & 4.2.2.2). Here also four energy minima were identified with the global minimum energy region at ϕ/ψ = -60^o /-60^o. The other three minimum energy regions were found to be close to ϕ/ψ = -40^o/60^o, 40^o/40^o and ϕ/ψ = -40/180 (Figure 4.12a). The potential energy surface for the R/S linkage of neomycin B was also found to resemble to that of ribostamycin (Figure 4.12b). Three energy minimum regions at ϕ/ψ = -30^o/40^o, 60^o/40^o and 60^o/70^o were detected in a larger area connected to each other through a shallow valley. Two other energy minimum regions are located at ϕ/ψ = 60^o/180^o and 180^o/30^o. For the I/R glycosidic linkage the global energy minimum was found to lie at ϕ/ψ = -60^o/-60^o with two other minimum energy regions at ϕ/ψ = -50^o/180^o and ϕ/ψ = 180/-60^o. Thus, the described potential energy surfaces suggested the large internal mobility of neomycin B as indicated by the NOE data.

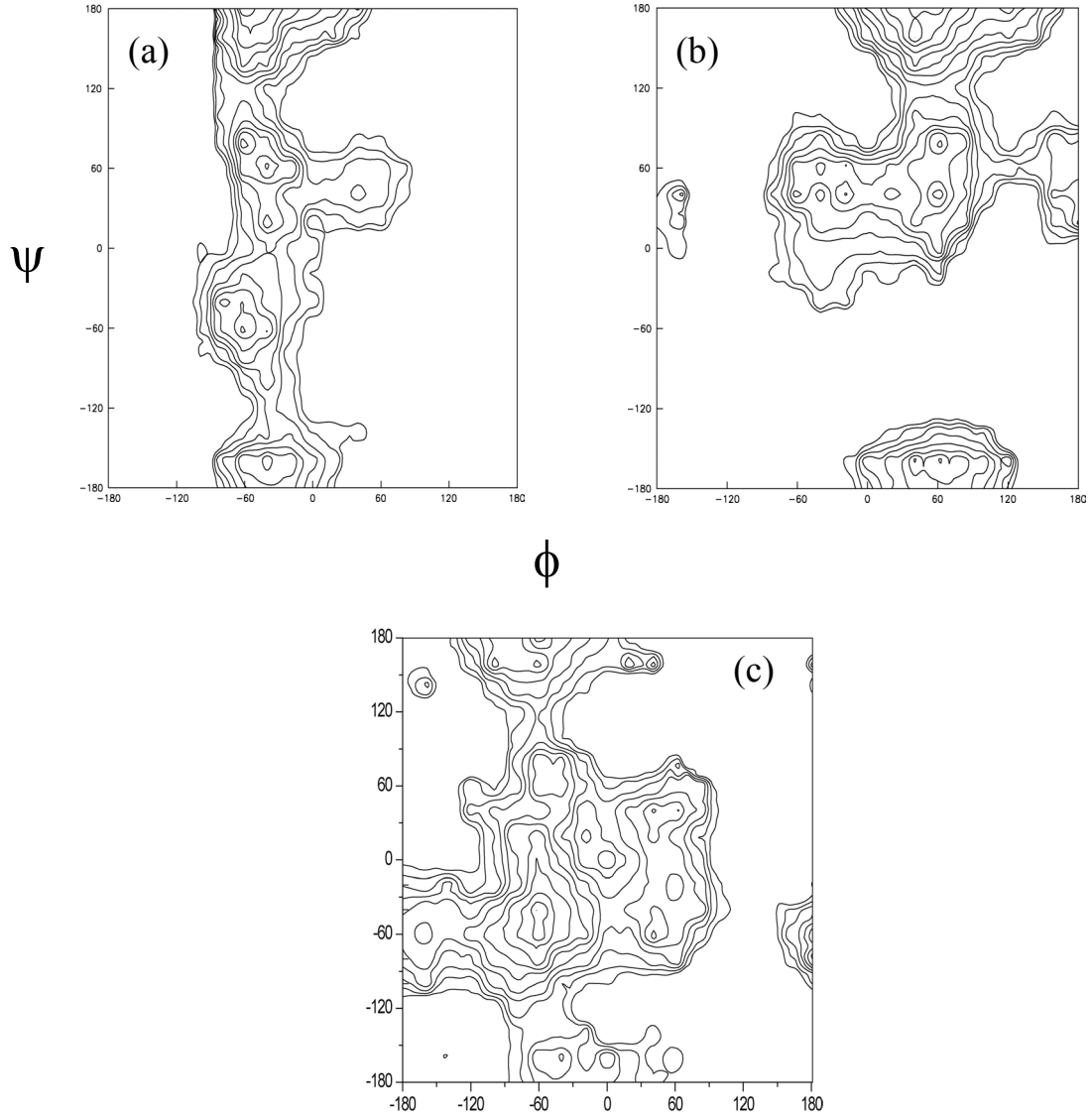

Figure-4.12: Potential energy plot for neomycin B. (a) G/S glycosidic linkage, (b) R/S glycosidic linkage and (c) I/R glycosidic linkage.

4.2.4 Ribose Ring Puckering in Ribostamycin and Neomycin B

Several NOE effects for hydrogen atoms of ribose ring (H1R-H2R, H1R-H3R, H1R-H4R, H2R-H5R, H3R-H4R, and H3R-H5R) were observed which indicated the conformational flexibility of ribose ring. Conformation of ribose ring in ribostamycin and neomycin B was determined by molecular dynamics simulations by calculating the sugar pucker phase angle (see section 6.4).

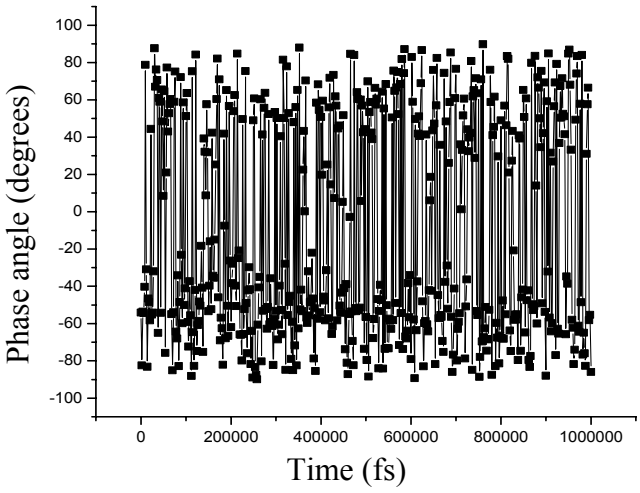

Figure-4.13: Distribution of phase angle of the ribose ring in ribostamycin.

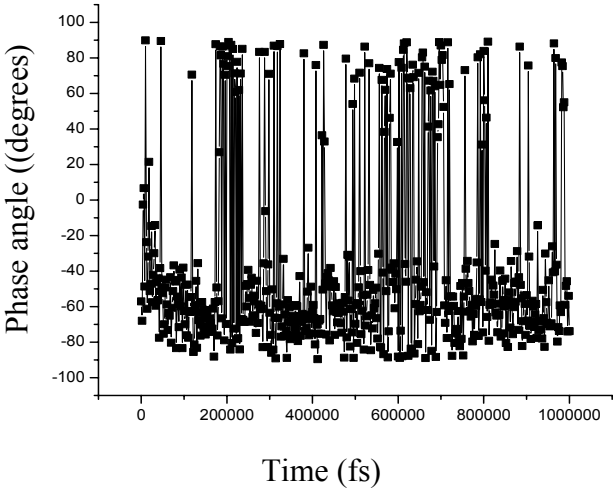

Figure: 4.14: Distribution of phase angle of the ribose ring in neomycin B.

MD simulation data showed that the phase angle of ribose ring in ribostamycin varied from -80^{o} to 80^{o} over the period of MD simulation. That corresponds to variation of a ring puckering from a C1-endo to C4-exo type showing large degree of flexibility. (Figure 4.13). In case of neomycin B the major population of the ribose ring conformation was scattered in C1-endo region and minor population in C4-exo region of ring puckering (Figure 4.14). Based on these calculations of MD simulation, the ribose ring was found more flexible in ribostamycin as compared to that in neomycin B. This lower flexibility of ribose ring in

neomycin B could be attributed to the presence of 2,6-diamino-2,6-dideoxyidopyranose (I) ring in neomycin B.

These results suggested the large degree of conformational flexibility in three aminoglycosides. A detailed conformational analysis of these aminoglycosides was already described in literature (Asensio *et al.*, 2002; Botto & Coxon, 1984), and experimental and theoretical data described in previous sections was very similar to the published data. Therefore, no further attempt was made to correlate the NOE data with MD simulations. The presented data form the basis for the determination of the bioactive conformations of the aminoglycosides. Comparison of this data to that obtained through the experiments with the mixtures of aminoglycosides with tRNA in following sections, helped to obtain information of conformation selection of aminoglycosides by tRNA. Subsequent constraint MD simulations led to define the bioactive conformations of these aminoglycosides.

4.3 Determination of the $tRNA^{Phe}$-bound Conformation of Neamine

4.3.1 TrNOE Experiments

The bioactive conformation of neamine bound to $tRNA^{Phe}$ was determined with trNOE experiments. Negative NOE signals were observed in the NOESY spectra of neamine $tRNA^{Phe}$ mixture indicating the binding of neamine to $tRNA^{Phe}$. As discussed previously, due to the flexibility of the glycosidic linkage, free neamine displays a complex conformational equilibrium and several NOEs appeared. In the mixture with $tRNA^{Phe}$, two large (H1G-H4S and H1G-H5S) and three small (H1G-H6S, H1G-3S and H5G-H4S) inter ring trNOE contacts of neamine were observed. TrROE experiments suggested these three very small NOE effects to be spin diffusion. In the trNOE experiments no additional NOE effect was observed as compared to the effects of free neamine (Figure 4.15, Table 4.1). Disappearance of H1G-H3S NOE in the trNOE experiments indicated that a conformer selection occurred during the binding event at the glycosidic linkage. In order to determine the $tRNA^{Phe}$-bound conformation of neamine, distances between hydrogen atoms were extracted from trNOE build up curves (Figure 4.16 and Table 4.2).

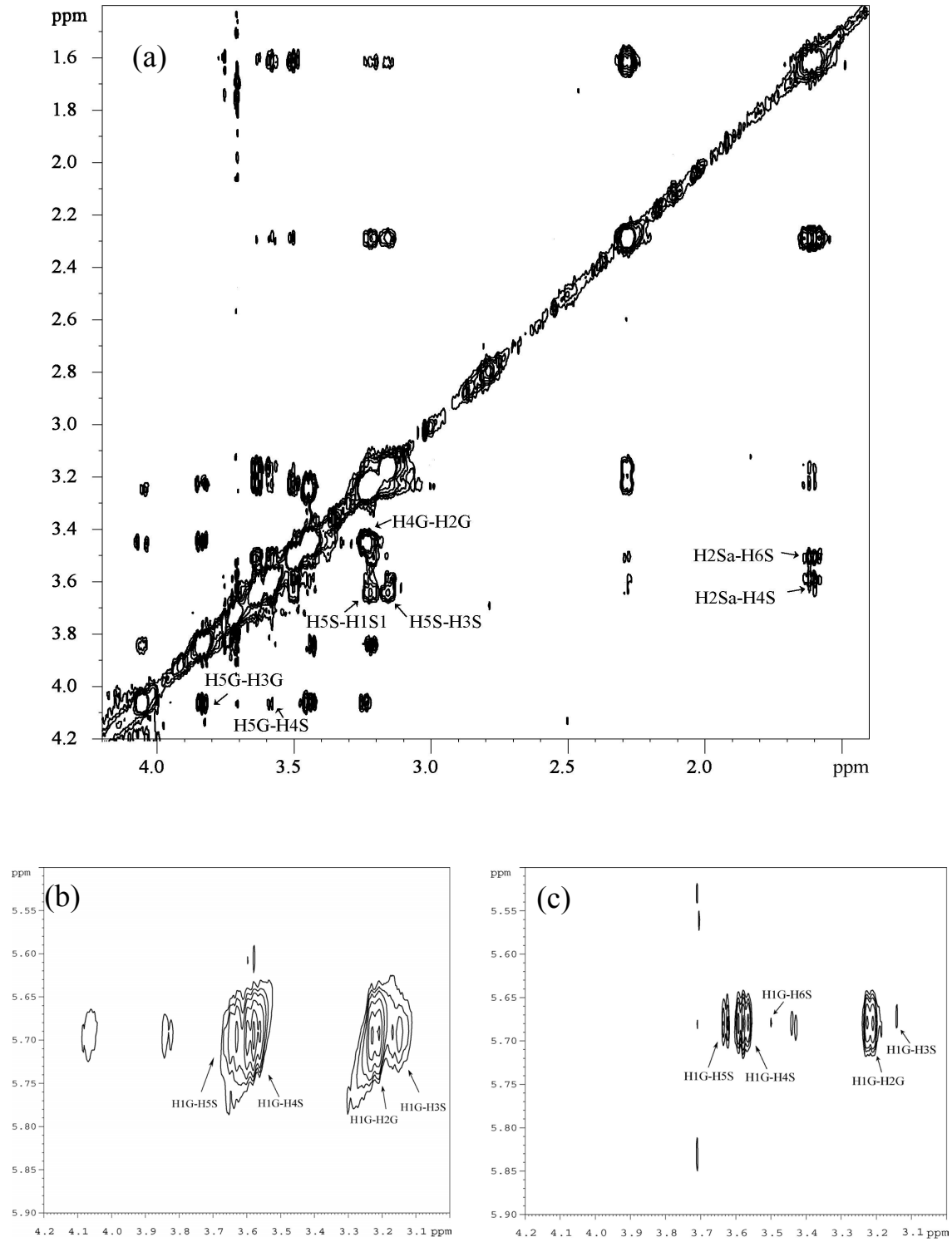

Figure-4.15: (a) Expanded region of a trNOE spectrum of the neamine-tRNA^{Phe} complex. Only conformational relevant trNOEs are labelled. (b) Expanded region of a NOESY spectrum of neamine in tris buffer showing NOE contacts of the anomeric hydrogen atom in the 2,6-diamino-2,6-dideoxy-□-D-glucopyranose ring (G). (c) Same expanded region from the trNOE spectrum of the neamine-tRNA^{Phe} complex.

Table-4.1: Inter ring NOE effects and trNOE effects of neamine.

Inter ring NOE effects of neamine	Inter ring trNOE effects of the neamine-tRNA^{Phe} complex
H1G-H4S	H1G-H4S
H1G-H5S	H1G-H5S
H1G-H3S	
H5G-H4S	

Table-4.2: Inter hydrogen atom distances in neamine extracted from the trNOE build up curves.

TrNOE effects of neamine	Distances
H1G-H4S	2.4 Å
H1G-H5S	3.1 Å
H3G-H5G	2.3 Å
H3S-H5S	2.3 Å

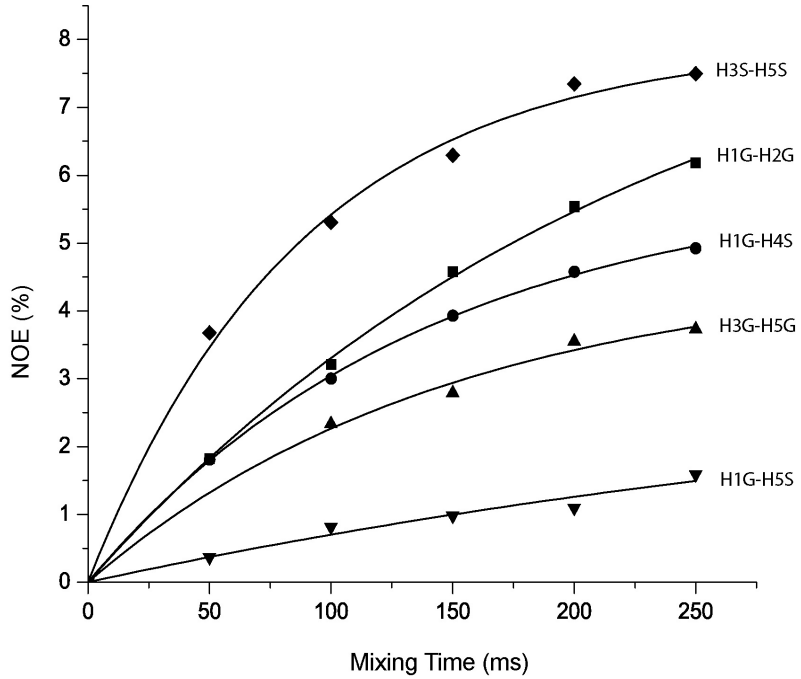

Figure-4.16: Build up curves for conformational relevant trNOE effects of the neamine-tRNA^{Phe} complex.

4.3.2 MD Simulations to Determine the Bioactive Conformation of Neamine

In order to define the bioactive conformation of neamine, four experimentally derived inter hydrogen atom distances (H1G-H4S, H1G-H5S, H3G-H5G and H3S-H5S) were used as constraints in the molecular dynamics simulations of neamine. Two MD simulations were performed with different starting conformations (see the methodology chapter) and identical results were obtained in each case. A plot for the distribution of conformers obtained through these constraint MD simulations has been overlaid to the potential energy plot of neamine previously produced as function of the ϕ and ψ glycosidic angles (Figure 4.17). In these constraint MD simulations only a region around $\phi/\varphi = -45^{o}/-40^{o}$ was found to be populated. This populated area is very close to the global minimum energy conformation of neamine. From this it could be concluded that a low potential energy conformation of neamine with glycosidic torsion angles of approximately $\phi/\varphi = -45^{o}/-40^{o}$ was bound by $tRNA^{Phe}$.

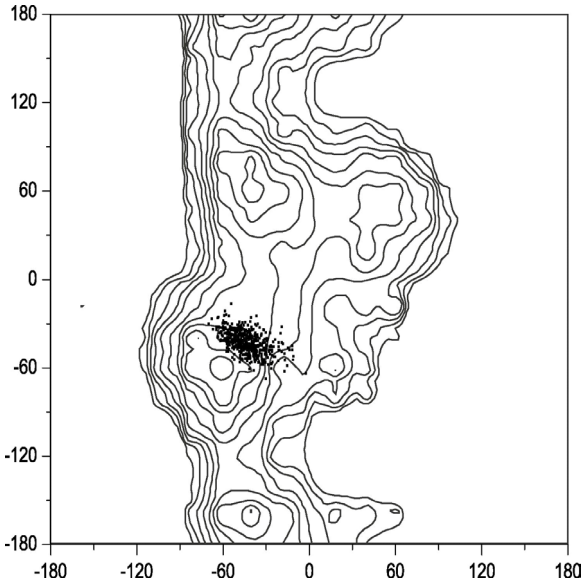

Figure-4.17: Distribution of conformers form the constraint MD simulations superimposed on the potential energy plot of neamine.

4.4 Determination of the tRNA^{Phe}-bound Conformation of Ribostamycin

4.4.1 TrNOE Experiments

The bioactive conformation of ribostamycin bound to tRNAPhe was determined by trNOE methodology. Negative trNOE signals were observed in the NOESY spectra of a mixture of ribostamycin tRNAPhe indicating the binding of ribostamycin to tRNAPhe. Close inspection of the trNOE spectra of the complex showed that out of twelve inter ring NOE signals of ribostamycin, only five appeared in the trNOE experiments (Table 4.3). No additional trNOE effect was observed as compared to the NOE effects of free ribostamycin (see section 4.2.2) (Figures 4.18 and 4.19). Similar inter ring trNOE pattern was observed across the G/S glycosidic linkage as was observed in case of neamine. Therefore, the tRNAPhe-bound conformation around this glycosidic linkage of ribostamycin was expected to be similar to that found in neamine. Four trNOE effects (H1R-H5S, H1R-H6S, H1R-H4S and H2R-H6S) were observed across the R/S glycosidic linkage. The trROE experiment suggested that the small trNOE effect H1R-H4S, was a contribution of spin diffusion. Disappearance of H1R-H4S, H1G-H2R, H1G-H3R, H1G-H5R and H2G-H5R NOE signals in the trNOE experiments suggested a conformer selection also at R/S glycosidic linkage. In order to determine the tRNAPhe-bound conformation of ribostamycin, inter hydrogen atom distances were calculated from the trNOE build up curves (Table 4.4).

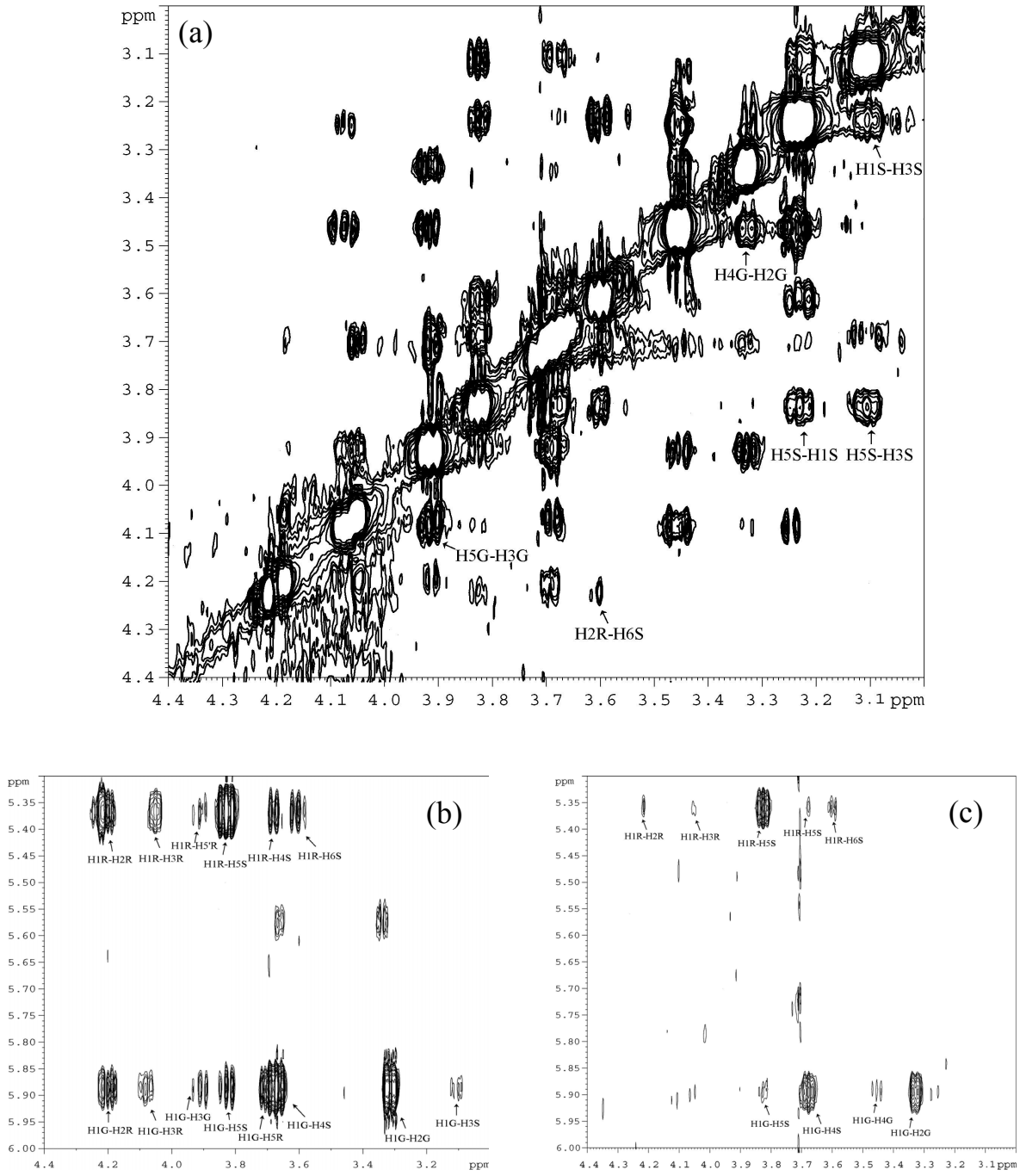

Figure-4.18: (a) Expanded region of a trNOE spectrum of the ribostamycin-tRNA^{Phe} complex. Only the conformational relevant trNOE signals are labelled. (b) Expanded region of a NOESY spectrum of ribostamycin showing NOE contacts of anomeric hydrogen atoms. (c) Same expanded region of the trNOE spectrum of ribostamycin-tRNA^{Phe} complex.

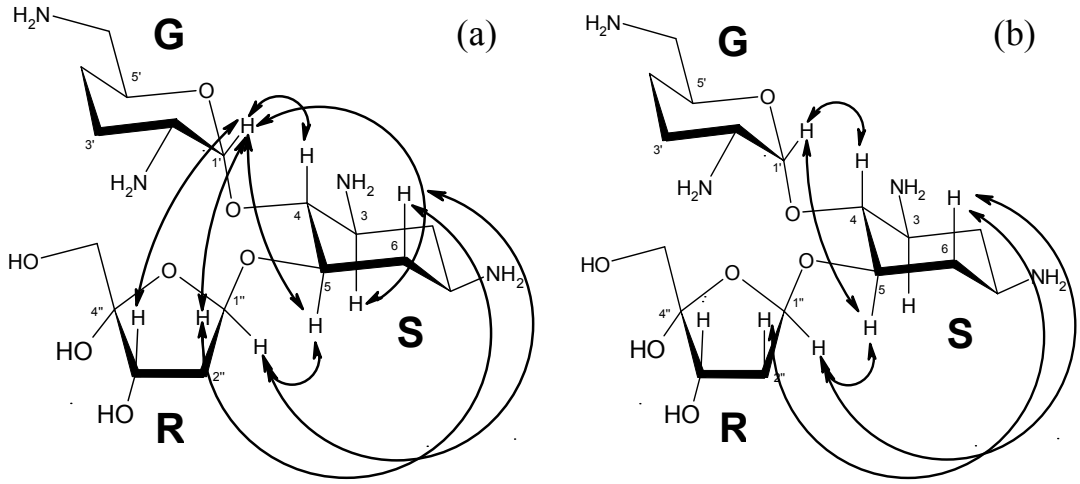

Figure-4.19: (a) Inter ring NOE contacts in ribostamycin. (b) Inter ring trNOE contacts in the $tRNA^{Phe}$-ribostamycin complex.

Table-4.3: Inter ring NOE effects and trNOE effects of ribostamycin.

Inter ring NOE effects of ribostamycin	Inter ring trNOE effects of the ribostamycin-$tRNA^{Phe}$ complex
H1G-H4S	H1G-H4S
H1G-H5S	H1G-H5S
H1G-H3S	H1R-H5S
H1G-H2R	H1R-H6S
H1G-H3R	H2R-H6S
H1G-H5R	
H1R-H5S	
H1R-H4S	
H1R-H6S	
H2R-H6S	
H2G-H5R	
H5G-H4S	

Table-4.4: Inter hydrogen atom distances in ribostamycin extracted from trNOE build up curves.

TrNOE effects in ribostamycin	Distances
H1G-H4S	2.3 Å
H1G-H5S	3.5 Å
H2G-H4G	2.6 Å
H1R-H5S	2.5 Å
H1R-H6S	3.4 Å
H2R-H6S	3.3 Å
H3S-H5S	2.3 Å

4.4.2 Constraint MD Simulations to Determine the Bioactive Conformation of Ribostamycin

Seven inter hydrogen atom distances were used (Table 4.4) as constraints in MD simulations for 1 ns. Two MD simulations were performed with different starting conformations and identical results were obtained in each case. To visualize the results of these MD simulations, plots for the distribution of conformers for both glycosidic linkages obtained through the MD simulations are superimposed on the potential energy plots for the respective glycosidic linkages in Figure 4.20. For G/S glycosidic linkage, conformers were populated in the region around $\phi/\psi = -45^{o}/-40^{o}$. This is consistent with the result obtained for neamine and suggested the same conformational space at this glycosidic linkage of these two aminoglycosides bound by $tRNA^{Phe}$. For R/S glycosidic linkage conformers were populated in a region between $\phi/\psi = -30^{o}/60^{o}$ and $\phi/\psi = 20^{o}/30^{o}$ (Figure 4.20 b) showing a little higher mobility in the ϕ than in the ψ angle.

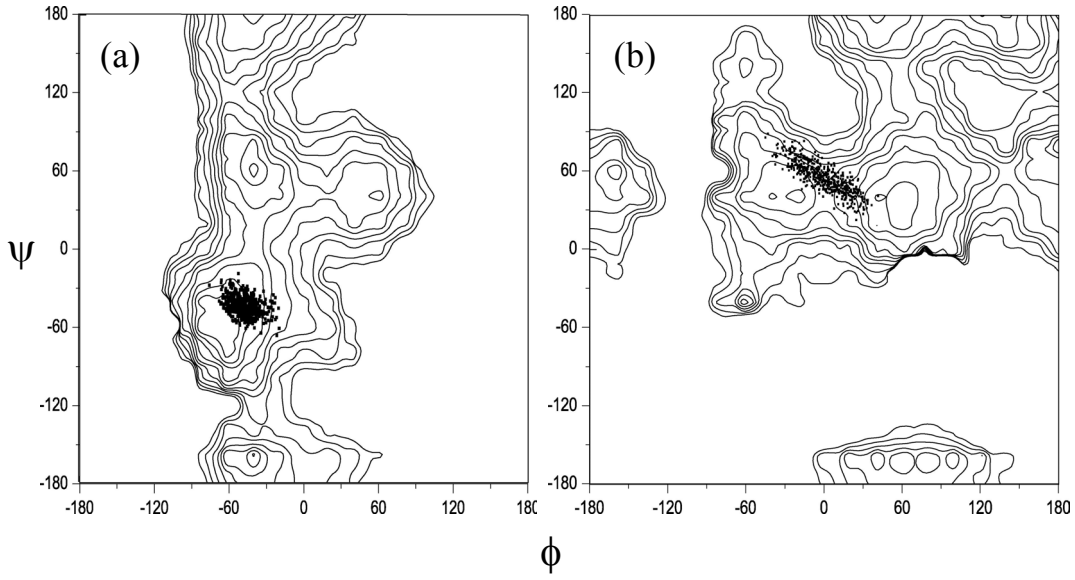

Figure-4.20: Distributions of conformers obtained through constraint MD simulations, are superimposed on the potential energy plots for the respective glycosidic linkages of ribostamycin. (a) G/S glycosidic linkage and (b) R/S glycosidic linkage.

4.4.3 Ribose Ring Puckering in tRNA^{Phe}-Bound Ribostamycin

The ribose ring pucker in bound ribostamycin was determined by calculating the phase angle of the ribose ring over the period of the constraint MD simulation (see the methodology section). Phase angle was found mainly populated in the region from 20^o to 70^o, which correspond to C3-endo and C4-exo type of ring puckering, respectively. A small population was also scattered in the region extended up to -80^o, which corresponds to C1-endo and C2-exo ring conformations (Figure-4.21). An unconstrained MD simulation of ribostamycin has shown equally populated C1-endo and C4-exo regions (Figure 4.13, section 4.5) with large degree of flexibility in the ribose ring (phase angle varied from -80^o to 80^o). Thus, besides a conformer selection the distance constraint MD simulations also showed less flexibility of the ribose ring as compared to the unconstrained MD simulation.

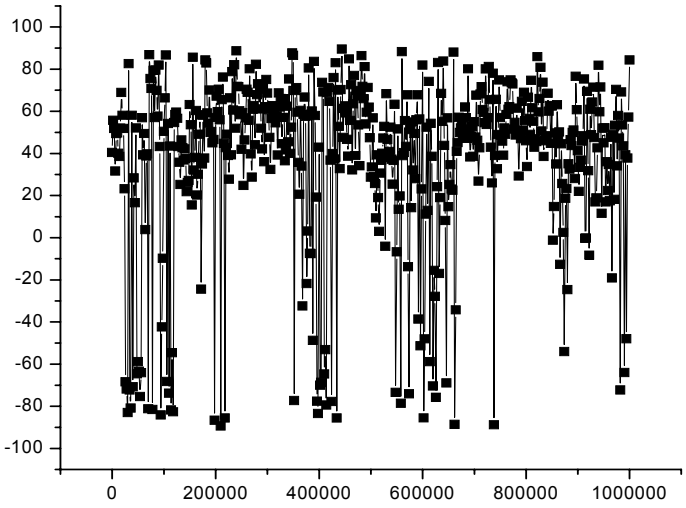

Figure-4.21: Phase angle distribution of ribose ring of ribostamycin calculated from the 1 ns constraint MD simulations.

4.5 Determination of the tRNA^{Phe}-bound Conformation of Neomycin B

4.5.1 TrNOE Experiments

In order to determine the tRNA^{Phe}-bound conformation of neomycin B, trNOE techniques were used as was done with other two aminoglycosides. Again, a significant difference in the NOE and trNOE pattern of neomycin B was observed. The trNOE pattern across the G/S glycosidic linkage found to be very similar as was observed in case of neamine and ribostamycin. This indicated that in all three aminoglycosides very similar conformer selection occurred at this glycosidic linkage during the binding event. Three trNOE signals, H1R-H5S, H1R-H4S and H2R-H6S were observed across the R/S glycosidic linkage. Whereas H1R-H6S NOE found in the NOESY spectra of free neomycin B was not observed in the trNOE experiments of the neomycin B tRNA mixture (Figures 4.22 and 4.23). This observation was contrary to that in ribostamycin where a H1R-H6S trNOE effect was observed and the NOE effect H1R-H4S was absent. This observation indicated that ribostamycin and neomycin B bound to tRNA in different conformations at the R/S glycosidic linkage. Four inter ring NOE effects between rings G and R, H1G-H2R, H1G-H3R, H1G-H5R and H2G-H5R found in free neomycin B also did not appear as trNOE effects. The trNOE effect, H2R-H6S was observed in ribostamycin as well as in neomycin B. This effect is consistent with the negative ϕ angle of the R/S linkage.

Three inter ring trNOE effects H1I-H3R, H1I-H2R and H1I-H4R were observed across the I/R glycosidic linkage. However, the trROE experiments suggested that the H1I-H4R effect was the contribution of spin diffusion. Another NOE effect, H2I-H2R that was found in the NOESY spectra of neomycin B, was also not observed as trNOE effect (Figure 4.23). Moreover, no further trNOE was observed as compared to the NOE effects of free neomycin B indicating the conformer selection of neomycin B during the binding with $tRNA^{Phe}$. In order to define the conformational space of neomycin B bound by the $tRNA^{Phe}$, inter hydrogen atom distances were calculated from the trNOE build up curves for all conformational relevant trNOE effects (Figure 4.24).

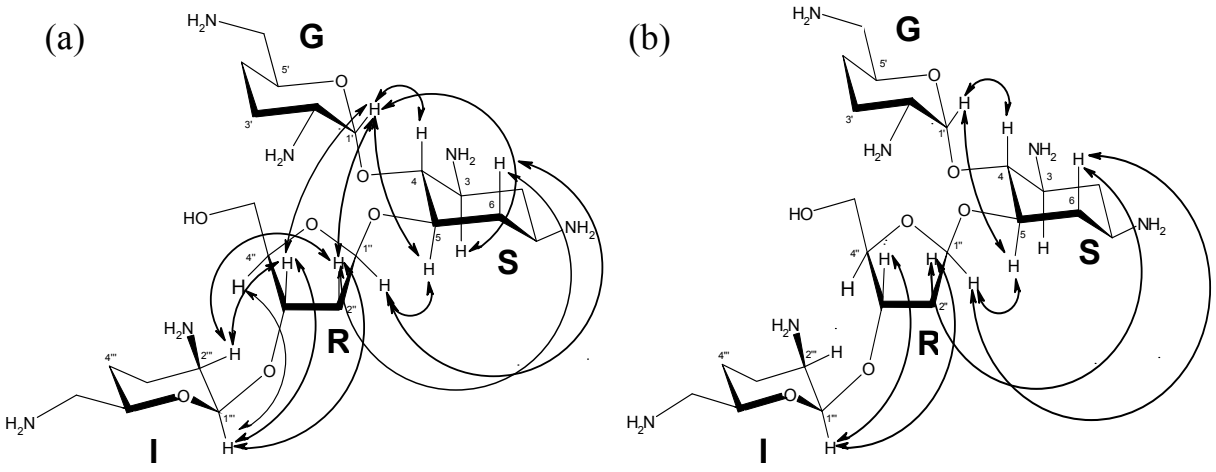

Figure-4.22: (a) Inter ring NOE contacts in neomycin B. (b) Inter ring trNOE contacts in the neomycin B-$tRNA^{Phe}$ complex.

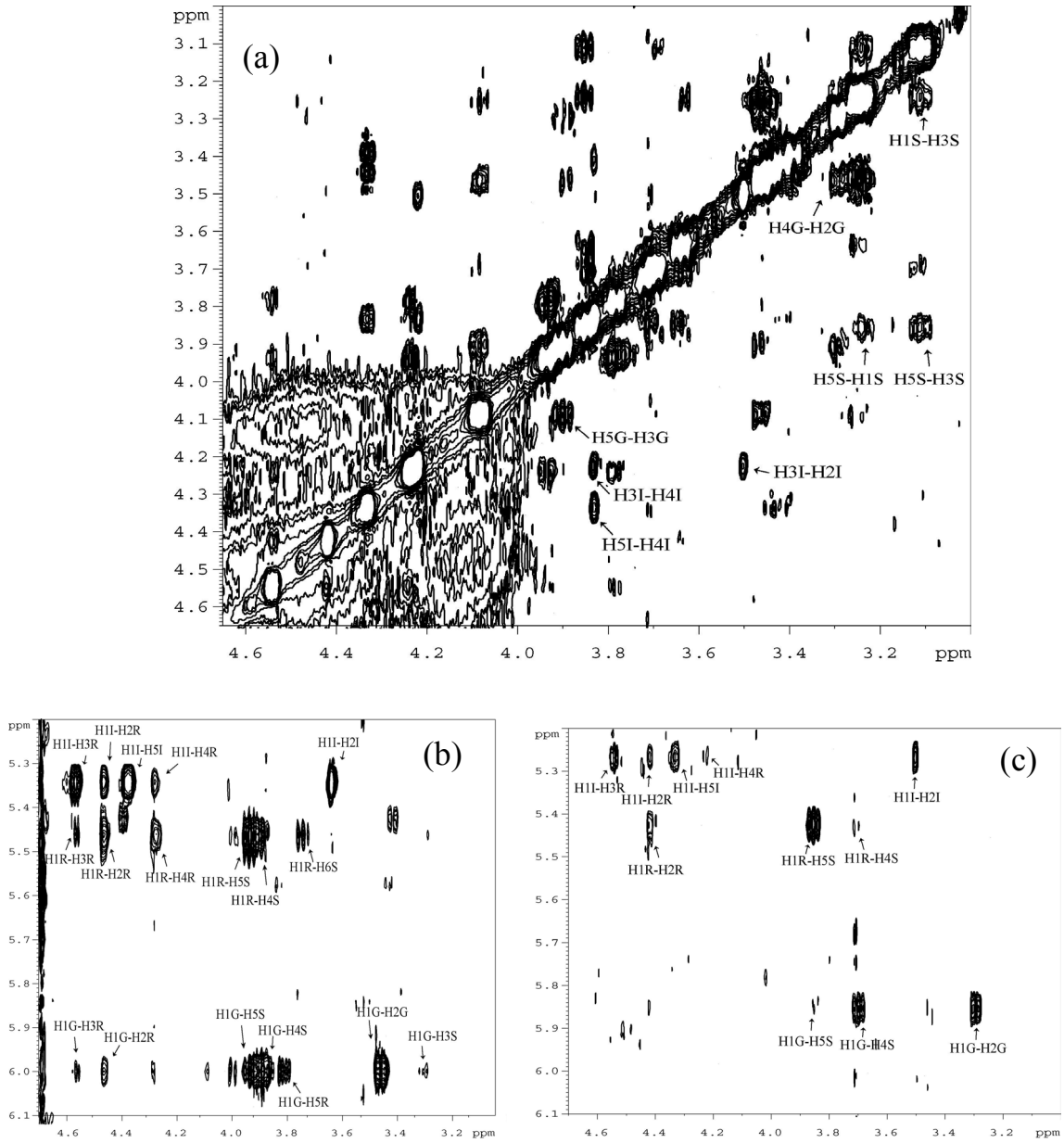

Figure-4.23: (a) Expanded region of a trNOE spectrum of the neomycin B-tRNA^{Phe} complex. Only the conformational relevant trNOE signals are labelled. (b) Expanded region of a NOESY spectrum of neomycin B showing NOE contacts of anomeric hydrogen atoms. (c) Same expanded region of the trNOE spectrum of the neomycin B-tRNA^{Phe} complex.

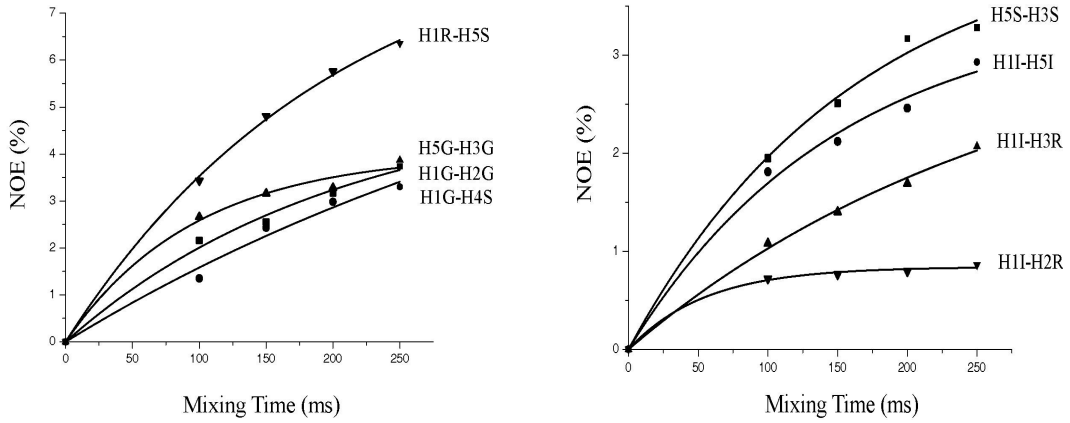

Figure 4.24: Build up curves for the trNOE effects of the neomycin B-tRNA^{Phe} complex. These build up curves were used to calculate the inter hydrogen atom distances.

Table-4.5: Inter hydrogen atom distances in neomycin B calculated from the trNOE build up curves.

TrNOE effects in neomycin B	Distances
H1G-H4S	2.6 Å
H1G-H5S	3.6 Å
H3G-H5G	2.3 Å
H1G-H2G	2.4 Å
H1R-H5S	2.3 Å
H2R-H6S	3 Å
H5S-H3S	2.4 Å
H1I-H5I	2.5 Å
H1I-H2R	2.7 Å
H1I-H3R	2.7 Å

4.5.2 MD Simulations to Determine the Bioactive Conformation of Neomycin B

Two MD simulations with different starting conformations of neomycin B were performed by including 10 inter hydrogen atom distances (Table 4.5) as constraints. The conformational space obtained from these constraint MD simulations represented the conformational family bound by tRNA^{Phe}. The distribution of conformers for all three glycosidic linkages obtained through these MD simulations have been superimposed on the potential energy maps of respective glycosidic linkages in Figure 4.25. For the G/S glycosidic linkage it was found that only one region of

conformers were in accordance with the experimental constraints as was found in case of neamine and ribostamycin (see sections 4.6.2 & 4.7.2) This region was centered around ϕ/ψ = -45°/-40° (Figure 4.25 a). In the case of the R/S glycosidic linkage conformers were populated in a single region around ϕ/ψ = -30°/0° (Figure 4.25b). This region differed from that found in ribostamycin for the R/S linkage (see section 4.7.2). For the I/R linkage, the constraint MD simulations populated conformers in the region of the global energy minimum (ϕ/ψ = -60°/-60°) (Figure 4.25 c).

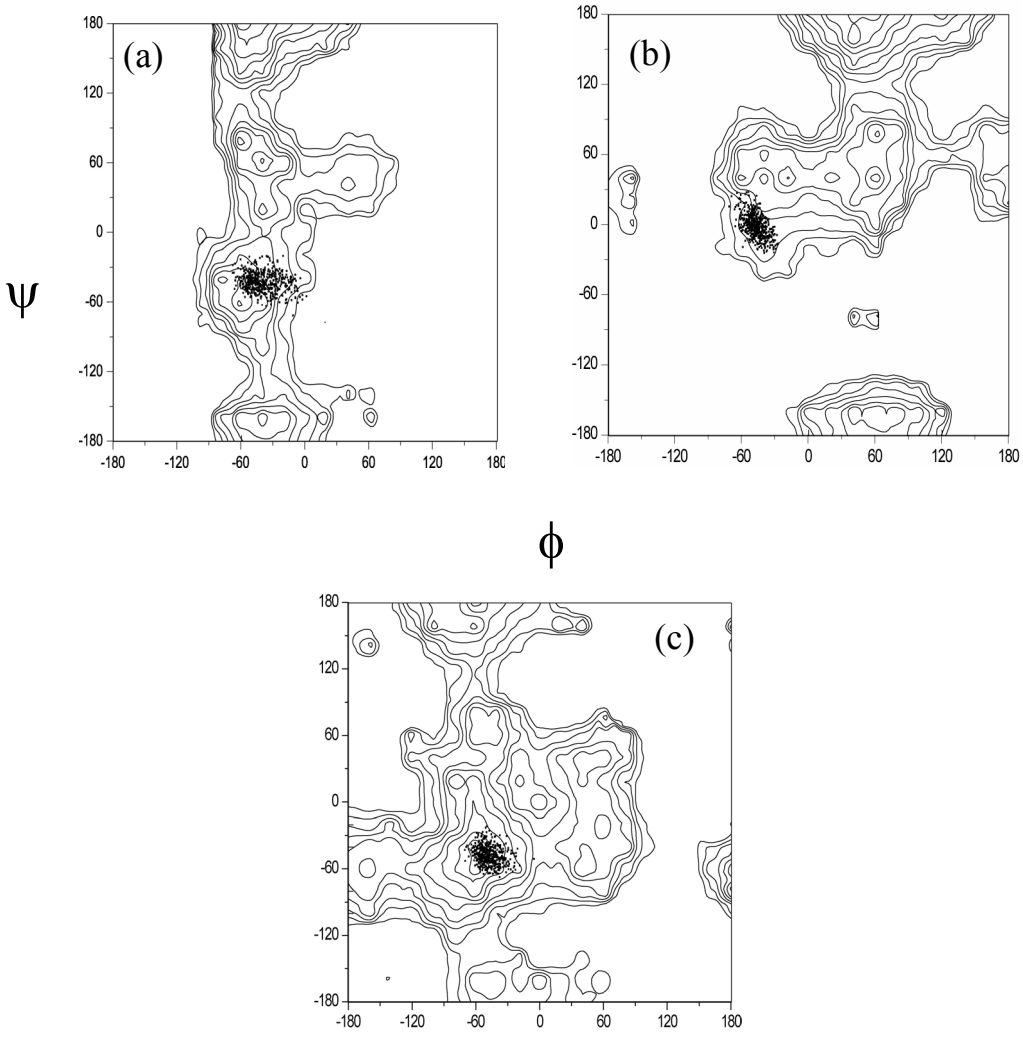

Figure-4.25: Distribution of conformers obtained through a distance constraint MD simulations for the three glycosidic linkages of neomycin B are super imposed on the potential energy maps of the respective glycosidic linkages. (a) G/S glycosidic linkage, (b) R/S glycosidic linkage and (c) I/R glycosidic linkage.

4.5.3 Ribose Ring Puckering in tRNA^{Phe}-bound Neomycin B

The conformation of the ribose ring in tRNA^{Phe}-bound neomycin B was determined by calculating the phase angle of the ribose ring from the distance constraint MD simulations. It was observed that the phase angle varied between 40^{o} to 75^{o} during the MD simulations (Figure 4.26). This range of phase angle corresponds to a C4-exo type of ring puckering. In the unconstraint MD simulation of neomycin B, C1-endo was major and C4-exo was minor populated with a large degree of flexibility in the ring (compare section 4.5, Figure 4.14). The distance constraint MD simulations showed less flexibility in the ribose ring. The strong trNOE effect, 1I-2R was in agreement with the C4-exo ring conformation in the bound state. In C4-exo and C3-endo ring conformations, H2R resides in a pseudo equatorial orientation and can generate a strong NOE effect with H1I across the glycosidic linkage. This NOE effect is very less probable when H2R resides in a pseudo axial orientation as in the C2-endo conformation. Asensio *et al.* have described that in neomycin B the conformation at the I/R glycosidic linkage and the ribose ring conformation are correlated. A negative ψ angle at the I/R linkage correlates with the pseudo axial orientation of OH2R (pseudo equatorial H2R) (Asensio *et al.*, 2002). Therefore, the results discussed in the previous section, with the I/R glycosidic linkage at ψ = –60^{o} and a C4-exo ribose ring conformation are in agreement with the results described by Asensio *et al*.

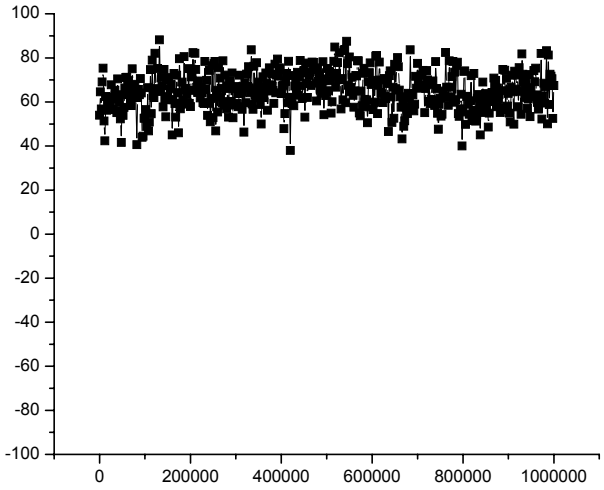

Figure-4.26: Distribution of Phase angle of ribose ring over the period of the constraint MD simulations of neomycin B.

4.6 Discussion of the tRNA^{Phe}-bound Conformations of Three Aminoglycosides

The NOE data for all three aminoglycosides (in the free state) suggested a high degree of flexibility in all glycosidic linkages. The trNOE data for the mixtures of aminoglycosides and tRNA^{Phe}, and subsequent inter hydrogen atom distance constraint MD simulations showed that the recognition process by tRNA^{Phe} leads to a conformational selection at all glycosidic linkages.

The conformational space at the G/S glycosidic linkage of all three aminoglycosides was found to be the identical when bound by tRNA^{Phe}. Moreover, all the key polar groups of neamine moiety of all three aminoglycosides, which play important roles in the binding of these molecules to tRNA^{Phe}, were found to occupy the same position in the three-dimensional space (Figure 4.27). These results suggested that the specific interactions of the neamine moiety of all three aminoglycosides with tRNA^{Phe} are similar. The conformational space at the R/S glycosidic linkage being bound by tRNA^{Phe} was found different in ribostamycin and neomycin B. Since ribostamycin and neomycin B differ in the idose ring of neomycin B, these observed variations of conformational space in the bound state can be attributed either to an interaction of the idose ring with tRNA^{Phe} or to a steric repulsion of the additional ring with the large RNA.

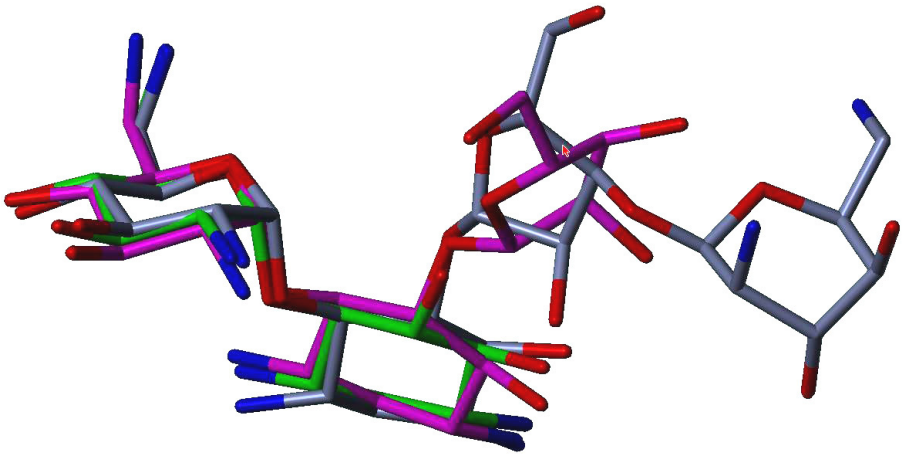

Figure-4.27: Three aminoglycosides, neamine, ribostamycin and neomycin B are superimposed on each other in their tRNA^{Phe}-bound conformations. Each structure has been taken from the middle of the populated regions of conformers obtained through the constraint MD simulations.

4.7 An Attempt to Determine the Binding Epitope of the Aminoglycosides by STD NMR Experiments

In order to define the contact area of the aminoglycosides with $tRNA^{Phe}$ Saturation Transfer Difference-NMR (STD-NMR) experiments were performed. Unfortunately, these experiments were not successful. The reason for this could be that RNA molecules in general have a very low density of hydrogen atoms as compared to proteins and magnetization transfer in the RNA molecule might not be sufficient enough for a saturation transfer to the small ligand molecule. Secondly, the crystal structure of the $tRNA^{Phe}$-neomycin B complex (Mikkelsen *et al.*, 2001) shows that the binding site of neomycin B at the $tRNA^{Phe}$ is mainly surrounded by phosphoric esters with very few hydrogen atoms (Figure 4.28) which again does not provide an adequate source for the transfer of magnetization.

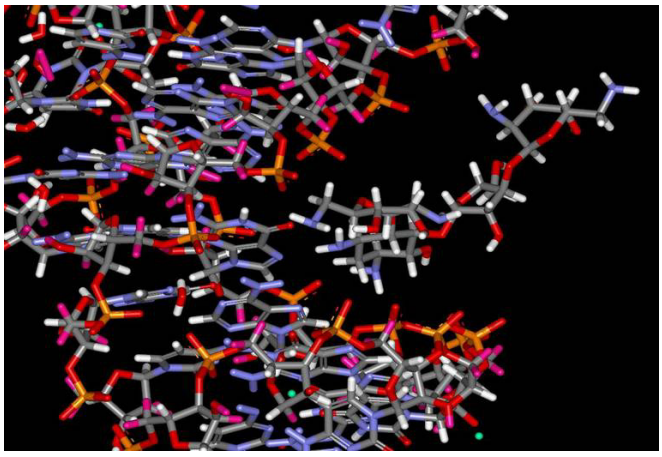

Figure-4.28: Part of the crystal structure of the $tRNA^{Phe}$-neomycin B complex showing the binding site of neomycin B.

4.8 Comparison of trNOE-derived $tRNA^{Phe}$-bound Conformation of Neomycin B with its Crystal Structure

A closer inspection of neomycin B in the crystal structure of its complex with tRNAPhe (Mikkelsen et al., 2001) has revealed several configuration errors. Out of 19 chiral carbon atoms in neomycin B, only 8 displayed the correct absolute configuration. Atoms C1 in the glucopyranose (G) and C1 in the idopyranose (I) unit belong to these misconfigured carbon

atoms and therefore the 2,6-dideoxy-2,6-diamino-α-D-glucopyranose unit (G) is β-configured and the 2,6-dideoxy-2,6-diamino-β-L-idopyranose unit (I) is α-configured in the crystal structure of neomycin B. (Figure 4.29).

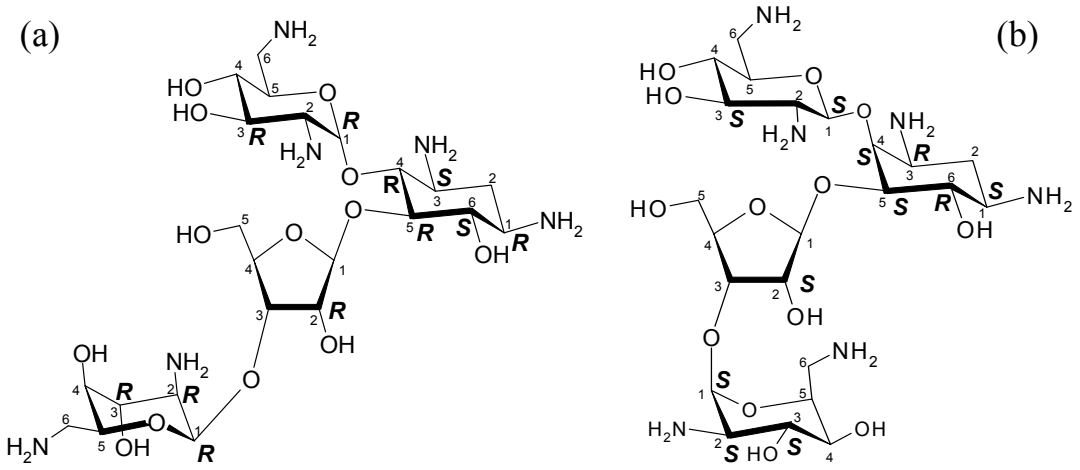

Figure-4.29: Neomycin B (a) NMR structure (b) crystal structure. Both have configuration differences at eleven different positions indicated by the respective type of absolute configuration (*R* or *S*).

These configuration errors might be due to badly resolved crystal structure especially in the part of complex containing ligand molecule. This crystal structure has been resolved at 2.6 Å resolutions, which is not good enough to define the proper configuration of the ligand. Comparison of trNOE-derived bound conformation of neomycin B with its crystal structure is presented in Figure 4.30. The conformer of neomycin B was picked up from the middle of populated region of conformers obtained through distance constraint MD simulations and overlaid to the crystal structure. Figure 4.30 shows that the key polar groups of neamine region in both structures occupy the same positions in three-dimensional space despite the few wrong configurations in the crystal structure. Remaining part of neomycin B shows different orientations as in both structures.

It can be concluded from this comparison that the positions of key polar groups of neamine part of the crystal structure has been confirmed by the NMR methodology. The configuration errors in the crystal structure have also been corrected by NMR experiments. However, the orientation

of ribose and idose ring found to be different by trNOE methodology as compared to that in the crystal structure.

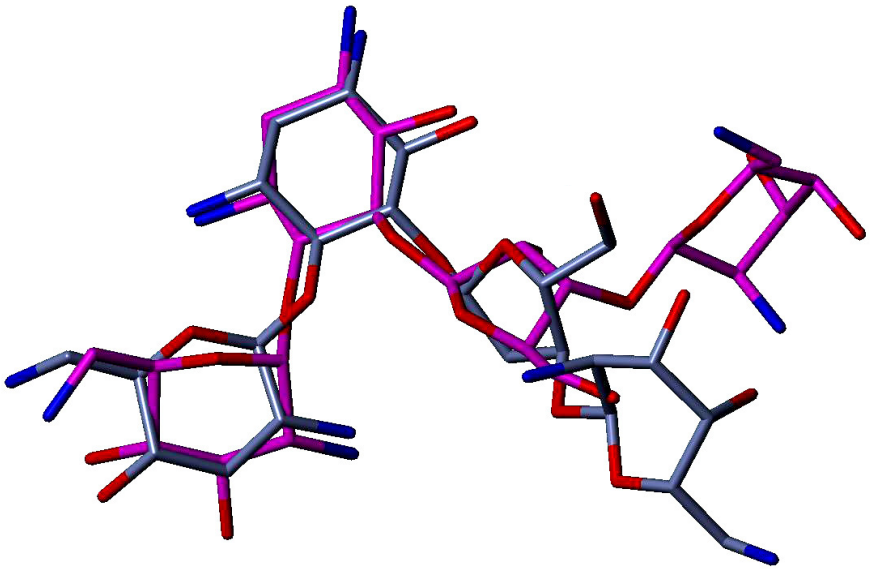

Figure-4.30: Neomycin B in $tRNA^{Phe}$-bound conformation determined through NMR (purple carbon atom) superimposed on neomycin B from crystal structure of the complex (grey carbon atoms).

4.9 Inhibition Studies on α-Glucosidase Enzymes by Sesquiterpenoid Derivatives

During this study, α-glucosidase enzyme inhibition effect of eleven natural sesquiterpenoid derivatives (compounds **1**-**11**) was investigated. All of these compounds were isolated from methanol extract of the roots of a medicinal plant, *Ferula mongolica* (Umbelliferae) by a fellow student Muhammad Irfan Baig. Structural information of these compounds are reported in references: (Choudhary *et al.*, 2001; Kojima *et al.*, 1999; Kojima *et al.*, 1999; Kojima *et al.*, 1998). Inhibitory activity of these compounds against yeast and intestinal α-glucosidase enzymes was determined (see the methodology chapter). Their IC_{50} values are listed in Table-4.7.

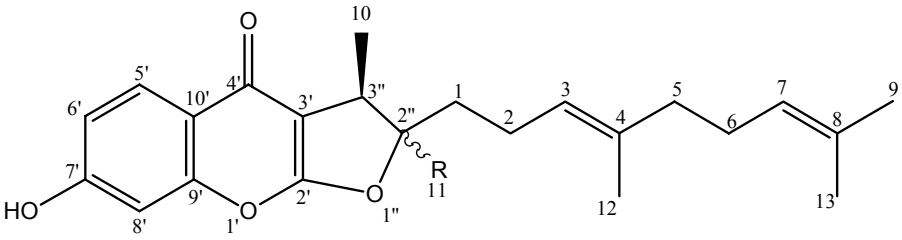

1 R = α-CH_3

2 R = β-CH_3

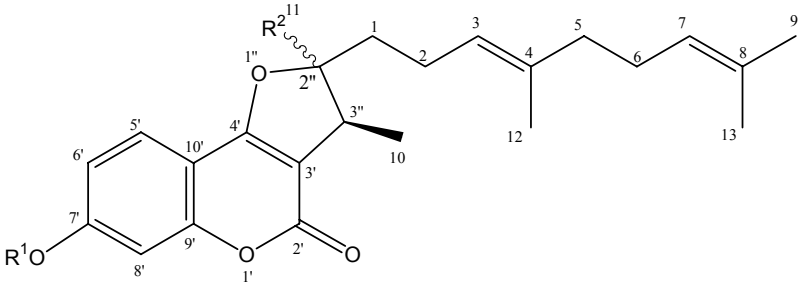

3 R^1 = H, R^2 = α-CH_3
4 R^1 = CH_3, R^2 = α-CH_3
5 R^1 = CH_3, R^2 = β-CH_3

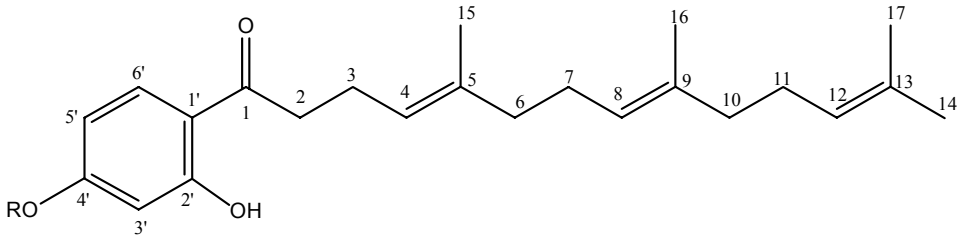

6 R=H
7 R= CH_3

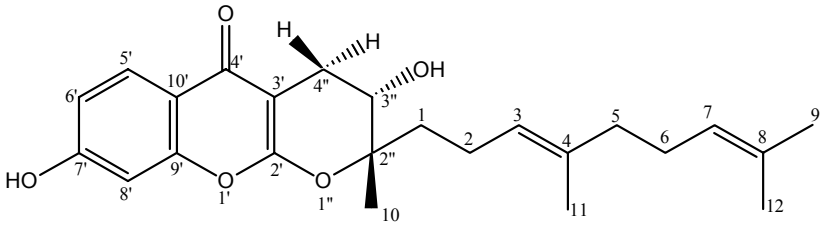

8

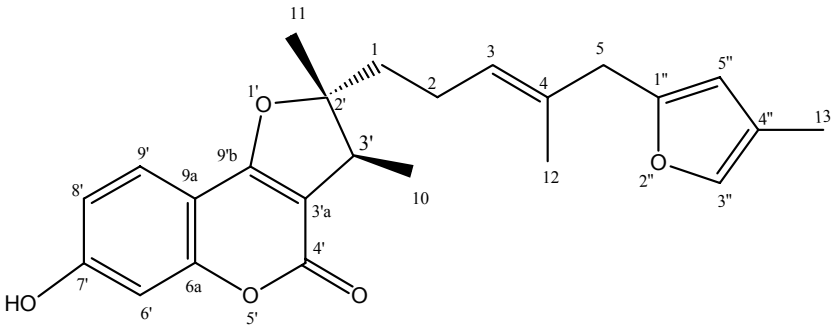

9

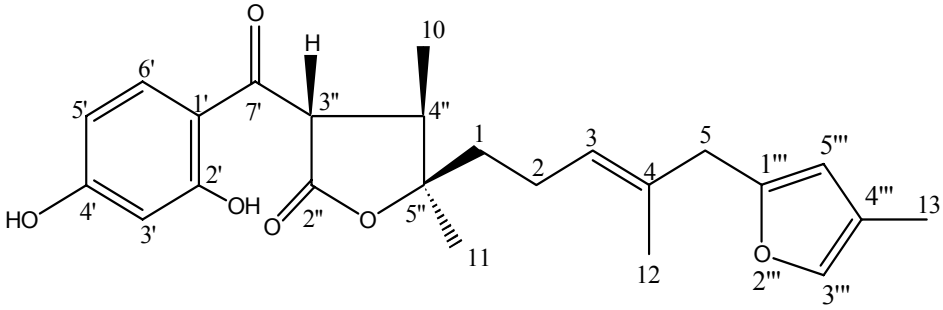

10

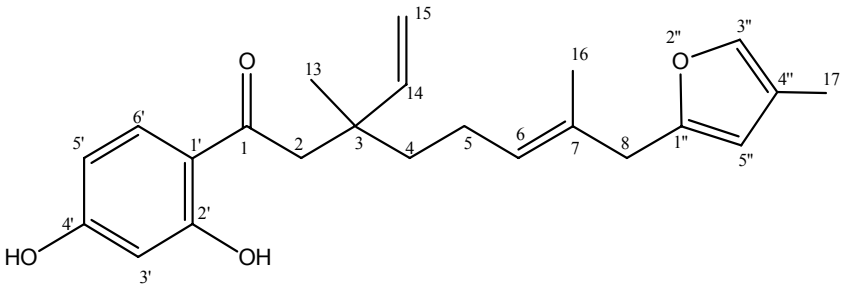

11

Table-4.6: IUPAC Names of Compounds **1**-**11**.

Compounds	IUPAC names
1	7'-Hydroxy-2"*R*,3"*R*-dimethyl-2"-(4,8-dimethyl-3(*E*),7-nonadienyl)-2",3"-dihydro-furo(2",3"-b)benzopyran-4'-one
2	7'-Hydroxy-2"*S*,3"*R*-dimethyl-2"-(4,8-dimethyl-3*(E),*7-nonadienyl)-2",3"-dihydro-furo(2",3"-b)benzopyran-4'-one
3	7'-Hydroxy-2"*R*,3"*R*-dimethyl-2"-(4,8-dimethyl-3(*E*),7-nonadienyl)-2",3"-dihydro-furo(3",2"-c)coumarin
4	7'-Methoxy-2"*R*,3"*R*-dimethyl-2"-(4,8-dimethyl-3(*E*),7-nonadienyl)-2",3"-dihydro-furo(3",2"-c)coumarin
5	7'-Methoxy-2"*S*,3"*R*-dimethyl-2"-(4,8-dimethyl-3(*E*),7-nonadienyl)-2",3"-dihydro-furo(3",2"-c)coumarin
6	1-(2',4'-Dihydroxybenzoyl)-4,8,12-trimethyl-3(*E*),7(*E*),11-tridecatriene
7	1-(2'-Hydroxy-4'-methoxybenzoyl)-4,8,12-trimethyl-3(*E*),7(*E*),11-tridecatriene
8	(2"*S,*3"*R*)-7',3"-Dihydroxy-2"-methyl-2"-(4,8-dimethyl-3(*E*),7-nonadienyl)-3",4"-dihydro-pyrano(2",3"-b)benzopyran-4'-one
9	7-Hydroxy-2'*S**,3'*R**-dimethyl-2'-[4-methyl-5-(4"-methyl-2"-furyl)-3(*E*)-pentenyl]-2',3'-dihydro-furo[3',2'-c]-2H-benzopyrane-4'-one
10	3"*S**-(2',4'-Dihydroxybenzoyl)-4'*R**,5"*R**-dimethyl-5"-{4-methyl-5-(4'"-methyl-2'"-furyl)-3(*E*)-pentenyl}tetrahydro-2"-furanone
11	1-(2',4'-Dihydroxyphenyl)-3,7-dimethyl-3-vinyl-8-(4"-methyl-2"-furyl)-6(*E*)-octen-1-one

Table-4.7: IC_{50} values of sesquiterpenoid derivatives against α-glucosidase from yeast and small intestine of rat.

Compounds	IC_{50} (μM) ± SEM	
	Yeast α-glucosidase	**Intestinal α-glucosidase**
1	32.21 ±1.38	120 ± 5.9
2	20.50 ±1.62	109.1 ± 4.7
3	63.68 ±2.68	136 ±6.5
4	79.87 ±2.97	138.9 ±7.2
5	200	[a]
6	9.31 ±0.15	109.1 ± 4.7
7	82.41 ±3.21	208 ± 9.1
8	56.06 ±2.56	123.8 ± 7.1
9	66.3 ±2.17	130 ± 5.6
10	60.75 ± 0.961	129.1 ±7.8
11	29.158 ±0.148	110.3 ±8.2

[a] Negligibly active, SEM = standard error of the mean = standard deviation/√n; n = number of replicates for IC_{50} value (n =3).

4.9.1 Kinetic Studies

Kinetic studies on all sesquiterpenoid derivatives were conducted against yeast α-glucosidase. Kinetic studies of four of these compounds were also conducted against intestinal α-glucosidase. The K_m value of the substrate (P-NPG) was determined as 0.5 mM ± 0.03 with yeast enzyme and 6.6 mM ± 0.4 with intestinal enzyme. Plots of steady state kinetics for compounds **1** and **6** are presented in Figures 4.31 and 4.32 against both enzymes.

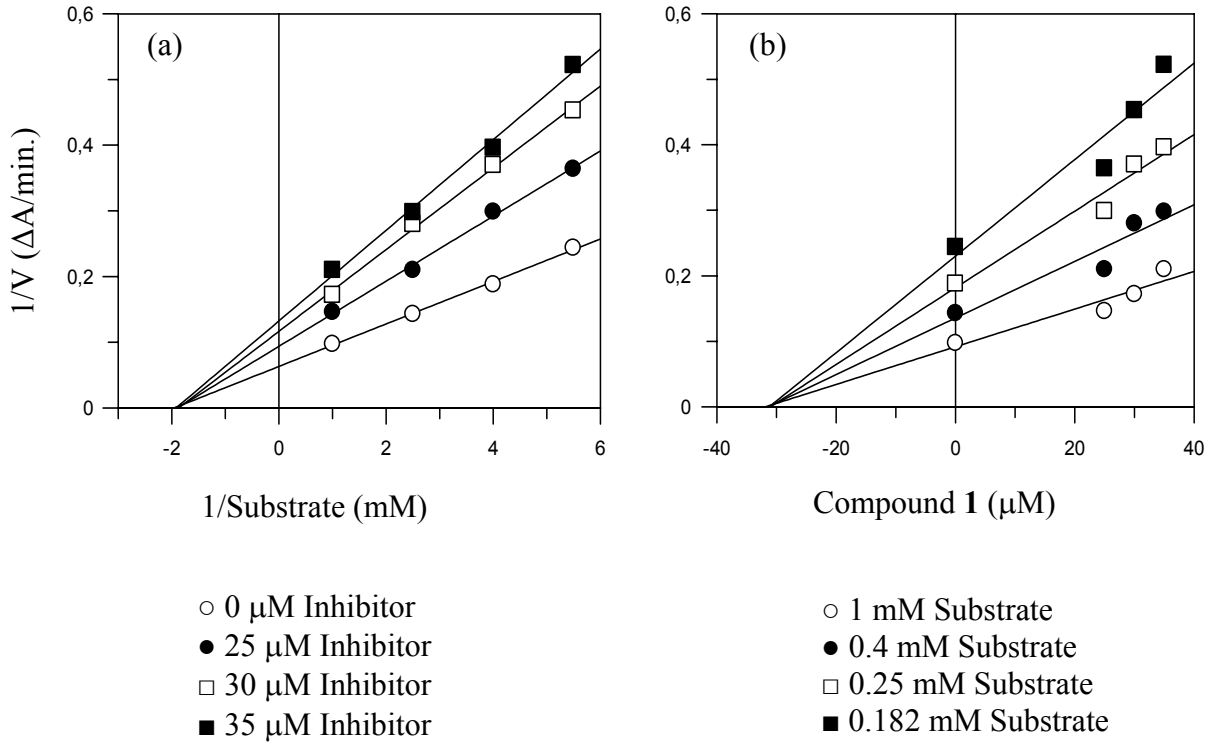

Figure-4.31: Steady state inhibition studies on compound **1** against yeast α-glucosidase. (a) Lineweaver-Burk plot, reciprocals of initial reaction velocities versus various concentrations of substrate (PNP-G) (b) Dixon plot, reciprocals of initial reaction velocities versus different concentrations of compound **1**. Both plots show the noncompetitive inhibition of α-glucosidase by compound **1**.

Table-4.8: Values of K_i and types of inhibition for compounds **1-11** against yeast α-glucosidase.

Compounds	K_i (μM) ± SEM	Type of inhibition
1	31 ± 1.2	Noncompetitive
2	19 ± 1.1	Noncompetitive
3	61 ± 1.21	Noncompetitive
4	75.5 ± 2.4	Noncompetitive
5[a)]		
6	10.2 ± 0.7	Mixed-type
7	59 ± 2.1	Mixed-type
8	45 ± 2.3	Mixed-type
9	64.5 ± 1.4	Noncompetitive
10	56 ± 4.1	Noncompetitive
11	18 ± 1.2	Mixed-type

[a)] Negligibly active, SEM = standard error of the mean = standard deviation/√n; n = number of replicates for K_i value (n =3)

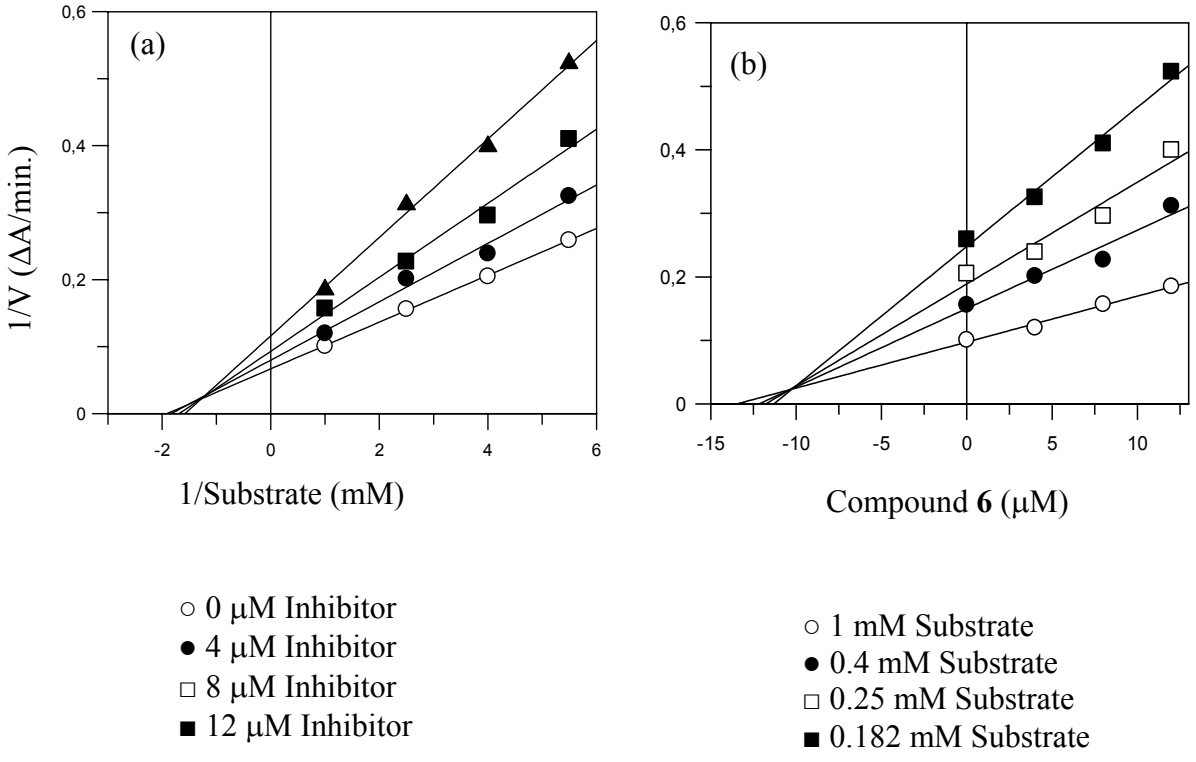

Figure-4.32: Steady state inhibition studies on compound **6** against yeast α-glucosidase. (a) Lineweaver-Burk plot, reciprocals of initial reaction velocities versus various concentrations of substrate (PNP-G) (b) Dixon plot, reciprocals of initial reaction velocities versus different concentrations of compound **6**. Both plots show the mixed-type inhibition of α-glucosidase by compound **6**.

Table-4.9: Values of K_i and types of inhibition for compounds **6**, **7**, **9** and **11** against rat intestinal α-glucosidase.

Compounds	K_i (μM) ± SEM	Types of Inhibition
6	97 ± 8.1	Mixed-type
7	132 ± 9.5	Mixed-type
9	116 ± 10.4	Mixed-type
11	110 ± 7.1	Mixed-type

SEM = standard error of the mean = standard deviation/√n; n = number of replicates for K_i value (n = 3)

Compounds **1**, **2, 3**, **4**, **9** and **10** were found to be noncompetitive inhibitors of yeast α-glucosidase. Lineweaver-Burk plots of these compounds showed that K_m values did not change with the increase of inhibitor concentrations they remained the same as in the absence of inhibitor. V_{max} values decreased with the increase of inhibitor concentrations. This was indicative of noncompetitive inhibition that in turn indicated that substrate and inhibitor

bound to the enzyme independent of each other. K_i values of these compounds determined through Dixon Plot are presented in Table 4.8.

Compounds **1** and **2** are structurally similar, except the configuration at C2". Their inhibitory activities were also not much different (with K_i values 31 μM and 19 μM respectively). However, these two compounds represented the most active compounds among six sesquiterpenoid derivatives. K_i values of compounds **3**, **4**, **9** and **10** were also in similar range (Table 4.8). These four compounds have structural similarities with each other but it is very difficult to predict the binding epitope or structure activity relationship with certainty based on this data.

Compounds **6**, **7**, **8** and **11** were found to be mixed-type inhibitors of yeast α-glucosidase. Lineweaver-Burk plots for these compounds showed that values of V_{maxi} (maximum velocity of enzymatic reaction in the presence of inhibitor) were less than the values of V_{max} (maximum velocity of enzymatic reaction in the absence of inhibitor) and decreased with the increase of inhibitors concentrations. Inhibitors also affected the K_m values of the substrate. All the lines representing different inhibitor concentrations intercepted each other on a point behind the y-axis but before the x-axis. This type of inhibition was apparently a mixture of competitive and noncompetitive inhibition referred to as mixed-type inhibition (see section 3.4.4). K_i values of these compounds determined through Dixon plot are presented in Table 4.3. Hydroxyl moiety on aromatic ring seems to have a major role in the inhibitory activities of these compounds. Compounds **6** and **11** showed comparable inhibitory activity with K_i values of 10.2 μM and 18 μM, respectively. Each of these compounds has two hydroxyl groups on the aromatic ring (see section 4.7). Compounds **7** and **8** showed K_i values of 59 μM and 45 μM, respectively. Compound **7** is structurally similar to compound **6**, except the presence of a methoxy group at C4 in compound **7,** in place of hydroxyl group at this position in compound **6**. Compound **8** has also one hydroxyl group on aromatic ring. Stronger inhibitory activity of compounds **6** and **11**, as compared to the compounds **7** and **8** can therefore, be attributed to the presence of two hydroxyl groups on aromatic ring in compounds **6** and **11**.

Four compounds **6**, **7**, **9** and **11** were subjected to kinetic studies also against rat intestinal α-glucosidase. Rest of compounds did not have enough quantities for kinetic studies against this enzyme and for *in vivo* studies as well. Compounds **6**, **7**, **9** and **11** showed mixed-type

inhibition against the intestinal α-glucosidase with weak inhibitory potential as predicted from their K_i values (Table 4.9).

4.9.2 Determination of Cytotoxicity of Sesquiterpenoid Derivatives

Five sesquiterpenoid derivatives were subjected to the test of cytotoxicity (see the methodology section). All the five compounds were found to be non-cytotoxic as their inhibition against the yeast in DNA damaging assay was negligible. Three of these compounds were also tested in brine shrimp lethality assay to determine their toxicity. None of these compounds showed significant toxic effect in brine shrimp assay.

4.9.3 *In vivo* Studies on Sesquiterpenoid Derivatives as α-Glucosidase Inhibitors

In vivo studies to determine the inhibitory activity of four sesquiterpenoid derivatives were conducted (see the methodology section). Values of blood glucose levels at different intervals after oral administration of these compounds are presented in Table 4.10. Pathological control group that was orally administered with saline, in place of any test compound showed significant rise in blood glucose levels at 30 minutes. This was followed by a steady decline in blood glucose levels until 90 minutes (Figure 4.31). Positive control group that was orally administered with acarbose, a standard inhibitor, showed very slow increase of blood glucose levels (Figures 4.33 and 4.34). At 30 minutes, rise in blood glucose was much less as compared to pathological control. Similarly, decline in blood glucose was also slow which actually indicated the prolonged glucose absorption after maltose was orally given in the presence of acarbose. Similar effect was exhibited by the groups of rats that were given compounds **6**, **7**, **9** and **11** separately. All of these four groups showed less significant rise in blood glucose levels as compared to pathological control (Figures 4.33 and 4.34). They also showed a slow decline in blood glucose levels. The hypoglycaemic effect in animals with test compounds was not as prominent as in case of positive control but they certainly showed prolongation of glucose absorption from the intestine. The prolongation of glucose absorption can be attributed to the inhibition of maltase activity of α-glucosidase enzymes that results in slow hydrolysis of maltose to glucose. This delayed absorption of glucose into blood is the key stage to avoid hyperglycaemia especially after meal.

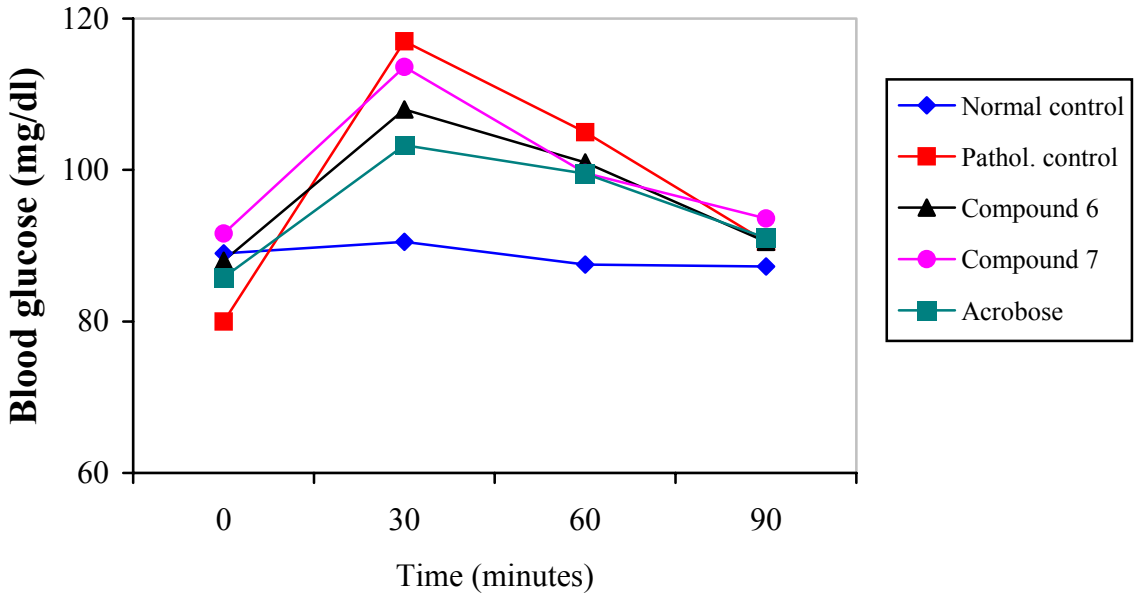

Figure-4.33: Effect of compounds **6** and **7** on serum glucose elevation in maltose loaded rats.

Table-4.10: Effect of compounds **6**, **7**, **9** and **11**, on blood glucose levels at different times, 0 minute, 30 minutes, 60 minutes, and 90 minutes after 1 mg/kg body weight maltose was orally given 20 minutes after oral administration of test compounds.

	Serum glucose concentration (mg/dl) at different time intervals			
Groups of animals	**0-time**	**30-minutes**	**60-minutes**	**90-minutes**
Normal control	89.5 ± 2.304	90.5 ± 3.0	87.5 ± 1.47	87.2 ± 2.63
Pathological control	80.7 ± 1.67	117.5*± 1.34	105.2*± 1.63	90.5*± 2.16
Administered with compound **6**	88 ± 3.37	109.2*± 3.28	102.5*± 4.03	90.5 ± 4.90
Administered with compound **7**	91.6 ± 3.49	113.6*± 4.2	99.6 ± 3.68	93.6 ± 4.10
Administered with compound **9**	87 ± 2.66	109*± 4.75	100.3*± 3.57	92*± 3.74
Administered with compound **11**	90.5 ± 3.09	114*± 3.37	105.7 ± 4.56	100.5 ± 3.76
Administered with acarbose (Positive control)	87.8 ± 3.76	104.2*± 7.94	99.5 ± 3.58	91.2 ± 4.32

Each value represents the mean of six ± SEM. *P< 0.05, significantly different from the zero time observation.

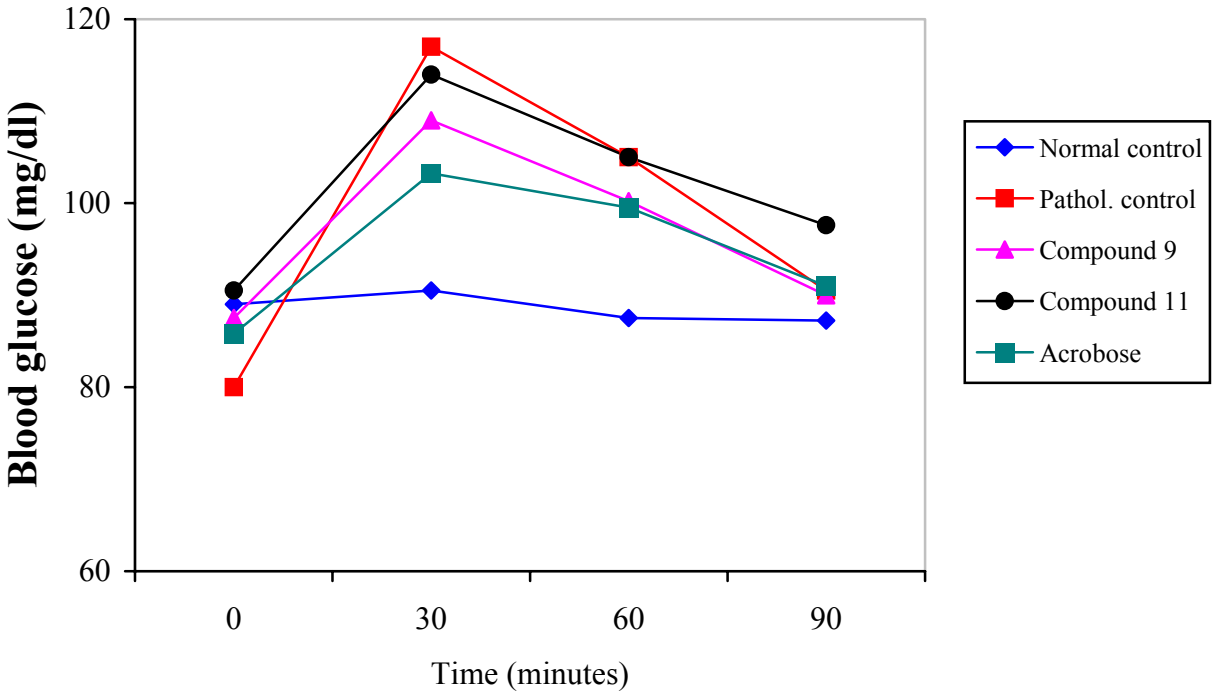

Figure-4.34: Effect of compounds **9** and **11** on serum glucose elevation in maltose loaded rats.

4.9.3.1 Experiments with Glucose-loaded Rats

Few experiments were also carried out with glucose-loaded rats, instead of maltose loaded-rats, to further verify that hypoglycaemic effect of these compounds was due to the inhibition of intestinal α-glucosidase enzyme. Since α-glucosidase does not have any role in the digestion of glucose (glucose is already an absorbable monosaccharide) therefore, any inhibitor of intestinal α-glucosidases should not have any effect on blood glucose levels in glucose-loaded rats. As shown in Table 4.11, when compound **9** and **11** were given to rats 20 minutes before glucose administration, rise in blood glucose was as significant as in case of pathological control. Therefore, this showed no glucose lowering effect of these compounds in glucose-administered rats.

Table-4.11: Effect of compounds **9** and **11** on elevation of blood glucose when these compounds were orally given twenty minutes before glucose administration. Both compounds showed no effect on glucose absorption.

Groups of animals	Serum glucose concentration (mg/dl) at different time intervals			
	0 time	**30 minutes**	**60 minutes**	**90 minutes**
Normal control	88.5 ± 3.34	90.1 ± 2.8	89.1±1.3	87.4±2.7
Pathological control	87.53 ± 3.54	129.66* ± 4.9	112*±3.15	104*±5.45
Administered with compound **9**	93.5 ± 2.95	132.25*± 3.26	114.75*±3.56	101.75*±4.64
Administered with compound **11**	84.8 ± 5.56	127* ± 3.94	112.20* ± 4.1	101.20* ± 7.2

Each value represents the mean of six ± SEM. *P< 0.05, significantly different from the zero time observation.

4.10 Inhibition Studies on α-Glucosidase by Oleanolic Acid Derivatives

Eight oleanolic acid derivatives (compounds **12-18**) were investigated as inhibitors of α-glucosidase. These compounds **12-18** (Ali *et al.*, 2002; Reddy *et al.*, 1975) showed inhibitory activity against the yeast α-glucosidase, but none of these compounds was active against mammalian intestinal α-glucosidase. Compound **12** (oleanolic acid) was isolated from the ethyl acetate extract of *Tridax procumbens* by Muhamamd Jahangir a fellow student who also prepared six derivatives of oleanolic acid (**13-17**). Compound **18** was isolated from *Spathodea companulate*. These seven compounds were subjected to kinetic studies to determine their mechanism of inhibition of yeast α-glucosidase.

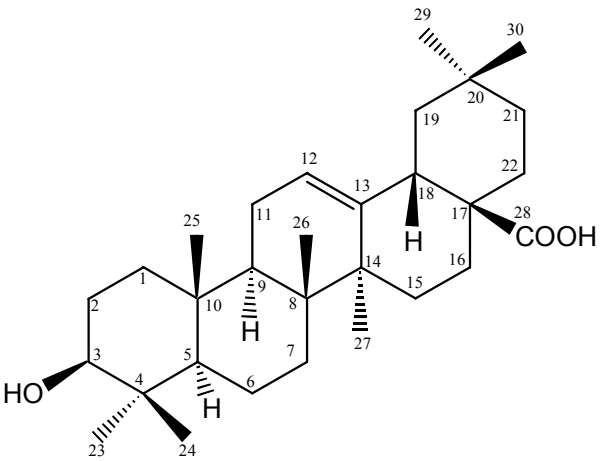

(**12**) Oleanolic acid

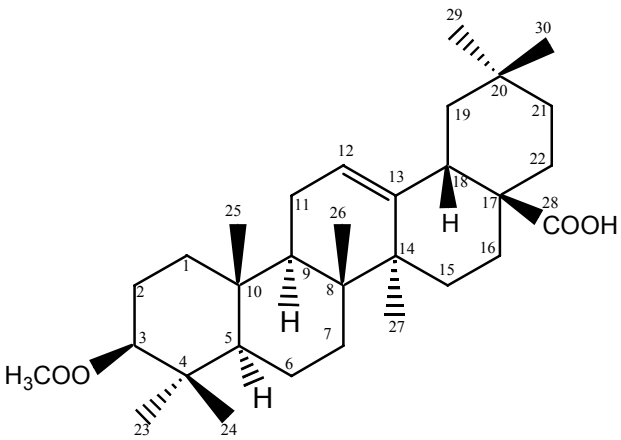

(**13**) 3β-Acetoxyoleanolic acid

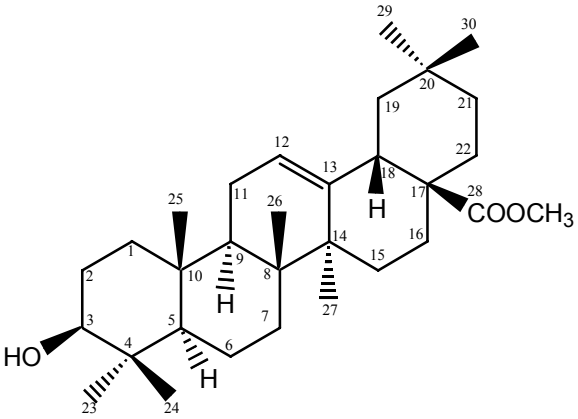

(**14**) Methyl oleanolate

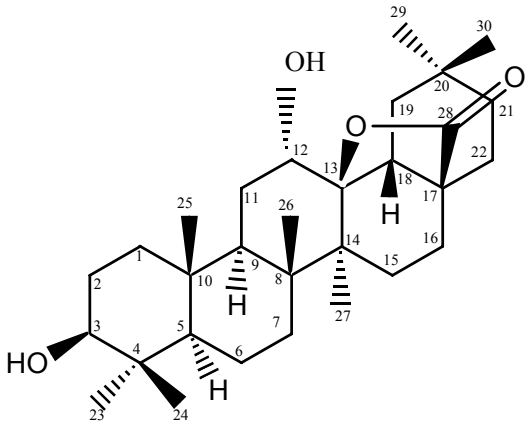

(**15**) 3β,12α,13β-Trihydroxy-28-oic acid-28→13-olide oleanane

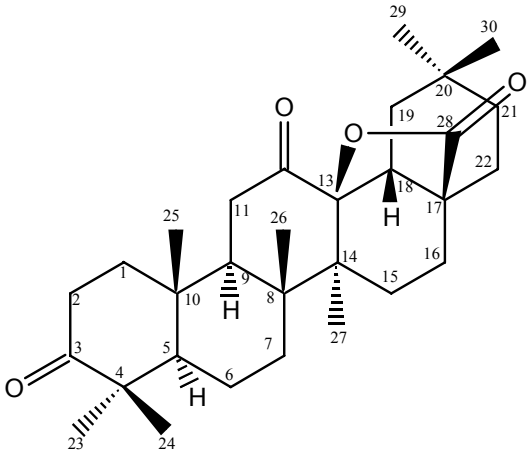

(**16**) 13β-Hydroxy 3,12-dioxo-28-oic acid-28→13-olide oleanane

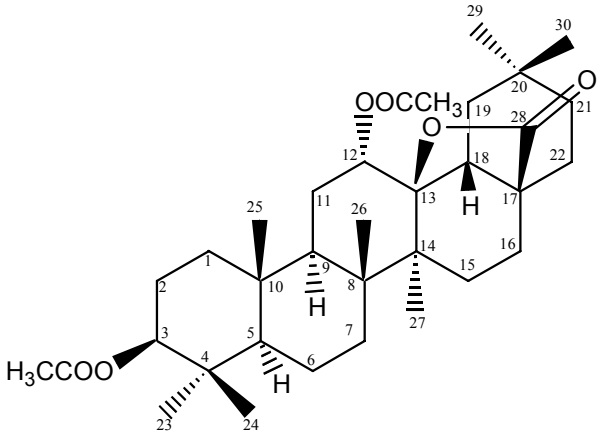

(**17**) 13β-Hydroxy-3β,12α-diacetoxy 28-oic acid-28→ 13-olide oleanane

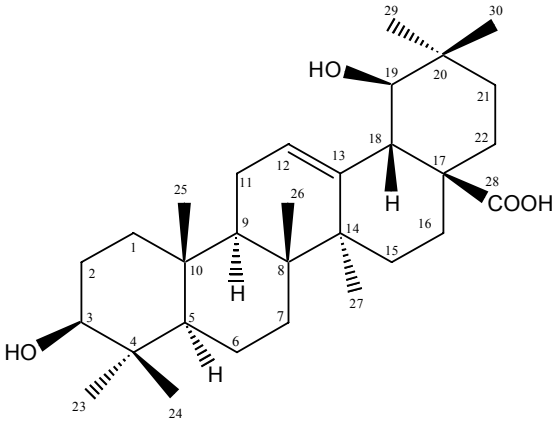

(**18**) 3β-19β-Dihydroxyolean-12-en-28-oic acid

4.10.1 Kinetic Studies

Steady state kinetic studies of oleanolic acid derivatives were conducted to determine the mechanism of inhibition of these compounds. All the oleanolic acid derivatives affected V_{max} but K_m values remained unaffected. This suggested that these compounds inhibited the enzyme noncompetitively. K_i values were obtained from the intercept of all the lines on x-axis in the Dixon plot (Figure 4.35 and Table 4.12) Mode of inhibition of these compounds indicates that the substrate and the inhibitors (Oleanolic acid derivatives) bind to the enzyme independent of each other at different locations and do not affect the dissociation constants of each other.

Table-4.12: IC_{50} and K_i values of oleanolic acid derivatives against yeast α-glucosidase.

Compounds	IC_{50} (μM) ± SEM	K_i (μM) ± SEM
12	11.16 ± 0.49	12.5 ± 1.22
13	55.1 ± 2.63	65.0 ± 4.35
14	19.0 ± 0.83	13.5 ± 0.91
15	7.97 ± 0.21	9.5 ± 0.85
16	21.63 ± 2.33	24.0 ± 1.82
17	89.7 ± 2.1	95.0 ± 5.33
18	12.0 ± 0.07	13.0 ± 1.1

Every value represent the mean of three ± SEM, SEM = standard error of the mean = standard deviation/√n; n = number of replicates for IC_{50} and K_i values (n = 3).

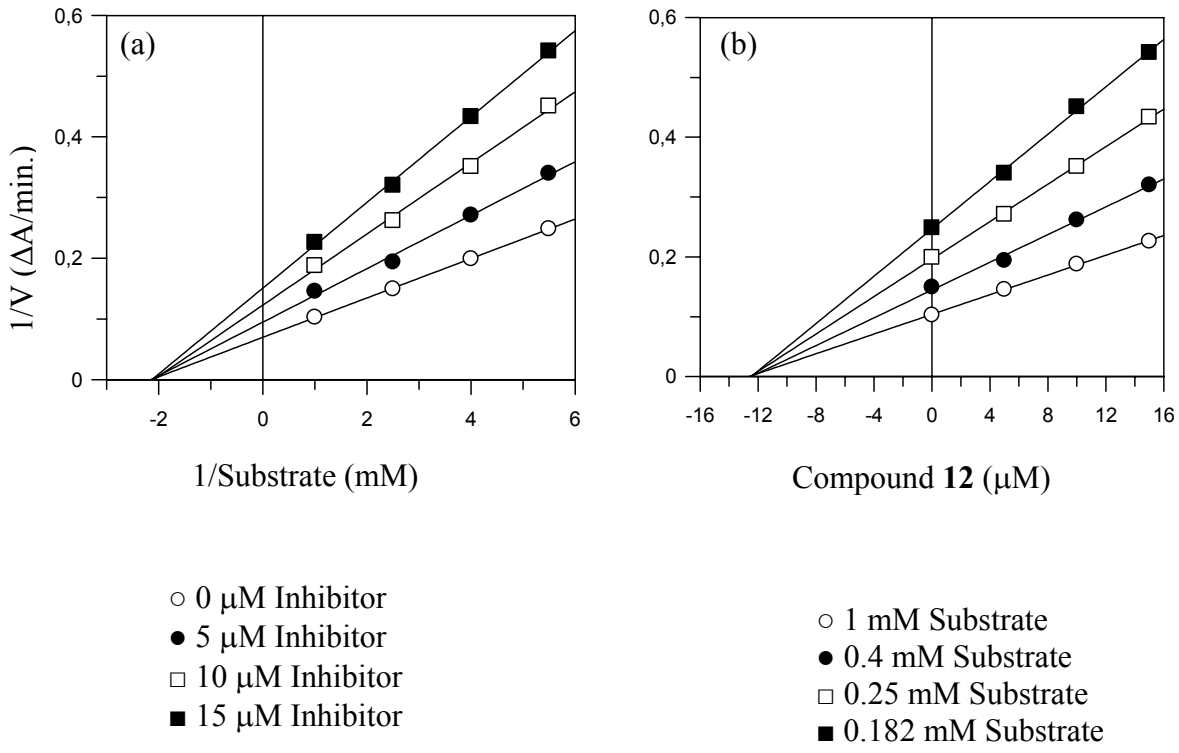

Figure-4.35: Steady state inhibition of yeast α-glucosidase by compound **12**. (a) Lineweaver-Burk plot, reciprocals of initial reaction velocities versus various concentrations of substrate (PNP-G). (b) Dixon plot, reciprocals of initial reaction velocities versus different concentrations of compound **12**. Both plots show the noncompetitive inhibition of α-glucosidase enzyme.

It was inferred from the IC_{50} and K_i values of various inhibitors (Oleanolic acid derivatives) (Table 4.12) that the hydroxyl group at C3 is the most contributing functionality towards the inhibitory activity of these compounds, against the α-glucosidase enzyme. Oleanolic acid (**12**) has shown a K_i value = 12.5 μM. Activity decreased very slightly when carboxyl group at C28 was methylated as in compound **14** (see section 4.8) showing a K_i value = 13.5 μM. When hydroxyl group at C3 was acetylated as in compound **13**, activity decreased significantly (Table 4.12). Compound **13** has shown a K_i value = 65 μM. Compound **15**, which has an additional hydroxyl group at C12 showed a K_i value = 9.5 μM. Compound **15** showed only slightly better inhibitory activity than compound **12**. This indicated that the C12 hydroxyl group does not have any major role in the inhibitory activity. In compound **17**, which is a C3 and C12 acetylated product of compound **15**, activity was significantly lowered (K_i value = 95 μM) as compared to compound **15**. Compound **16**, which has ketonic functions at C3 and C12, in place of hydroxyl functions as in compound **15**, also showed a decreased activity as compared to compound **15**, showing K_i value = 24 μM. This was not a very

significant decrease, which indicated that the presence of a polar functionality (hydroxyl or carbonyl) at C3 plays a crucial role in the inhibitory activity of these compounds against yeast α-glucosidase. Compound **18** has an additional hydroxyl group at C19 as compared to compound **12**. However, this hydroxyl group does not seem to contribute to the inhibitory activity, since compound **18** showed a K_i value = 13 μM, comparable to that observed for compound **12** (11.16 μM). This observation again indicated the importance of polar group at C3 in the inhibitory potential of this class of compounds.

4.11 Inhibition Studies on α-Glucosidase Enzymes by Steroidal lactones (Withanolides)

Two steroidal lactones (withanolides) **19** and **20** (Atta-ur-Rahman *et al.*, 1998) have been studied as inhibitors of yeast and intestinal α-glucosidase. *In vitro* studies of these compounds were followed by *in vivo* experiments on rats. These two compounds were isolated from a plant *Withania coagulance*.

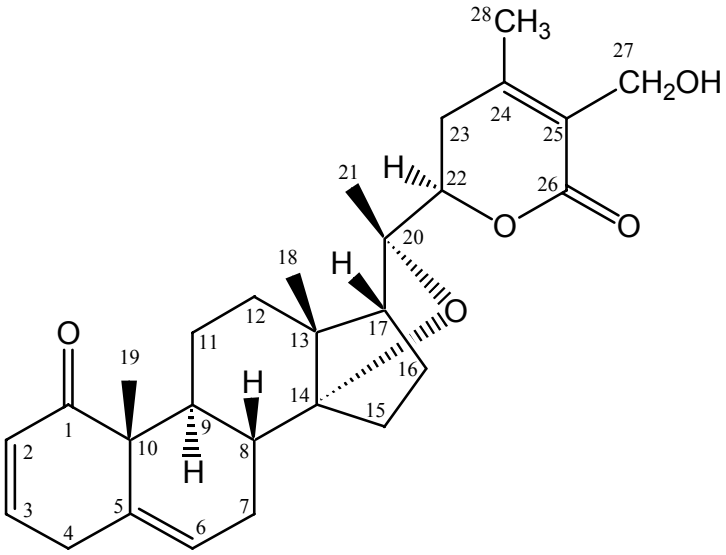

(**19**) 14α,20α-Epoxy-25-hydroxymethyl-1-oxowitha-5,24-dienolide

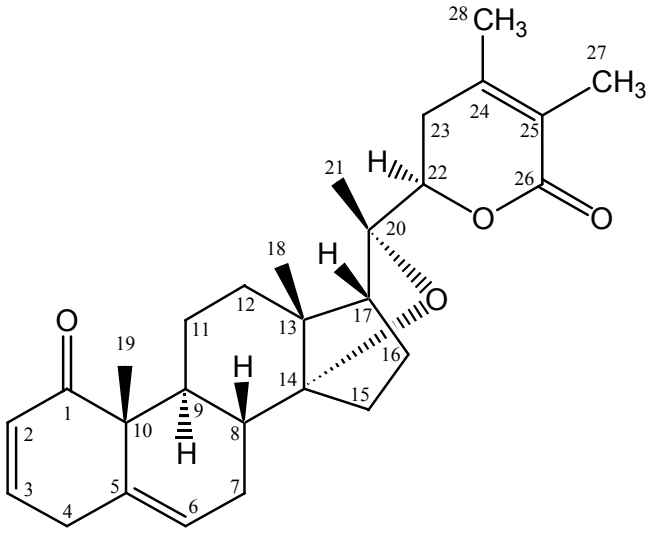

(**20**) 14α,20α-Epoxy-1-oxowitha-5,24-dienolide

Table-4.13: IC_{50} values of two steroidal lactones against α-glucosidase from yeast and mammalian intestine. Every value represents the mean of three.

Compounds	**IC_{50} (μM) ± SEM** Yeast α-glucosidase	**IC_{50} (μM) ± SEM** Intestinal α-glucosidase
19	54.4 ± 2.4	108 ± 6.5
20	53.3 ± 2.8	114 ± 4.8

SEM = standard error of the mean = standard deviation/√n, n = number of replicates for IC_{50} values (n=3).

4.11.1 Kinetic Studies

Steady state kinetic studies on steroidal lactones were conducted to determine their mode of inhibition, as well as the inhibition constant (K_i). Type of inhibition was determined by producing Lineweaver-Burk plot and the inhibition constant (K_i) values were determined from the Dixon plot (Figures 4.36-4.39).

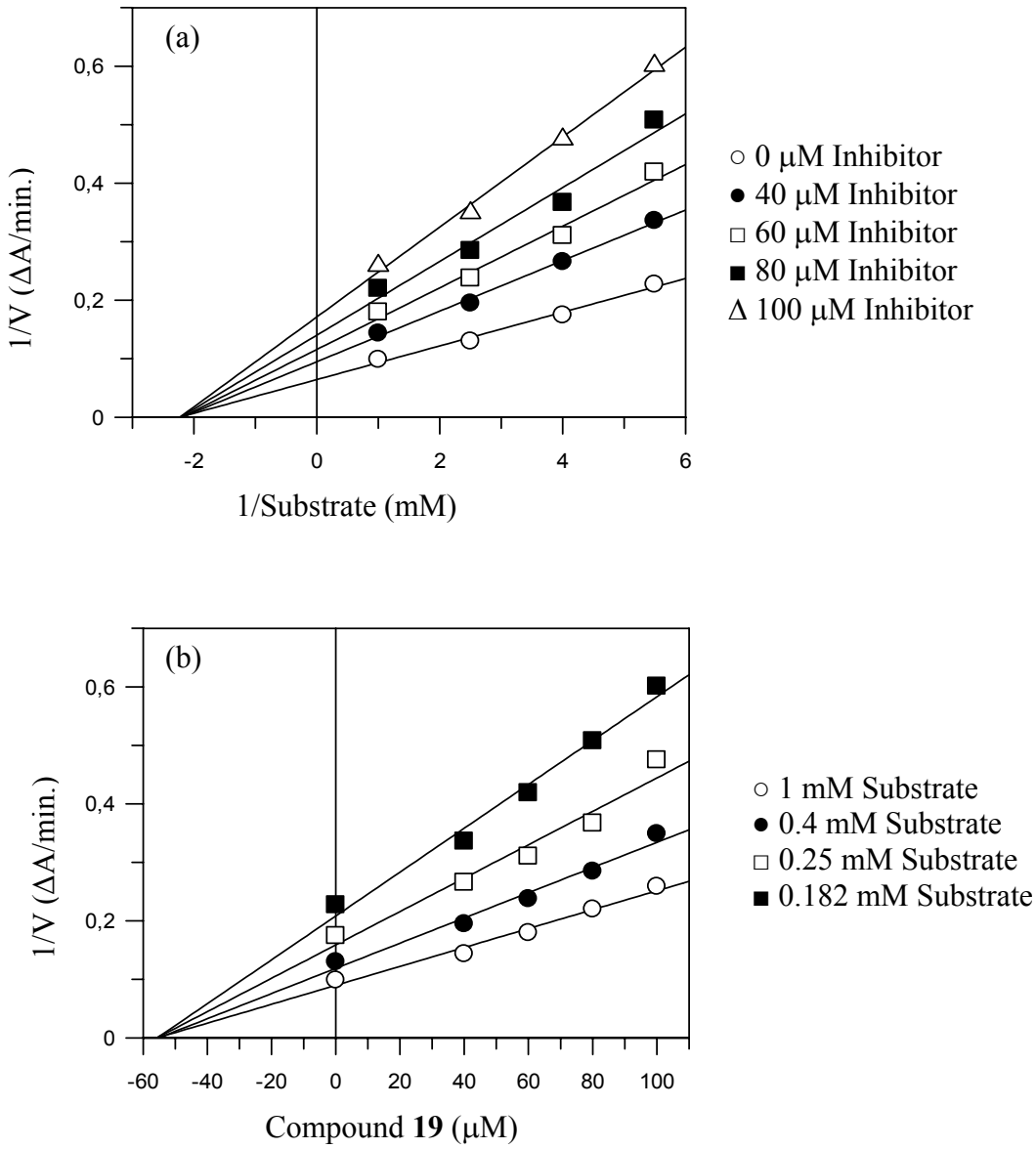

Figure-4.36: Steady state inhibition of yeast α-glucosidase by compound **19**. (a) Lineweaver-Burk plot, reciprocals of initial reaction velocities versus various concentrations of substrate (PNP-G). (b) Dixon plot, reciprocals of initial reaction velocities versus different concentrations of compound **19**. Both plots show noncompetitive inhibition of yeast α-glucosidase by compound **19**.

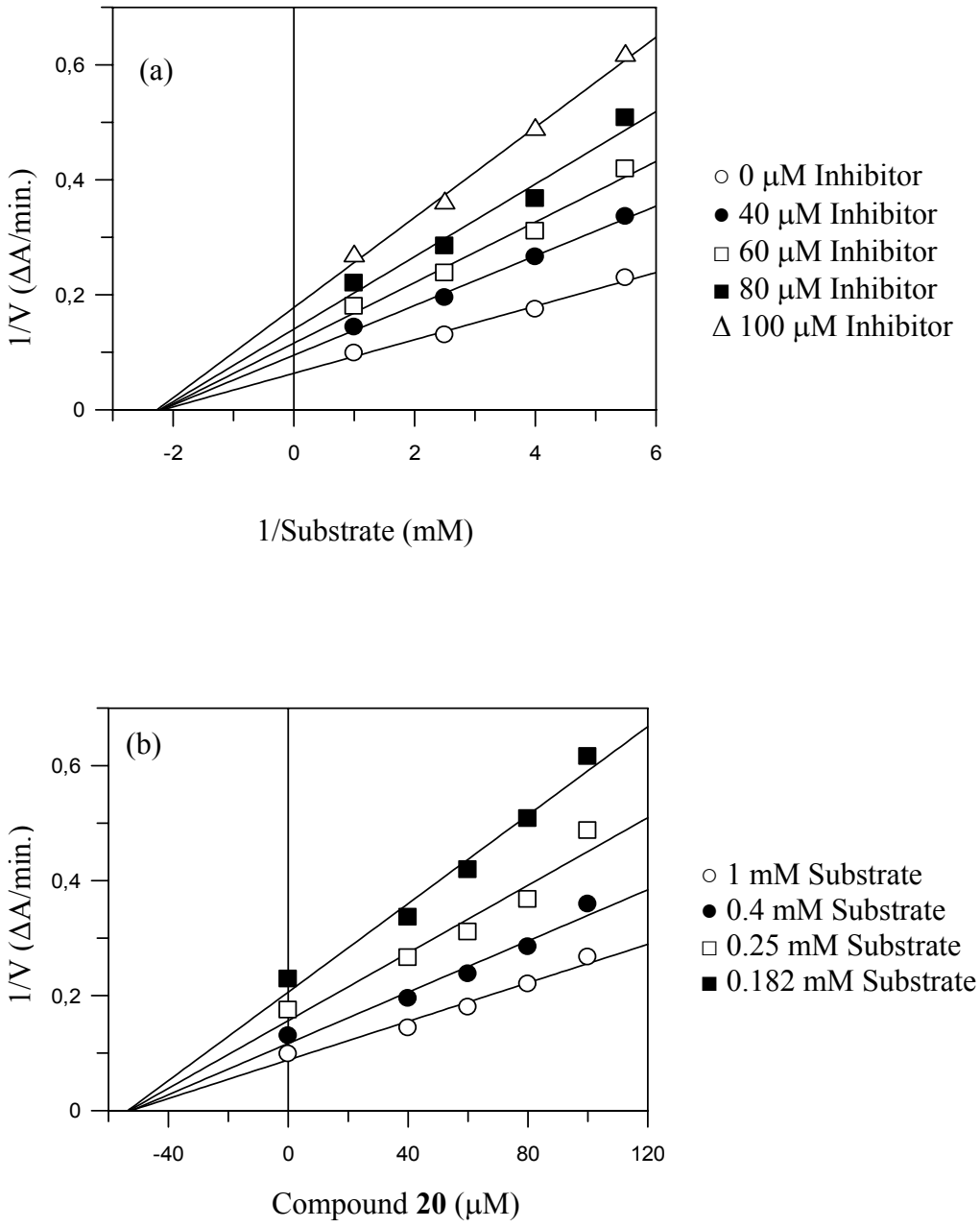

Figure-4.37: Steady state inhibition of yeast α-glucosidase by compound **20**. (a) Lineweaver-Burk plot, reciprocals of initial reaction velocities versus various concentrations of substrate (PNP-G). (b) Dixon plot, reciprocals of initial reaction velocities versus different concentrations of compound **20**. Both plots show noncompetitive inhibition of yeast α-glucosidase by compound **20**.

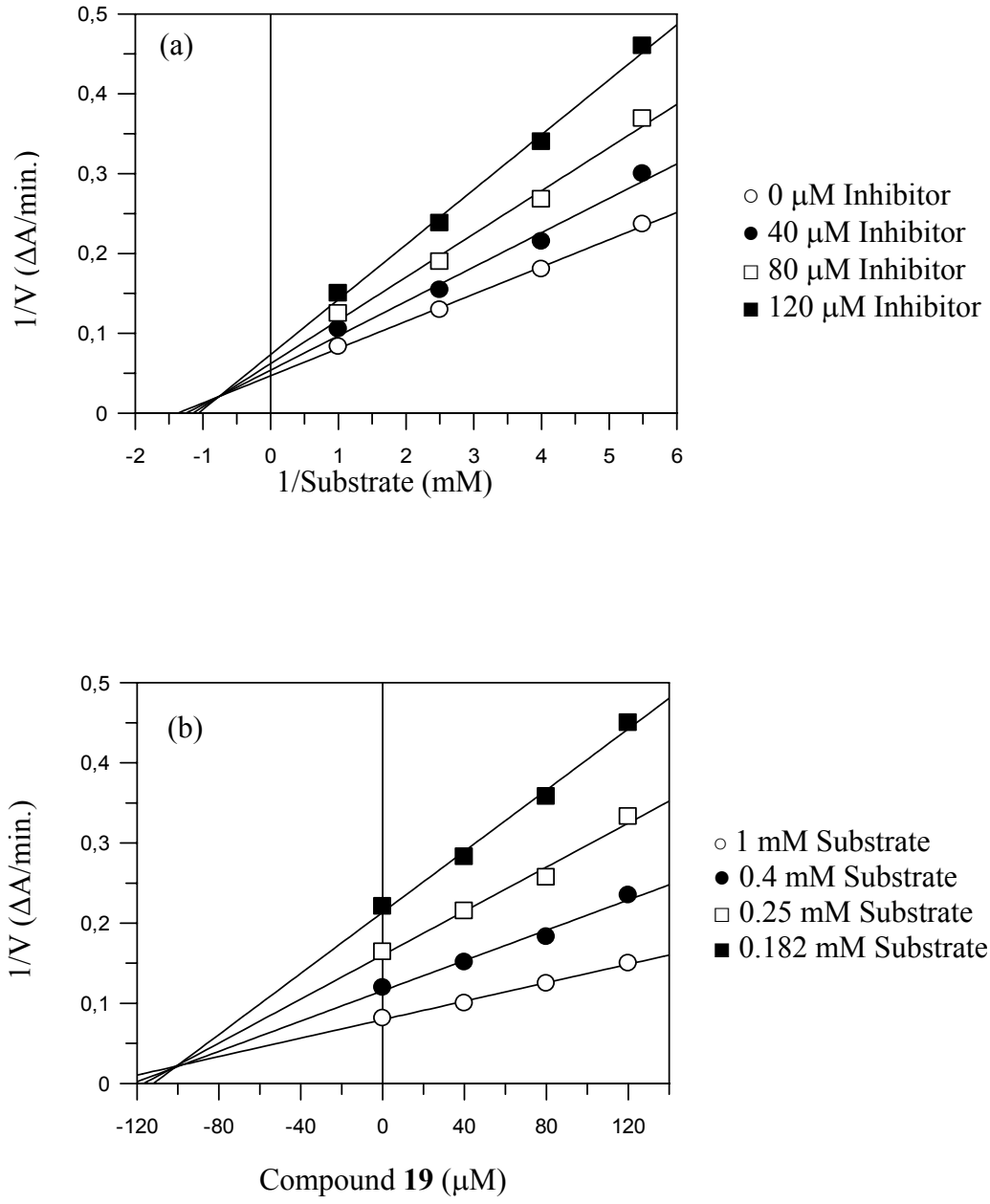

Figure-4.38: Steady state inhibition of intestinal α-glucosidase by compound **19**. (a) Lineweaver-Burk plot, reciprocals of initial reaction velocities versus various concentrations of substrate (PNP-G). (b) Dixon plot, reciprocals of initial reaction velocities versus different concentrations of compound **19**. Both plots show mixed-type inhibition of intestinal α-glucosidase by compound **19**.

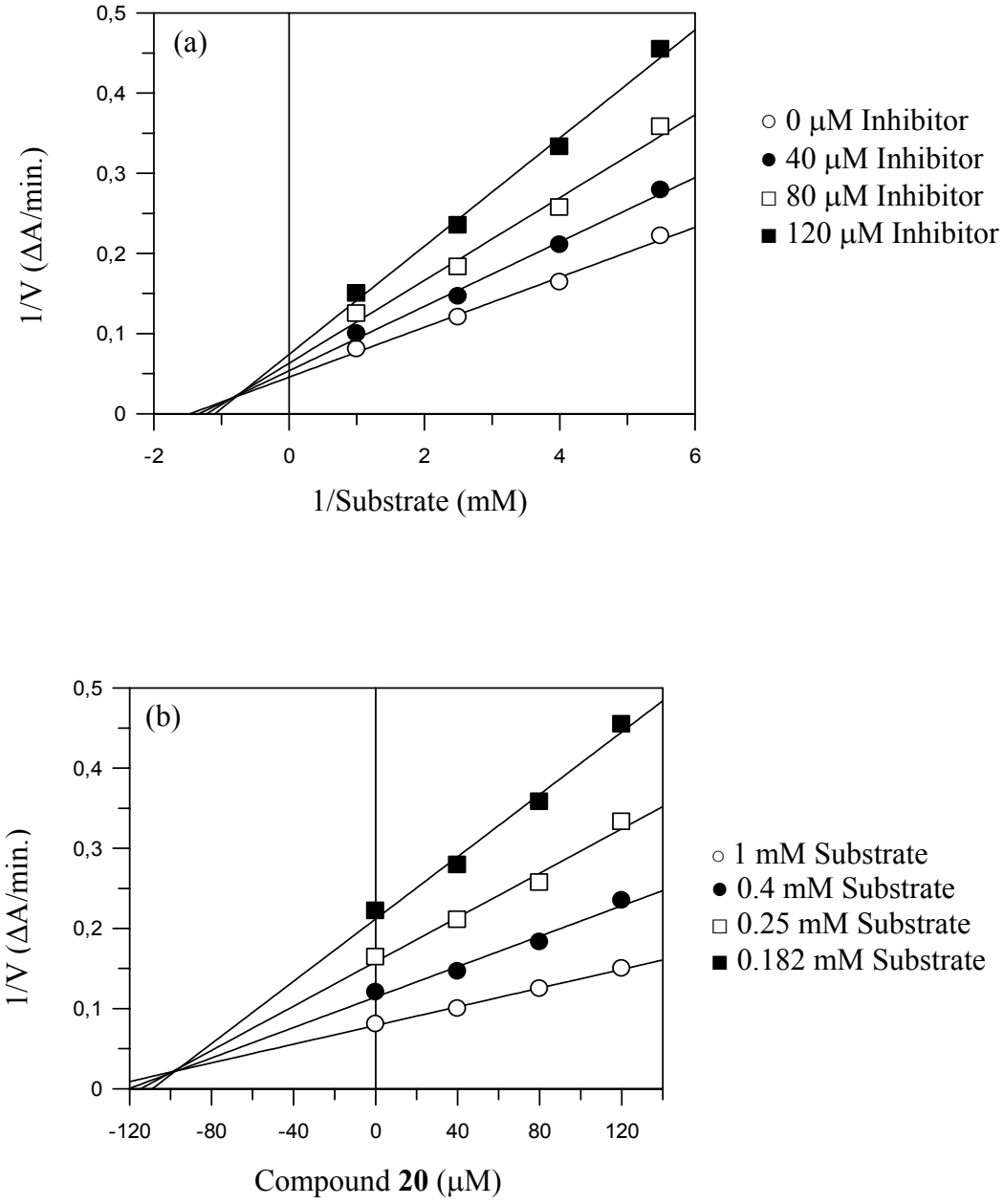

Figure-4.39: Steady state inhibition of intestinal α-glucosidase by compound **20**. (a) Lineweaver-Burk plot, reciprocals of initial reaction velocities versus various concentrations of substrate (PNP-G). (b) Dixon plot, reciprocals of initial reaction velocities versus different concentrations of compound **20**. Both plots show mixed-type inhibition of intestinal α-glucosidase by compound **20**.

Table-4.14: K_i values of two steroidal lactones against yeast and intestinal α-glucosidase enzymes. Every value represents the mean of three values.

Compounds	K_i (μM) ± SEM Yeast α-glucosidase	K_i (μM) ± SEM Intestinal α-glucosidase
19	53 ± 3.3	100 ± 6.1
20	51.5 ± 1.9	96 ± 5.3

SEM = standard error of the mean = standard deviation/√n, n = number of replicates for K_i values (n = 3).

Both of these steroidal lactones showed noncompetitive inhibition against the yeast α-glucosidase. Increased concentration of the compounds affected the V_{max} values but the K_m values of substrate remained unaffected. These compounds showed mixed-type inhibition against intestinal α-glucosidase. In this case, K_m as well as V_{max} values were affected in the presence of inhibitors (compounds **19** and **20**). IC_{50} and K_i values (Tables 4.13 and 4.14) of these compounds indicated that both of these compounds inhibit intestinal α-glucosidase with less affinity as compared to the yeast α-glucosidase. Compounds **19** and **20** do not have any structural similarity to maltose, substrate of α-glucosidase. Therefore, due to this dissimilarity these compounds were expected to inhibit α-glucosidase noncompetitively or through mixed type inhibition. Experimental results also suggested noncompetitive inhibition of yeast α-glucosidase and mixed type inhibition of intestinal enzyme by these steroidal lactones.

4.12.2 *In vivo* Studies on Steroidal Lactones as α-Glucosidase Inhibitors

In vivo studies on steroidal lactones were also conducted to determine their inhibitory activities in the animal models (see the methodology section). Effect of these compounds on increase in blood glucose levels is presented in Figure 4.40 and values of blood glucose levels at different time intervals after oral administration of these compounds are given in Table 4.15.

Both of these compounds showed slow rise, slow decline and lower maximum levels of blood glucose as compared to pathological control (Figure 4.40 & Table 4.15). This indicated the prolonged glucose absorption from intestine to blood that in turn could be attributed to the inhibition of maltase activity of intestinal α-glucosidase enzymes. This effect was not as

pronounced as in case of positive control. Nevertheless, these steroidal lactones showed the hypoglycaemic effect in animal models due to the inhibition of intestinal α-glucosidase enzymes and represent the another new class of compounds having inhibitory potential against yeast and intestinal α-glucosidase enzymes.

Table-4.15: Effect of steroidal lactones, **19** and **20**, on blood glucose levels at different time intervals, 0 minute, 30 minutes, 60 minutes, and 90 minutes after 1 mg/kg body weight maltose was orally given. These compounds were ingested separately 20 minutes prior to the oral dose of maltose.

	Blood glucose levels (mg/dL) at different time intervals			
Groups of animals	**0-times**	**30-minutes**	**60-minutes**	**90-minutes**
Normal control	89.5 ± 2.3	90.5 ± 3.0	87.5 ± 1.47	87.2 ± 2.63
Pathological control	80.7 ± 1.6	117.5*± 1.3	105.25*± 1.63	90.5*± 2.16
Administered with compound **19**	89 ± 3.7	112.2 ±*2.9	102.2*± 4.03	95 ± 4.18
Administered with compound **20**	98.7 ± 3.4	120.5*± 4.2	109.6* ± 3.68	103.7 ± 4.10
Positive control (acarbose)	87.8 ± 3.8	104.2*± 7.9	99.5 ± 3.58	91.2 ± 4.32

Each value represents the mean of six ± SEM. *P< 0.05, significantly different from the zero time observation.

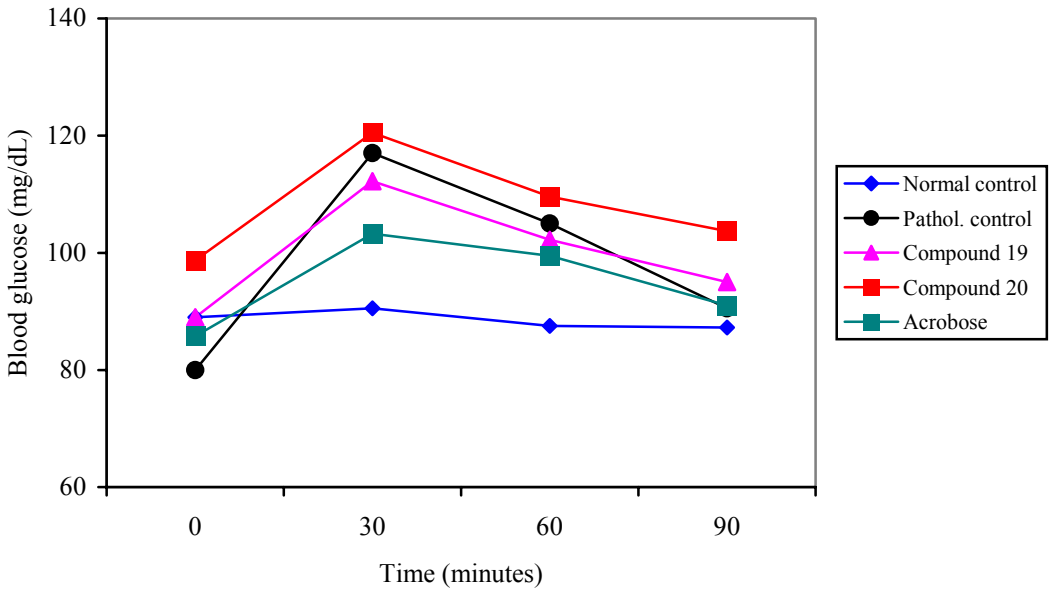

Figure-4.40: Effect of compounds **19** and **20** on blood glucose rise in maltose-loaded rats. Compounds were orally given 20 minutes prior to the maltose dose

5 Summary

In this thesis, binding of small ligand effectors with bio-macromolecules has been investigated. Studies were conducted on the effectors of two types of bio-macromolecules, $tRNA^{Phe}$ and α-glucosidase enzymes.

5.1 Investigation of complexes of Aminoglycosides with $tRNA^{Phe}$

This work presents the investigations of complexes of three aminoglycosides of the neomycin B family, neamine, ribostamycin and neomycin B with $tRNA^{Phe}$. Goal of these studies was to determine the bioactive conformations of these aminoglycosides by trNOE methodology.

Before performing trNOE experiments, the conditions were optimized to minimize the electrostatically driven unspecific interactions between positively charged aminoglycosides and negatively charged RNA backbone. The unspecific interactions were significantly minimized using high concentrations of Mg^{2+} ions and the experimental protocol was carefully validated with other techniques (SPR and CD). Then the NMR experiments with free aminoglycosides were performed and the obtained results were found similar to the reported results. These results suggested the large degree of conformational flexibility in the aminoglycosides. Comparison of NOE results of free aminoglycosides with those obtained by trNOE experiments with the mixtures of aminoglycosides with $tRNA^{Phe}$, formed the basis for the determination of bioactive conformations of these molecules. TrNOE experiments suggested the conformer selection in all aminoglycosides during binding. In order to determine the $tRNA^{Phe}$-bound conformations of aminoglycosides, inter hydrogen atom distances were extracted from the trNOE build up curves and these distances were used in MD simulations as constraints. All the aminoglycosides were found with identical $tRNA^{Phe}$-bound conformations at G/S glycosidic linkage (neamine moiety). However, the conformational space at the R/S glycosidic linkage being bound by $tRNA^{Phe}$ was found different in ribostamycin and neomycin B which could be attributed either to a steric repulsion or interaction of idose ring of neomycin B with $tRNA^{Phe}$. In order to determine the binding epitopes of these aminoglycosides, STD experiments were performed. These experiments were not successful. Failing of the STD experiments could be the low density of hydrogen atoms in RNA structure that might not be sufficient for saturation transfer to the ligand. Finally, the comparison of trNOE-derived $tRNA^{Phe}$-bound conformation of neomycin B with its structure from crystal was made. It was found that all the key polar groups of the

neamine moiety, which are involved in hydrogen bonds and electrostatic interactions with RNA, occupy the same positions in three-dimensional space in both structures.

The presented results, confirmed the positions of the key polar groups in the neamine part of the crystal structure, led to correct the configuration errors in the crystal structure of neomycin B and validated the experimental approach to avoid the unspecific interactions between aminoglycosides and RNA. This work successfully transferred the trNOE methodology to RNA-aminoglycoside complexes and presents an important lead for future work with such complexes to get insight into the interactions of ligands with RNA targets which in turn will be very useful for drug discovery.

5.2 Inhibition Studies on α-Glucosidase Enzymes

This work presents the inhibition of α-glucosidase enzymes from two different sources, yeast and rat intestine, by three classes of compounds, sesquiterpenoid derivatives, oleanolic acid derivatives and steroidal lactones. Initial screening of potential inhibitors was followed by the determination of their IC_{50} values. Subsequently, the kinetic parameters of these inhibitors were determined by Michaelis-Menten kinetics, which provided the information about the binding mode and binding affinities of these compounds to the enzymes. All the compounds inhibited the yeast enzyme noncompetitively except four sesquiterpenoid derivatives, which showed mixed-type inhibition. Oleanolic acid derivatives were found to be inactive against intestinal α-glucosidase however, they showed potent inhibitory potential against yeast α-glucosidase. Sesquiterpenoid derivatives and steroidal lactones inhibited both yeast and intestinal α-glucosidases. Their mode of inhibition of intestinal enzyme was found to be the mixed-type. These compounds showed a potent inhibitory potential against yeast enzyme with K_i values in lower micromolar range but they inhibited intestinal enzyme with comparatively weaker affinities. Sesquiterpenoid derivatives and steroidal lactones were then subjected to toxic studies in DNA damaging assay and brine shrimp lethality assay. These compounds were found to be non-toxic in both assays. Finally, these inhibitors were subjected to *in vivo* studies to determine their effect on serum glucose levels in maltose-loaded rats. All of these compounds showed hypoglycaemic effect in rat models. Their hypoglycaemic effect was not as significant as was observed in case of standard drug, acarbose but still significant enough to justify further studies as new classes of α-glucosidase inhibitors keeping in view the therapeutic significance of α-glucosidase inhibitors.

6 Methodology

6.1 NMR Spectroscopy

6.1.1 Sample Preparations

6.1.1.1 Aminoglycoside Samples

Ribostamycin and neomycin B were purchased from Sigma-Aldrich and neamine was a gift from Professor B. Westermann (Halle). 25 mM of each aminoglycoside was dissolved in D_2O (Sigma-Aldrich) and lyophilized three times. Tris buffer (40 mM tris, pH 7.2, 20 mM NaCl) was prepared with H_2O, lyophilized and redissolved in D_2O five times (pD not corrected for kinetic isotope effect). After optimizing the buffer conditions, 30 mM $MgCl_2$ after its deuteration was added to tris buffer. Finally, the aminoglycosides were dissolved in this deuterated tris buffer for NMR experiments.

6.1.1.2 Aminoglycosides $tRNA^{Phe}$ Samples

Phenylalanine specific transfer RNA ($tRNA^{Phe}$ 25.2 kDa) from yeast was purchased from Sigma-Aldrich. $tRNA^{Phe}$ was first dialyzed against millipore water to remove all salts and additives using Pierce membrane with a 3.5 kDa exclusion size. The RNA was then dissolved in deuterated buffer and aminoglycoside was added. This solution was then lyophilized and redissolved in D_2O three times. Every sample was prepared containing 25 µM $tRNA^{Phe}$ and 375 µM aminoglycoside (1:15) in 600 µl deuterated tris buffer as described above.

6.1.2 NMR Experiments

All the NMR measurements were done at 308 K. Data acquisition and processing were performed with XWINNMR software (Bruker). Chemical shifts were calibrated relative to the internal reference, 3-(trimethylsilyl) propionic acid (TSP).

6.1.2.1 NMR Experiments with Free Aminoglycosides

All NMR experiments with free aminoglycosides were performed on Bruker Avance DRX 500 spectrometer (Institute of Chemistry, University of Luebeck, Germany) which was operating at 500.25 MHz. One-dimensional ^1H spectra were acquired with 10 ppm spectral

width, 16 k data points and 64 scans. TOCSY spectra were acquired with 2 k data points, 512 increments and 16 scans using the MLEV17 sequence. A mixing time of 60 ms, 12 dB power level for TOCSY spin-lock and -3 dB power level for 90º pulse was used. COSY spectra were acquired with 2 k data points, 512 increments and 16 scans. For NOESY experiments, the standard NOESY pulse sequence was used. All NOESY experiments were performed with 4096 data points, 512 increments, 32 scans and 900 ms mixing time and 10 ppm spectral width. Two-dimensional data were zero-filled to give a 4096 × 1024 data matrix before fourier transformation that used a squared cosine function for apodisation.

6.1.2.2 NMR Experiments with Aminoglycoside-tRNA^{Phe} Complexes

All NMR spectra of mixtures of neamine tRNA^{Phe} and ribostamycin tRNA^{Phe} were acquired on a DRX 700 spectrometer (Bruker) equipped with a cryoprobe at the Institute of Chemistry University of Hamburg, Germany. The NMR spectra of the neomycin B tRNA^{Phe} mixture were acquired on a DRX 600 spectrometer (Dr. Till Maurer, Boehringer, Ingelheim). The standard NOESY pulse sequence with an additional watergate sequence was used to suppress the residual water signal (Piotto *et al.*, 1992). All NOESY spectra of the complexes were acquired with 4096 data points, 512 increments, 32 scans and 3 s recycling delay. TrNOE spectra of different mixing times, 50, 100, 150, 200 and 250 were acquired to obtain trNOE build up curves for every complex. TrROE spectra were acquired with 150 ms spin lock, 4096 data points and 512 increments using standard ROESY sequence with an additional watergate sequence.

6.1.2.3 Integration and Distance Determination

Volumes of the trNOE cross peaks were obtained from the spectra with the program, Sparky (Goddard and Kneller). The resulting data points were fitted to an exponential function of the form $f(t) = a(1-e^{-bt})$ where a and b were adjustable parameters and t the experimental mixing time. Initial slopes of the curves were determined from the first derivative of the function ($f(0) = a \times b$) and were used to calculate the experimental inter hydrogen atom distances with the isolated two spin approximation (Weimar *et al.*, 2000). using the H1G-H2G (Figure 1.1) distance of 2.45 Å as reference. In case of the trNOE effects H1G-H5S and H2R-H6S, which were very small at low mixing time, the integration was performed from one dimensional cross-sections of the two dimensional spectra. The areas from signals in these one-dimensional spectra were obtained using mixed Gaussian/Lorentzian line deconvolution. Subsequently, inter hydrogen atom distances were calculated through an isolated two spin

approximation using the area of the cross peak H1G-H2G as reference. Another intra ring hydrogen atom distance, H5S-H3S (Figure 1.1) was used as calibration distance besides H1G-H2G and experimental error for the distance determination was found to be 0.3 Å.

6.1.2.4 STD Experiments

One-dimensional STD experiments with aminoglycosides $tRNA^{Phe}$ mixtures were performed on DRX 500 and DRX 700 spectrometer an STD pulse sequence with an additional watergate sequence (Mayer & Meyer, 1999). Train of Gausian pulses of 50 ms length each separated by 1 ms delay were used to selectively saturate the aromatic region (7.4 ppm) of RNA resonances. In different experiments, different duration of saturation (0.5, 1, 2 and 3 s) was used by adjusting the numbers of selective pulses. The on-resonance irradiation of the RNA was done at chemical shift of 7.3 ppm and off-resonance irradiation was applied at 40 ppm. Subtraction of the 1D STD was performed internally by phase cycling after every scan.

6.2 Molecular Modelling and MD Simulations

All calculations were performed with Sybyl (Tripos) on SGI computers using the standard Tripos force field (Sybyl). To obtain potential energy maps of the aminoglycosides, grid search calculations were performed in which the glycosidic torsion angles ϕ and ψ were allowed to vary at 20° intervals over the complete conformational space. Isothermal contours were plotted by interpolation at 1 kcal/mol intervals relative to the global minimum energy conformation defined to be at 0 kcal/mol up to 10 kcal/mol. The glycosidic torsion angles ϕ and ψ in all three molecules were defined as under:

For G/S glycosidic linkage

ϕ = H1G-C1G-O-C4S ψ = C1G-O-C4S-H4S

For R/S glycosidic linkage

ϕ = H1R-C1R-O-C5S ψ = C1R-O-C5S-H5S

For I/R glycosidic linkage

ϕ = H1I-C1I-O-C3R ψ = C1I-O-C3R-H3R

Constraint MD simulations of aminoglycosides started from different low energy conformations. Protonation of amino groups were followed by conjugate gradient

minimization for 1000 iterations. The distance derived from trNOE experiments were used as constraints with ± 0.3 Å range and a force constant of 600 kcal/mol $Å^{-1}$. Simulations were carried out *in vacuo* using a dielectric constant of 40.00. Equilibration was obtained by increasing the temperature from 50 K in steps of 50 K to 300 K during 2 ps each. The simulations continued at a temperature parameter of 300 K for 1 ns with a step of 1 fs. Snapshots were taken after every 2 ps (James & Engin, 1997).

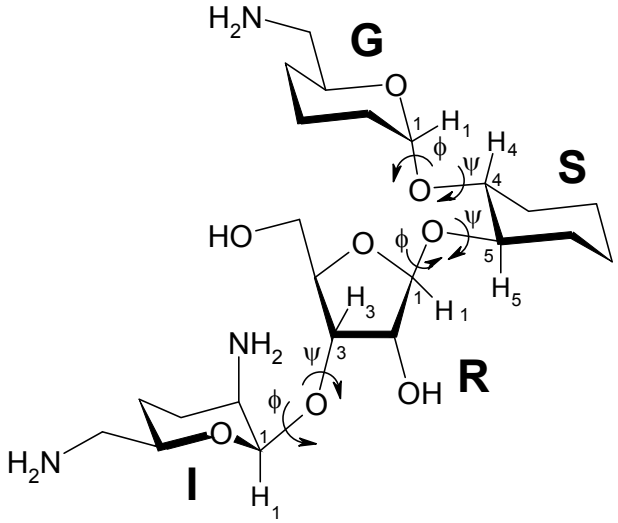

Figure-6.1: Schematic representation of the carbohydrate skeleton of neomycin B with the torsion angles discussed in the text.

6.3 Circular Dichroism (CD) spectroscopy

Samples were heated prior to each titration to 85° C for 2 min. and equilibrated to room temperature for 5 min. CD spectra were acquired with a Jasco J-715 spectrapolarimeter equipped with a thermoelectrically controlled cell holder in the continuous wave mode. A quartz cell with a path length of 0.5 cm was used. Three spectra were averaged with a spectral width from 320 to 220 nm at 1 nm resolution, a time constant of 1 s and a scan speed of 50 nm min^{-1}. Experiments were carried out with 200 µl samples (8 µM $tRNA^{Phe}$, Tris-HCl, pH 7.2) at 308 K. During the titrations, reagents (aminoglycosides and salts) were added in 1 µl volumes. Following each addition of reagents the samples were allowed to equilibrate for 5 min prior to the acquisition of the CD spectra. After baseline correction the spectra were scaled to take the dilution into account and normalized to the number of nucleotides of $tRNA^{Phe}$.

6.4 Determining the Ribose Ring Puckering

The conformation of the ribose ring in ribostamycin and neomycin B was determined by determining the phase angle of the ribose ring from 1 ns molecular dynamics simulations of these two molecules. The phase angle is defined as (IUPAC-IUB Joint Commission on Biochemical Nomenclature):

$$\text{Phase angle} = \tan^{-1}\left[\frac{(\nu 4 + \nu 1) - (\nu 3 + \nu 0)}{2\nu 2(\sin 36^\circ + \sin 72^\circ)}\right]$$

The torsion angles are defined as in the following figure

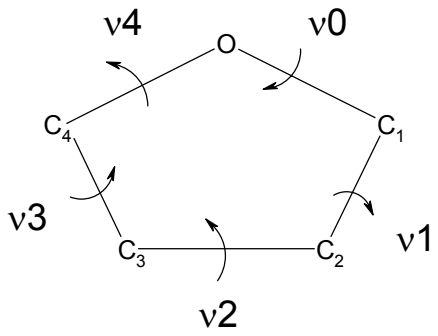

Figure-6.2: Ribose ring with details of the torsion angles used to define the phase angle of the ring.

The phase angle was calculated also from the constraint MD simulation of these two aminoglycosides to determine the ribose ring conformation in their $tRNA^{Phe}$-bound state.
Inhibition study against α-glucosidase enzymes from two different sources, yeast and rat intestine were carried out in following stages:

6.5 *In vitro* Enzyme Assays

6.5.1 For Yeast α-Glucosidase

Method reported by Matsui *et al*. was used with slight modifications (Matsui *et al.*, 1996). α-Glucosidase (EC 3.2.1.20) from yeast and substrate *p*-nitrophenyl-α-D-glucopyranoside (PNP-G) were purchased from Sigma. Enzyme and substrate solutions were prepared with 100 mM sodium phosphate buffer containing 50 mM sodium chloride (pH 6.8). 0.017 Units/ml enzyme and 0.7 mM substrate were adjusted as the final concentrations in the reaction mixture. Enzyme-catalyzed reaction was studied with a spectrophotometer, micro-titer plate reader (Molecular Devices USA). The change in absorption observed at 400 nm due to the hydrolysis of PNP-G by α-glucosidase was monitored continuously with one-minute interval in 96-well plate. Increase of absorption was considered as function of enzyme activity as enzyme hydrolyses the PNP-G to release *p*-nitorphenolate ion (Figure 6.3). Temperature was maintained at 37^{o} C during the experiment.

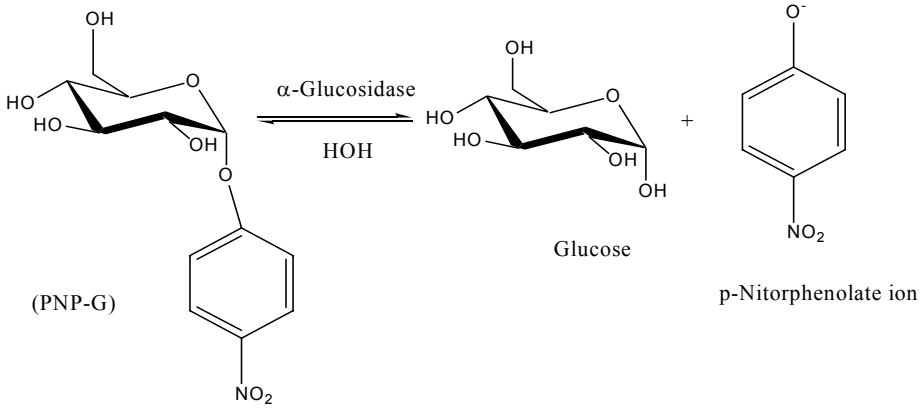

Figure-6.3: Mechanism of hydrolysis of PNP-G by α-glucosidase.

Change of optical density (OD) per unit time was considered as rate of reaction. During the inhibition study, enzyme was incubated with the test compound for 15 minutes before adding the substrate to this solution. After that, the reaction was monitored for 30 minutes. Every reaction was carried out in triplicate and control was taken as enzyme-catalyzed reaction in the absence of any inhibitor. Percentage inhibition of enzyme by the test compounds was calculated with the formula:

$$\% \text{ Inhibition } = 100 - \left[\frac{\text{Rate of reaction for the test sample}}{\text{Rate of reaction for the control}} \times 100 \right]$$

6.5.2 For Intestinal α-Glucosidase

For intestinal α-glucosidase inhibition, rat intestinal acetone powder (Sigma) was used following the method of (Oki *et al*., 1999).

6.5.2.1 Preparation of α-Glucosidase Solution from Rat Intestinal Acetone Powder

100 mg Intestinal acetone powder was added to 3 ml of 0.9 % NaCl solution and sonicated for 30 seconds 12 times in ice bath. Subsequently, it was subjected to centrifugation at 11,000 rpm for 30 minutes and resultant supernatant was collected and directly used for inhibitory assay. Same inhibition assay was used, as described in previous section.

6.6 Determination of the Validity of *In vitro* Assays

1-Deoxynojirimycin and acarbose were used as positive controls in the inhibition assay of yeast α-glucosidase and intestinal α-glucosidase, respectively. IC_{50} value of 1-deoxynojirimycin was determined (0.3 mM) and found to be similar to the value reported by (Asano *et al.*, 1994). The IC_{50} value of acarbose was also determined (50 μM) and found to be the similar as reported by (Oki *et al*., 1999). Reproduction of the reported result provided better validity of the enzyme assays.

6.7 Determination of IC_{50} Values

Concentrations of inhibitors that inhibit the hydrolysis of PNP-G by 50 % (IC_{50}), by enzyme, were determined by monitoring the effect of different concentrations of inhibitors on percentage inhibition and were calculated by EZ-Fit enzyme kinetics software.

6.8 Kinetic Studies

In order to determine the mechanism of inhibition of different compounds, Michaelis Menten kinetics was conducted. K_m value of the substrate (PNP-G) was determined by Lineweaver-Burk plot where reciprocals of initial rates of enzymatic reactions were plotted against reciprocals of four different concentrations of substrate (0.182 mM, 0.25 mM, 0.4 mM and 1 mM). The K_m value of the substrate was determined as 0.5 mM ± 0.03. Then the experiments were performed with different concentrations of test compounds as inhibitors in combination with each of four concentrations of substrate, in triplicate and the effect of these inhibitor concentrations on K_m and V_{max} values was determined through Lineweaver-Burk plot (Segel, 1993). Type of inhibition determined was further confirmed by the Dixon plot where different

concentrations of inhibitors were plotted against reciprocals of initial rates of enzyme-catalyzed reactions (Dixon, 1953). K_i (dissociation constant for enzyme inhibitor complex) values were determined from the intercept of all the lines on x-axis in Dixon plot.

6.9 Determination of Toxicity of the Active Compounds

Following two methods were used to determine the toxicity of test compounds:

a) Brine shrimp lethality assay

b) DNA damaging assay

6.9.1 Brine Shrimp Lethality Assay for Cytotoxicity

Eggs of the brine shrimp, *Artemia salina*, were purchased from the market as fish food. 50 mg of these was sprinkled on filtered brine solution (38 g/l of sea salt in distilled water, pH 7.4) and incubated at 37^{o}C. This process was done in a hatching tray (rectangular dish with perforated partitions). Test compounds were taken with three concentrations, 10 μg/ml, 100 μg/ml and 1000 μg/ml in separate vials and the organic solvent was allowed to evaporate overnight. Two days after the hatching 10 larvae/vial were placed along with 5 ml seawater per vial. All these were incubated at 25 to 27^{o} C under illumination along with the negative control containing only solvent and positive control containing cytotoxic compound, etoposide (Harwig & Scott, 1971).

6.9.2 DNA Damaging Micro Titer Assay

DNA damaging effect of active compounds was determined by using *Saccharomyces cerevisiae* strains, LF15 and RS322Y following the reported methods (Sancar *et al.*, 1995). These two strains were grown in YPD media overnight and adjusted to the following values of OD at 600 nm: LF15 (0.001 OD) and for RS322Y (0.01 OD). 5 μL of the test compound (after dissolving in 5 % MEOH) was mixed with 100 μL of YPD broth and added in 96-well flat bottom micro-titer plate. Then 95 μL of yeast suspension was added to all wells of the plate, which was then incubated at 30^{o}C for 24-48 hours. The plate was read at 600 nm on micro plate reader. Any compound that was showing >65% inhibition against the yeast RS322Y and >35% inhibition against yeast LF15 was considered a primary hit and retested in concentration response. Camptothecin was used as positive control for DNA damaging effect (Sancar *et al.*, 1995).

6.10 *In vivo* Inhibition Studies on α-Glucosidase Enzymes

6.10.1 Selection of Animals

Adult male rats weighing 100-120 gm from the animal house of the HEJ Research Institute of Chemistry were selected and housed in clean wire mesh cages. The animals were kept at 25^{o} C ± 2. Their normal diet was discontinued and they were starved for 18-20 hours prior to the experiments. Only water was provided *ad libitum*.

6.10.2 Biological Assay

During the *in vivo* experiments, 10 mg/kg body weight test samples were orally administered twenty minutes prior to the maltose dose of 1 g/kg body weight. Acarbose was orally given to the positive control group animals and saline was given to the pathological control group instead of test samples prior to the maltose dose. Normal control group animals were given only saline in the beginning and were not given any maltose. Blood was drawn from tail vein at every 30 minutes interval up to 90 minutes after oral administration of maltose. Blood glucose levels were determined using glucometer (Glucotrend® 2-Roche). Data obtained were statistically analysed. The significant values ($p< 0.05$) were assessed by performing T-test (one-way ANOVA) (Ye *et al.*, 2002).

Few experiments were also performed with glucose-loaded rats with the procedure described in previous paragraphs.

7 References

Akasaka, K., Konrad, M., Goody, R. S. (1978). Selective spin diffusion: A novel method for studying motional properties of biopolymers in solution. *FEBS Lett.*, **96**, 287-290.

Ali, M. S., Jahangir, M., Shahazad ul Hussan, S. and Choudhary, M. I. (2002). Inhibition of α-glucosidase by oleanolic acid and its synthetic derivatives *Phytochemistry*, **60**, 295-299.

Arepalli, S. R., Glaudemans, C. P., Daves, G. D. Jr., Kovac, P. and Bax, A. (1995). Identification of protein-mediated indirect NOE effects in a disaccharide-Fab' complex by transferred ROESY. *J. Magn. Reson. B.*, **106**, 195-8.

Arshag, D. M. and Jerome, E. T. (1999). Drug therapy of postprandial hyperglycaemia. *Drugs*, **57**, 19-29.

Asano, N., Oseki, K., Kaneko, E. and Matsui, K. (1994). Enzymatic synthesis of α and β-D-glucosides of 1-deoxynojirimycin and their glycosidase inhibitory activities. *Carbohydr. Res.*, **258**, 255-266.

Asensio, J. L., Hidalgo, A. Cuesta, I., Gonzalez, C., Canada, J., Vicent, C., Chiara, J. L., Cuevas, G. and Jimenez-Barbaero, J. (2002). Experimental evidence for the existence of non-exo-anomeric conformations in branched oligosaccharide: NMR analysis of the structure and dynamics of aminoglycosides of the neomycin family. *Chemistry*, **8**, 5228-5240.

Atta-ur-Rahman, Shabbir, M., Dur-e-Shahwar, Choudhary, M. I., Voelter, W. and Hohnholz, D. (1998). New Steroidal Lactones from *Withania coagulance. Heterocycles*, **47**, 1005-1012.

Balandrin, M. F., Kinghorn, A. D. and Fransworth, N. R. (1993). In: *Human medicinal agents from plants*. Symposium series No 531, American chemical society, Washington D. C., 2-12.

Barat, L. M. and Bloland, P. B. (1997). Drug resistance among malaria and other parasites. *Infect. Dis. Clin. North. Am*., **11**, 969-987.

Bischoff, H. (1994). Pharmacology of α-glucosidase inhibition. *Eur. J. Clin. Invest.*, **24**, 2-10.

Blanchard, S. C., Fourmy, D., Eason, R. G. and Puglisi, J. D. (1998). rRNA chemical groups required for aminoglycoside binding. *Biochemistry*, **37**, 7716-7724.

Botto, R. E. and Coxon, B. (1984). Two dimensional proton J-resolved NMR spectroscopy of neomycin B. *J. Carbohydr. Chem.*, **3**, 545-563.

Brownlee, M. (1992). Glycation products and the pathogenesis of diabetic complications. *Diabetes Care*, **15**, 1835-1843.

Bruce, H. R. W. and Timon, W. H. (1995). Prevention of complications in non-insulin-dependent diabetes mellitus. *Drugs*, **50**, 263-288.

Bush, A. C. and Martin-Paster, M. (1999). Structure and conformation of complex carbohydrates of glycoproteins, glycolipids, and bacterial polysaccharides. *Annu. Rev. Biophys. Biomol. Struct.*, **28**, 269-293.

Carter, A. P., Clemons, W. M., Brodersen, D. E., Morgan-Warren, R. J., Wimberly, B. T., and Ramakrishnan, V. (2000). Functional insights from the structure of the 30S ribosomal subunit and its interactions with antibiotics. *Nature*, **407**, 340-348.

Choudhary, M. I., Baig, I., Nur-e-Alam, M., Shahzad ul Hussan, S., Öndognii, P., Bunderya, M., Oyan, Z. and Atta-ur-Rahman (2001). New α-glucosidase inhibitors from the Mongolian medicinal plant *Ferula mongolica*. *Helv. Chim. Acta*, **84**, 2409-2416.

Claridge, T. D. W. (1999). High resolution NMR techniques in organic chemistry. Pergamon, an imprint of Elsevier Science, Amsterdam, New York and Tokyo.

Clouet-d'Orval, B., Stage, T. K. and Uhlenbeck, O. C. (1995). Neomycin inhibition of the hammerhead ribozyme involves ionic interactions. *Biochemistry*, **34**, 11186-11190.

Conner, C. S. (1985). β-Lactamase inhibitors. *Drug. Intell. Clin. Pharm.*, **19**, 475-6.

DeFronzo, R. A., Bonadonna, R. C. and Ferranini, E. (1992). Pathogenesis of NIDDM: a balanced overview. *Diabetes Care*, **15**, 737-768.

Dixon, M. (1953). *Biochem. J.*, **55**, 170-171.

Domschke, S. and Erdmann, W. D. (1969). Trial of a new antidotal principle to experimental poisoning with DFP. *Arch. Toxikol.* **25**, 127-39.

Donald, V. and Judith, G.V. (1990). In: *Biochemistry*, John Wiley and Sons, New York, pp. 328.

EZ-Fit: Enzyme Kinetics, version 5.03, Perrella Scientific Inc., Amherst, NH 03031, USA

Forge, A. and Schacht, J. (2000). Aminoglycosides antibiotics. *Audiol. Neurootol.*, **5**, 3-22.

Frank, R. N. (1994). The aldose reductase controversy. *Diabetes*, **43**, 169-172.

Goddard, T. D. and Kneller, D.G., SPARKY 3, University of California, San Francisco

Guerrier-Takada, C., Gardiner, K., Marsh, T., Pace, N. and Altman, S. (1983). The RNA moiety of ribonuclease P is the catalytic subunit of the enzyme. *Cell*, **35**, 147-157.

Harms, J., Schluenzen, F., Zarivach, R., Bashan, A., Gat, S., Agmon, I., Bartels, H., Franceschi, F. and Yonath, A. (2001). High resolution structure of the large ribosomal subunit from a mesophilic eubacterium. *Cell*, **107**, 679-688.

Harwig, J. and Scott, P. M. (1971). Brine shrimp (*Artemia salina* L.) larvae as a screening system for fungal toxins. *Appl. Microbiol.*, **21**, 1011-1016.

Holt, P. R., Atillasoy, E. and Lindenbaum, J. (1996). Effect of acarbose on fecal nutrients, colonic pH, and short chain fatty acids and rectal proliferative indices. *Metabolism*, **45**, 1179-1187.

Howard, S. and Wither, S. G. (1998). Labeling and identificaion of the postulated acid/base catalyst in the α-glucosidase from saccharomyces cerevisiae using a novel bromoketone C-glycosides. *Biochemistry*, **37**, 3858-3864.

IUPAC-IUB Joint Commission on Biochemical Nomenclature, Abbreviations and Symbols for the Descriptions of Conformations of Polynucleotide Chains.

Izaki, K. Matsuhashi, M. and Strominger, J. L. (1966). Glycopeptide-transpeptidase and D-alanine carboxypeptidase, penicillin-sensitive enzymatic reactions. *Proc. Natl. Acad. Sci. U.S.A.*, **55**, 656-663.

Jackman, L. M. and Cotton, F.A. (1975). Dynamic NMR spectroscopy, Academic Press, London and New York.

James, R. C. and Engin, H. S. (1997). Biologically important conformation of aminoglycoside antibiotics bound to an aminoglycoside 3'-phosphotransferase as determined by trNOE. *Biochemistry,* **36**, 2353-2359.

Jarrett, R. J. (1989). Epidemiology and public health aspects of non-insulin-dependent diabetes mellitus. *Epidemiol. Rev*., **11**, 151-71.

Jiang, L., Majumdar, A., Hu W., Jaishree, T. J., Xu, W. and Patel, D. J. (1999). Saccharide-RNA recognition in a complex formed between neomycin B and an RNA aptamer. *Structure Fold. Des***.**, **7**, 817-827.

Joe, M. C. and Arshag, D. M. (2000). A rational approach to drug therapy of type-2 diabetes mellitus. *Drugs*, **60**, 95-113.

Johnson, J. H., Ogawa, A. and Chen, L. (1990). Underexpression of the β cell high K_m glucose tansporters in non-insulin-dependent diabetes. *Science*, **250**, 546-449.

Judson, H. F. (1980). In:The eighth day of creation. Simon and Schuster, New York.

Kalk, A. and Berendsen, H. J. C. (1976). Proton magnetic relaxation and spin diffusion in proteins, *J. Magn. Reson.*, **24**, 343-366.

Kim, S. J. (2002). Current problems of drug-resistant tuberculosis and its control. *Kekkaku*, **77**, 735-740.

Kirk, S. R. and Tor, Y. (1999). tRNA binds aminoglycoside antibiotics. *Bioorg. Med. Chem.*, **7**, 1979-1991.

Kojima, K., Ishaka, K., Mizukami, H., Ogihara, Y. and Öndognii, P. (1999). Sesquiterpnoid derivatives from *Ferula ferulioides*. *Tennen Yuki Kagobutsu Toronkai Koen Yoshishu*, **41**, 211-216.

Kojima, K., Ishaka, K., Öndognii, P., Jargalsaikhan, G., Suran D., Mizukami, H. and Ogihara, Y. (1998). Sesquiterpnoid derivatives from *Ferula ferulioides*. *Chem. Pharm. Bull.*, **46**, 1781-1784.

Kojima, K., Ishaka, K., Öndognii, P., Zevgeeiin, O., Davgiin, K., Mizukami, H. and Ogihara, Y. (1999). Sesquiterpnoid derivatives from *Ferula ferulioides*. *Chem. Pharm. Bull.*, **47**, 1145-1147.

Kruger, K. (1982). Self-splicing RNA: autoexcision and autocyclization of the ribosomal RNA intervening sequence of Tetrahymena. *Cell*, **31**, 147-157.

Kuritzkes, D. (2002). Drug resistance. Navigating resistance pathways. *AIDS Read.*, **12**, 395-400.

Leach, A. R. (1996). Molecular Modelling Principles and Applications, Longman, London**.**

Mahidol, C., Ruchirawat, S., Parawat, H. and Picha, P. (1998). Biodiversity and natural product drug discovery. *Pure Appl. Chem.*, **70**, 2065-2072.

Martin, E. and Patricia, A. M. (1996). Acarbose: An α-glucosidase Inhibitor, *Am. J. Health Syst. Pharm.*, **53**, 2277-2290.

Matsui, T., Yoshimoto, C., Osajima, K., Oki, T. and Osajima, Y. (1996). *In vitro* survey of α-glucosidase inhibitory food components. *Biosci. Biotechnol. Biochem.*, **60**, 2019-2022.

Mayer, M. and Meyer, B. (1999). Characterization of ligand binding by saturation transfer difference NMR spectroscopy. *Angew. Chem. Int. Ed*., **38**, 1784-1787.

Mayer, M. and Meyer, B. (2001). Group epitope mapping by saturation transfer difference NMR to identify segments of a ligand in direct contact with a protein receptor. *J. Am. Chem. Soc.*, **123**, 6108-6117.

McCarter, J. D. and Withers, S. G. (1996). Unequivocal identification of Asp-214 as the catalytic nucleophile of *saccharomyces cerevisiae* α-glucosidase using 5-fluoro glycosyl fluorides. *J. Biol. Chem.*, **271**, 6889-6894.

McKeegan, K. S., Borges-Walmsley, M. I. and Walmsley, A. R. (2002). Microbial and viral drug resistance mechanisms. *Trends Microbiol*., **10**, 8-14.

Mei, H-Y., Galan, A. A., Halim, N. S., Mack, D. P., Moreland, D. W., Sanders, K. B., Truong, H. N. and Czarnik, A. W. (1995). Inhibition of an HIV-1 Tat-derived peptide binding to TAR RNA aminoglycoside antibiotics. *Bioorg. Med. Chem. Lett.*, **5**, 2755-2760.

Mikkelsen, N. E., Johansson, K., Virtanen, A. and Kirsebom, A. (2001). Aminoglycoside binding displaces a divalent metal ion in a tRNA-neomycin B complex. *Nat. Struct. Biol*., **8**, 510-514.

Moore, P. B. and Steitz, T. A. (2002). The involvement of RNA in ribosome function. *Nature*, **418**, 229-235.

Neuhaus, D. and Williamson, M. (2000). The Nuclear Overhauser Effect in structural and conformational analysis, Wiley-VCH, New York.

Newcommer, A. D. and McGill, D. B. (1966). Distribution of disaccharidase activity in the small bowel of normal and lactase-deficient subjects. *Gastroenterology*, **51**, 481-488.

Noggel, J. H. and Schirmer, R. E. (1971). The Nuclear Overhauser Effect. Chemical Applications, Academic Press, New York.

Oki, T., Matsui, T. and Osajima, Y. (1999). Inhibitory effect of α-glucosidase, inhibitors varies according to its origin. *J. Agric. Food Chem.*, **47**, 550-553.

Overval, B. C.-d, Stage, T. K. and Uhlenbeck, O. C. (1995). Neomycin inhibition of the hammerhead ribozyme involves ionic interactions. *Biochemistry*, **34**, 11186-11190.

Overval, B. C.-d, Stage, T. K. and Uhlenbeck, O. C. (1995). Neomycin inhibition of the hammerhead ribozyme involves ionic interactions. *Biochemistry*, **34**, 11186-11190.

Papandreou, M. J., Barbouche, R., Guieu, R., Kieny, M. P. and Fenouillet, E. (2002). The alpha-glucosidase inhibitor 1-deoxynojirimycin blocks human immunodeficiency virus envelope glycoprotein-mediated membrane fusion at the CXCR4 binding step. *Mol. Pharmacol.*, **61**, 186-193.

Parthasarathy, R. and Kim, H. (1988). Conformation and sandwiching of bases by azido groups in the crystal structure of 3'-azido-3'-deoxy-thymidine (AZT), an antiviral agent that inhibits HIV reverse transcriptase. *Biochem. Biophys. Res. Commun.*, **152**, 1-8.

Piotto, M., Saudeck, V. and Sklenar, V. (1992). Gradient-tailored excitation for single-quantum NMR spectroscopy of aqueous solutions. *J. Biomol. NMR*, **2**, 661-665.

Puls, W. Bischoff, H. (1983). Delaying absorption as therapeutic principle in metabolic diseases. *Ludwig-Heimeyer-Symposium of the Gesellschaft für Fortschritte auf dem Gebiet der Inneren Medizin*, Thieme-Stratton Inc., New York, pp.70-78.

Reaven, G. M. and Chen, Y. D. (1988), Role of insulin in regulation of lipoprotein metabolism in diabetes. *Diabetes Metab. Rev*., **4**, 639-52.

Reddy, G. C. S., Ayengar, K. N. N. and Rangaswami, S. (1975). Triterpenoids of *Gardenia latifolia*. *Phytochemistry*, **14**, 307-311.

Robert, E. B. and Coxon, B. (1983). Nitrogen-15 nuclear magnetic resonance spectroscopy of neomycin B and related aminoglycosides. *J. Am. Chem. Soc.*, **105**, 1021-1028.

Rogers, J., Chang, A. H., von Ahsen, U., Schroeder, R. and Davies J. (1996). Inhibition of the self-cleavage reaction of the human hepatitis delta visus ribozyme by antibiotics. *J. Mol. Biol.*, **259**, 916-925.

Sancar, G. B., Ferris, R., Smith, F. W. and Vanberg, B. (1995). Promoter elements of the PHR1 gene of Saccharomyces cerevisieae and their roles in the response to DNA damage. *Nucleic Acids Res.*, **23**, 4320-4328.

Schmidt, D. D., Frommer, W., Junge, B., Muller, L., Wingender, W., Truscheit, E. and Schafer, D. (1977). α-Glucosidase inhibitors, new complex oligosaccharides of microbial origin. *Naturwissenschaften*, **64**, 535-536.

Segel, I. H. (1975). In: *Biochemical Calculations,* 2nd ed., John Willey and Sons Inc. New York, pp. 214.

Segel, I. H. (1993). Behavior and analysis of rapid equilibrium and steady state enzyme systems. In: *Enzyme Kinetics*, John Willey and Sons Inc., New York, pp. 120-140.

Segel, I. H. (1993). Behavior and analysis of rapid equilibrium and steady state enzyme systems. In: *Enzyme Kinetics*, John Willey and Sons Inc., New York, pp. 46-47.

Seiya, C. (1997). Molecular mechanism in α-glucosidase and glucoamylase. *Biosci. Biotechnol. Biochem.*, **61**, 1233-1239.

Semenza, G. (1986). Anchoring and biosynthesis of stalked brush border membrane proteins: Glycosidases and peptidases of enterocytes and renal tubuli. *Annu. Rev. Cell Biol.,* **2**, 255-313.

Stage, T. K., Hertel, K. J. and Ulenbeck, O. C. (1995). Inhibition of the hammerhead ribozyme by neomycin. *RNA*, **1**, 95-101.

Stryer, L. (1995). In: *Biochemisty*, 4th ed., W. H. Freeman and Company, New York, pp 182.

Sybyl molecular modeling software, version 6.7, Tripose associates, 1699 South Hanely Road, St. Louis, MO 63144- 2917

Szilaghi, R., Shahzad, u. H. S., and Weimar, T. The RNA-bound conformation of neamine defined by transferred NOE experiments. *Chembiochem* (In press).

Tagboto, S. and Townson, S. (2001). Antiparasitic properties of medicinal plants and other naturally occurring products. *Adv. Parasitol.*, **50**, 199-295.

Taylor, D. L., Sunkara, P. S., Liu, P. S., Kang, M. S., Bowlin, T. L. and Tyms, A. S. (1991). 6-0-Butanoylcastanospermine (MDL 28,574) inhibits glycoprotein processing and the growth of HIVs. *AIDS*, **6**, 693-698.

Tor, Y. (2003). Targeting RNA with small molecules. *Chembiochem*, **4**, 998-1007.

Tor, Y., Herman, T. and Westhof, E. (1998). Deciphering RNA recognition: aminoglycoside binding to the hammerhead ribozyme. *Chem. Biol.*, **5**, 277-283.

Unger, R. H. and Grundy, S. (1985). Hyperglycaemia as an inducer as well as a consequence of impaired islet function and insulin resistance: implication for the management of diabetes. *Diabetologia,* **28**, 119-121.

Van Beers, E. H., Büller, H. A., Grand, R. J., Einerhand, A. W. C. and Dekker, J. (1995). Intestinal brush border glycohydrolases: Structure function and development. *Crit. Rev. Biochem. Mol. Biol.*, **30**, 197-262.

Van den Broek, L. A., Kat-Van Den Nieuwenhof, M. W., Butters, T. D., Van Boeckel, C. A. (1996). Synthesis of alpha-glucosidase I inhibitors showing antiviral (HIV-1) and immunosuppressive activity. *J. Pharm. Pharmacol.*, **48**, 172-178.

van Gunsteren, W. F. and Berendsen, H. J. C. (1982). Molecular dynamics: perspective for complex systems *Biochem. Soc. Trans*., **10**, 301-305**.**

Vane, J. R. (1971). Inhibition of prostaglandin synthesis as a mechanism of action for aspirin-like drugs. *Nature*, **231**, 232-235.

Vicens, Q. and Westhof, E. (2003). RNA as a drug target: the case of aminoglycosides. *Chembiochem*, **4**, 1018-1023.

von Ahsen, U., Davies, J. and Schroeder, R. (1991). Antibiotic inhibition of group I ribozyme fuction. *Nature*, **353**, 368-370.

Walter, F., Putz, J., Giege, R., and Westhof. E. (2002). Binding of tobramycin leads to conformational changes in yeast tRNA (Asp) and inhibition of aminoacylation. *EMBO J*. **21**, 760-768.

Wang, H. and Tor, Y. (1997). Electrostatic interactions in RNA aminoglycosides binding. *J. Am. Chem. Soc.*, **119**, 8734-8735.

Wank, H., Rogers, J., Davies, J. and Schroeder, R.(1994). Peptide antibiotics of the tuberactinomycin family as inhibitors of group I intron RNA splicing. *J. Mol. Biol.*, **236**, 101-110.

Weimar, T., Bukowski, R. and Young, N. M. (2000). The conformation of the T-antigen disaccharide bound to Maclura pomifera agglutinin in aqueous solution. *J. Biol. Chem.*, **275**, 37006-370010.

Wu, H. N., Lin, Y. J., Lin, F. P., Makino, S., Chang, M. F. and Lai, M. M. C. (1989). Human hepatitis delta virus RNA sub fragments contain an auto cleavage activity. *Proc. Natl. Acad. Sci. USA*, **86**, 1831-1835.

Ye, F., Shen, Z. and Xie, M. (2002). α-Glucosidase inhibition from a Chinese medical herb (*Ramulus mori*) in normal and diabetic rats and mice. *Phytomedicine*, **9**, 161-166.

Yoshikawa, K., Yamamoto, K. and Okada, S. (1994). Classification of some α-glucosidases and α-xylosidases on the basis of substrate specificity. *Biosci. Biotechnol. Biochem.,* **58**,1392-1398.

Zapp, M. L., Stern, S. and Green, M. R. (1993). Small molecules that selectively block RNA binding of HIV-1 Rev protein inhibit Rev function and viral production. *Cell*, **74**, 969-978.

8 Supplements

8.1 Lineweaver-Burk Plots and Dixon Plots Produced for Different Compounds

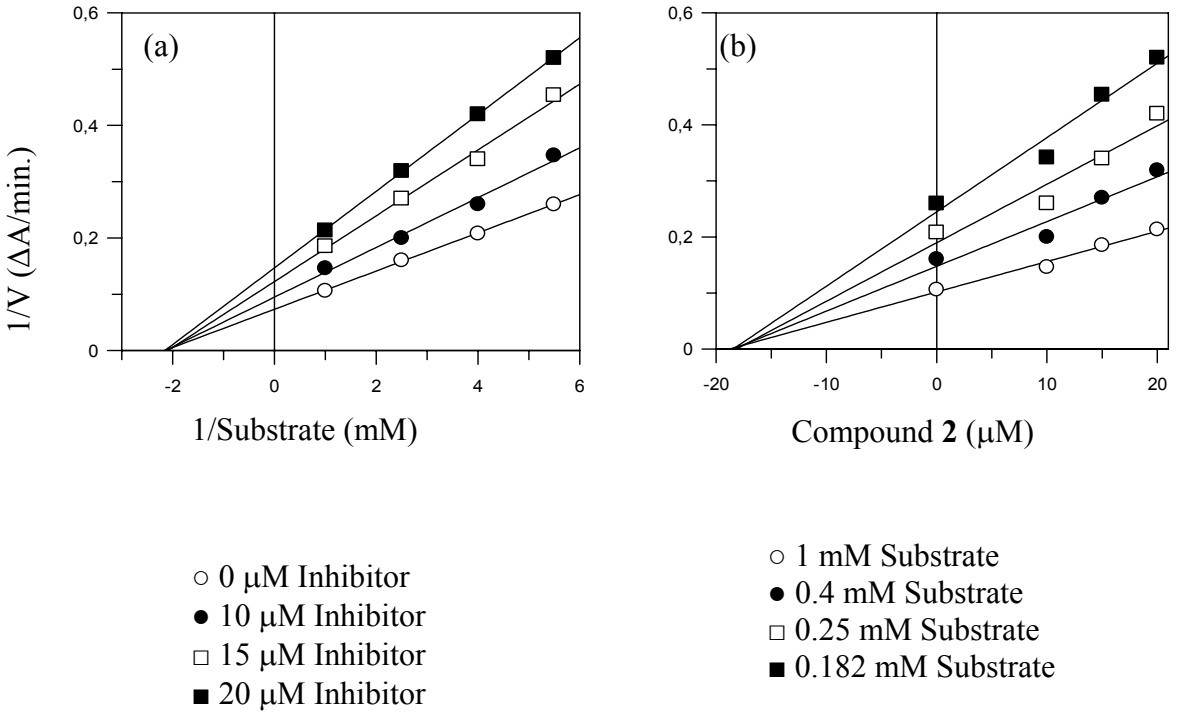

Figure-8.1: Steady state inhibition studies on compound **2** against yeast α-glucosidase. (a) Lineweaver-Burk plot, reciprocals of initial reaction velocities versus various concentrations of substrate (PNP-G) (b) Dixon plot, reciprocals of initial reaction velocities versus different concentrations of compound **2**.

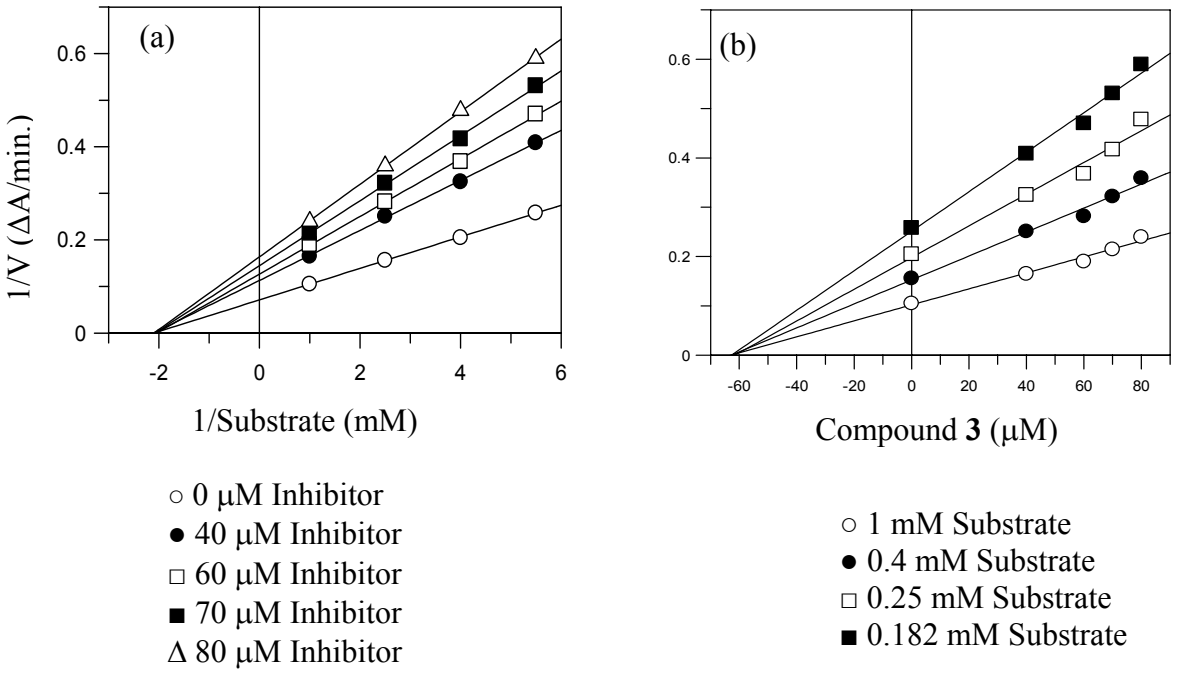

Figure-8.2: Steady state inhibition studies on compound **3** against yeast α-glucosidase. (a) Lineweaver-Burk plot (b) Dixon plot.

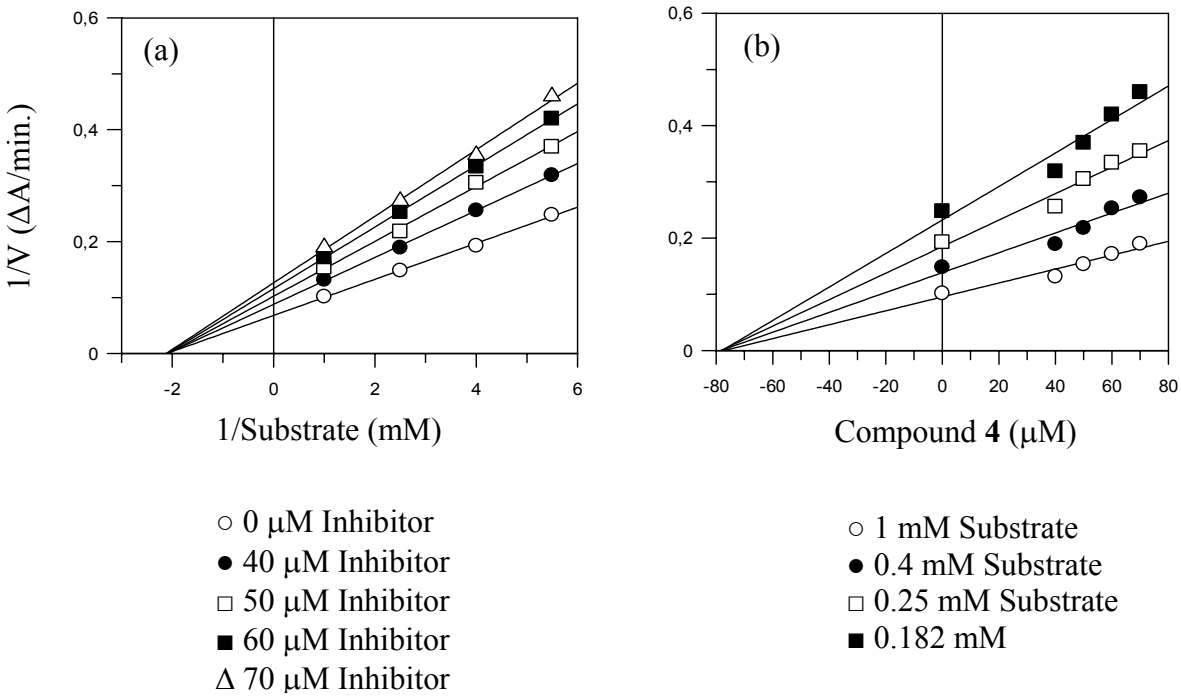

Figure-8.3: Steady state inhibition studies on compound **4** against yeast α-glucosidase. (a) Lineweaver-Burk plot (b) Dixon plot.

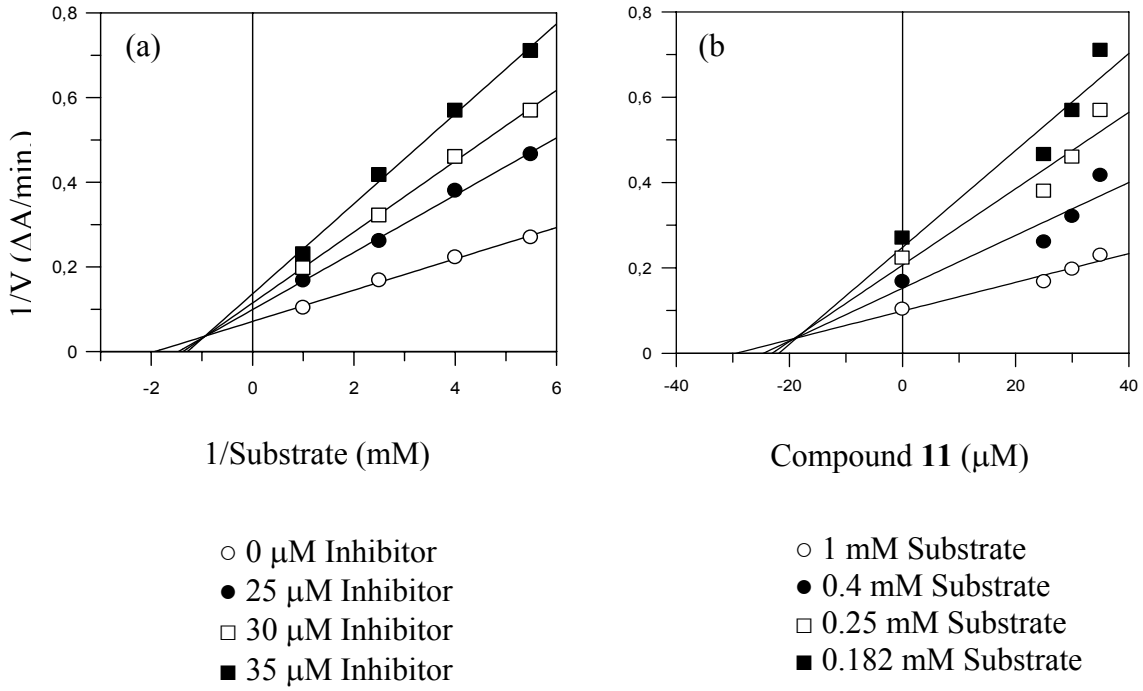

Figure-8.4: Steady state inhibition studies on compound **11** against yeast α-glucosidase. (a) Lineweaver-Burk plot (b) Dixon plot. Both plots show mixed-type inhibition.

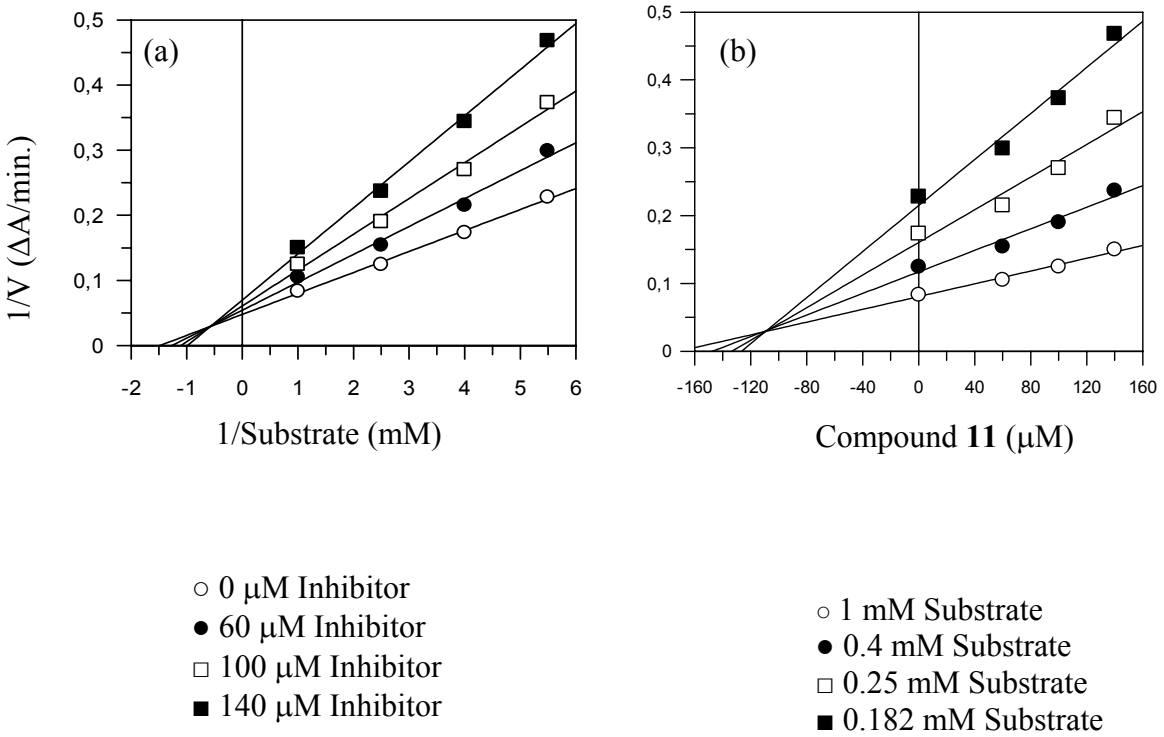

Figure-8.5: Steady state inhibition studies on compound **11** against intestinal α-glucosidase. (a) Lineweaver-Burk plot (b) Dixon plot.

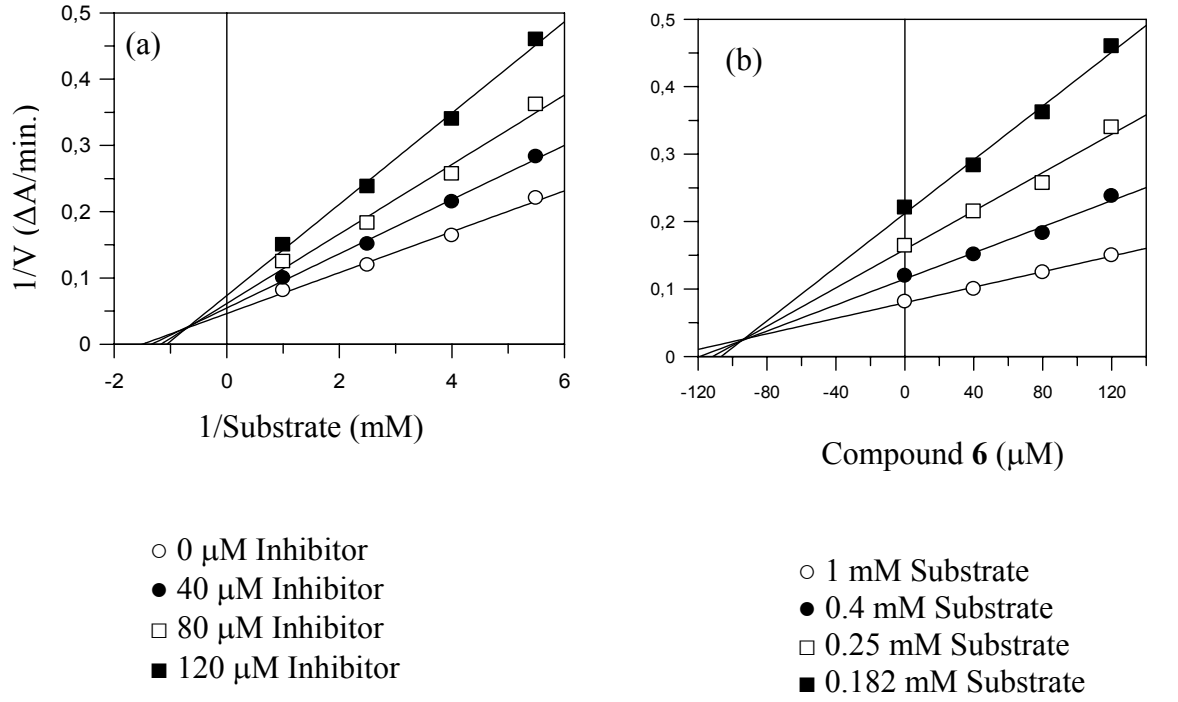

Figure-8.6: Steady state inhibition studies on compound **6** against rat intestinal α-glucosidase. (a) Lineweaver-Burk plot (b) Dixon plot.

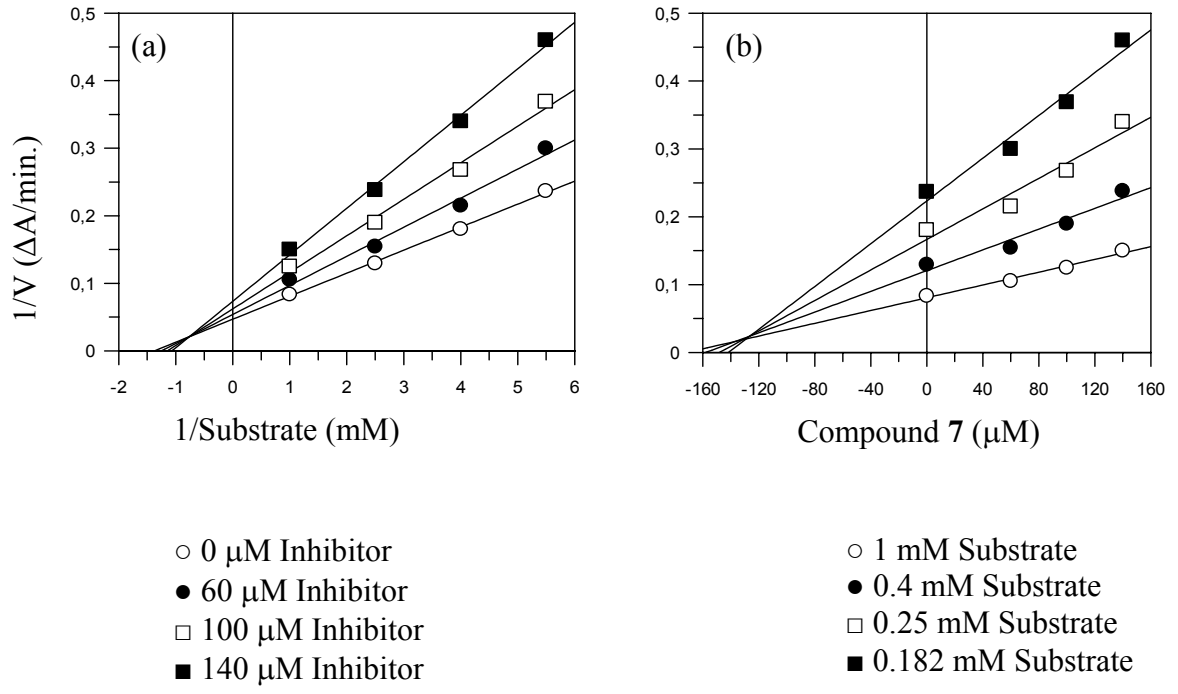

Figure-8.7: Steady state inhibition studies on compound **7** against rat intestinal α-glucosidase. (a) Lineweaver-Burk plot (b) Dixon plot.

Acknowledgements

I pay my special gratitude to my supervisor Dr. Thomas Weimar for his endless guidance, encouragements and motivations to complete this work. I would have never reached at this stage without his guidance.

I owe my warmest thanks to Prof. Dr. Thomas Peters for providing the research facilities, Professor Dr. Bernhard Westermann (Halle) for providing neamine sample, Dr. Till Maurer, (Boehringer, Ingelheim) for measuring few NMR spectra for us and Professor Dr. Bernd Meyer (Hamburg) for allowing us to measure NMR spectra in his institute.

I am highly indebted to Richard Szilaghi who helped a lot during my research work, and other colleagues for their cooperation and very friendly behaviour.

I pay my special gratitude to Professor Dr. Iqbal Choudhary for his guidance to complete α-glucosidase inhibition work.

I am highly indebted to my father and my wife for their great encouragement and sacrifice during my studies.

I am thankful to German Academic Exchange Service for the financial support to complete this thesis.

Curriculum Vitae

Personal Profile

Name:	Syed Shahzad ul Hussan
Address:	B1-87/3, Muhammadpura, Sialkot, Pakistan
Marital Status:	Married
Nationality:	Pakistani
Date of Birth:	08.11.1973

Education

Ph. D. (Bioorganic Chemistry)	Institute of Chemistry, University of Luebeck, (In process)
M. Sc. (Chemistry)	University of the Punjab, Lahore, Pakistan (1997)
B. Sc. (Chem., Zoology, Botany)	University of the Punjab, Lahore, Pakistan (1995)
F. Sc. (Science)	Murray College, Sialkot, Pakistan (1992)

Topic of Ph. D. Research

Small ligand effectors of bio-macromolecules: Exploration of novel α-glucosidase inhibitors and NMR investigation of $tRNA^{Phe}$-bound Aminoglycosides.

Institutes where worked during Ph. D.

From 1998 to 2002, at HEJ Research Institute of Chemistry, University of Karachi, Pakistan,
From 2002 to 2004, at Institute of Chemistry University of Luebeck .

Publications

1. Shahzad, u. H. S, Szilaghi, R., and Weimar, T., "Aminoglycosides bound by $tRNA^{Phe}$ studied by NMR-Spectroscopy" (In process)

2. Szilaghi, R., Shahzad, u. H. S., and Weimar, T., "The RNA-bound Conformation of Neamine Defined by Transferred NOE Experiments". Chembiochem (In press)

3. Shahzad, u. H. S., M. Iqbal Choudhary, Suad Naheed, and Attar-ur-Rahman, "Kinetics and *in vivo* Studies of Sesquiterpenoid Derivatives as α-Glucosidase Inhibitors". (Manuscript submitted)

4. Khan, T., Zahid, M., Shahzad, u. H. S., Nisar, M. and Ahmad, V. U. (2002) Pharmacological Activities of Crud Acetone Extract and Purified Constituents of *Salvia moorcraftiana. Phytomedicine*, **60**, 295-299.

5. Ali, M. S., Jahangir, M., Shahzad, u. H. S., Choudhary, M. I. (2002) Inhibition of α-glucosidase by Oleanolic acid *Phytochemistry*, **60**, 295-9.

6. Anis, E., Anis, I., Ahmed, S., Mustafa, G., Malik, A., Afza, N., Shahzad, u. H. S. and Choudhary, M. I. (2002) α-Glucosidase Inhibitory Constituents from *Cuscuta reflexa*. *Chemical and Pharmceutical. Bulletin,* **50**, 112-114.

7. Shahzad, u. H. S. and Choudhary, M. I., (2001) New Inhibitors of α-Glucosidase Enzyme from Natural Sources. *Scientific Sindh*, **7**, 40-42.

8. Atta-ur- Rahman, Choudhary, M. I., Baig, I., Shahzad, u. H. S., Odongii, P., Bunderya M.and Oyun, Z. (2001) New α-Glucosidase Inhibitors From Mongolian Medicinal Plant *Ferula mongolica*. *Helvetica Chimica Acta*, **84**, 2409-2416.

9. Ahmad, S., Shahzad, u. H. S., Jalal, A., Hussain, M. S. and Rafique, K. M. (2001) Determination of Selenium in Fruits. *Pakistan Journal of Biological Sciences*, **4**, 164-165.

10. Mustafa, G., Anis, E., Ahmed, S.,Anis, I., Malik, A., Shahzad, u. H. S., and Choudhary, M. I. (2000) Lupene-Type Triterpene From *Periploca aphylla*. *Journal of Natural Product*, **63**, 881-883.

11. Jahan, N., Malik, A., Afza N, Choudhary, M. I. and Shahzad, u. H. S.(2000) Triterpenes from *Mimusops elengi*. *Z. Naturforschung*, **55b**, 1206-1210.